NASA CR-152277

A THREE-DIMENSIONAL VISCOUS/POTENTIAL FLOW INTERACTION ANALYSIS METHOD FOR MULTI-ELEMENT WINGS

MODIFICATIONS TO THE POTENTIAL FLOW CODE TO ALLOW PART-SPAN, HIGH-LIFT DEVICES AND CLOSE-INTERFERENCE CALCULATIONS

BY: B. MASKEW

MARCH 1979

SUBMITTED TO:

NASA AMES RESEARCH CENTER
MOFFETT FIELD, CALIFORNIA 94035

CONTRACT NAS2-8788

SUBMITTED BY:

ANALYTICAL METHODS, INC.
100 - 116TH AVENUE S. E.
BELLEVUE, WASHINGTON 98004
(205) 454-6119

ABSTRACT

The scope of the VIP3D viscous/potential flow analysis method has been extended to include part-span, high-lift devices on general planforms. The description of the modified code includes details of a doublet subpanel technique in which panels that are close to a velocity calculation point are replaced by a subpanel set. This treatment gives the effect of a higher panel density without increasing the number of unknowns. In particular, the technique removes the close-approach problem of the earlier singularity model in which distortions occur in the detailed pressure calculation near panel corners. Removal of this problem allowed a complete wake relaxation and roll-up iterative procedure to be installed in the code. The geometry package developed for the new technique and also for the more general configurations is based on a multiple patch scheme. Each patch has a regular array of panels, but arbitrary relationships are allowed between neighboring panels at the edges of adjacent patches--this provides great versatility for treating general configurations. Preliminary tests of the modified code are encouraging, but further tests are needed, particularly for configurations with part-span, high-lift devices.

SUMMARY

The scope of the VIP3D program for the viscous/potential flow analysis of multi-element wings has been extended to cover more representative high-lift configurations. Particular objectives included part-span, high-lift devices and an improved representation of the interference between wakes and surfaces. To fulfill these objectives, each wake has to be fully relaxed (i.e., made force free) and allowed to roll up; however, this gives rise to close-approach problems associated with the potential flow panel methods. The close-approach problem arises because detailed pressure calculations near a surface represented by singularity panels have distortions near the panel edges. Since these distortions have a serious impact on free-wake analysis, ways of removing the close approach problem were investigated in the two-dimensional flow case. The investigation lead to the development of a doublet subpanel technique in which panels close to the velocity calculation point are represented by a set of subpanels. Subpanels are generated on the interpolated surface and have singularity values interpolated from local panel values. Subpanels, therefore, have the effect of higher panel density without increasing the number of unknowns.

The three-dimensional form of the doublet subpanel technique and also the objectives for part-span, high-lift devices on general planforms required the development of several new geometry routines. A versatile and user-oriented geometry package was developed based on multiple patches of panels. Each patch has a regular array of panels but arbitrary relationships are allowed between neighboring panels at the edges of adjacent patches. The patch, panel and subpanel arrangement is continued downstream on wakes which are allowed to relax and roll up in an iterative procedure in the potential flow code.

Preliminary test cases of the modified code are encouraging and compare closely with earlier solutions; however, further tests need to be carried out, particularly for the case of part-span, high-lift devices.

TABLE OF CONTENTS

Section			Page
ABSTRACT			i
SUMMARY			ii
TABLE OF CONTENTS			iv
LIST OF FIGURES			vi
1.0	INTRODUCTION		1
2.0	THE CLOSE-APPROACH PROBLEM AND ITS TREATMENT		2
	2.1	Occurrence of the Close-Approach Problem	2
	2.2	Singularity Model	6
	2.3	Close-Approach Techniques	9
		2.3.1 Interpolation	11
		2.3.2 Treatment of the Panel-Edge Singularity	11
		2.3.3 Internal Singularities	13
		2.3.4 Corner Panels	13
		2.3.5 Subpanel Technique	16
3.0	DOUBLET SUBPANEL TECHNIQUE		22
	3.1	Singularity Model	22
	3.2	Boundary Conditions	25
	3.3	Test Cases	28
4.0	OVERVIEW OF THE VIP3D CODE MODIFICATIONS		36
	4.1	General	36
	4.2	Geometric Model	36
	4.3	Singularity Model	46
	4.4	Solution Procedure	46
5.0	GEOMETRY ROUTINES		48
	5.1	Components	48
	5.2	Patches	50
		5.2.1 Convention	50
		5.2.2 Sections	53
		5.2.3 Chordwise Regions	58
		5.2.4 Spanwise Regions	62
	5.3	Special Routines	64
		5.3.1 Copying Routine	64
		5.3.2 Automatic Patch Generator	66

TABLE OF CONTENTS (Continued)

Section			Page
	5.4	Panels and Subpanels	71
		5.4.1 Automatic Paneling Routine	71
		5.4.2 Panel and Subpanel Geometry	71
		5.4.3 Panel Neighbor Routine	78
		5.4.4 Subpanel Usage	81
	5.5	Wake Routines	84
		5.5.1 Initial Wake Geometry	84
		5.5.2 Wake Panels and Subpanels	86
		5.5.3 Wake Relaxation	87
6.0	SURFACE DOUBLET DISTRIBUTION		89
	6.1	Doublet Multipliers	89
	6.2	Augmented Patch	92
	6.3	Influence Coefficient	94
		6.3.1 Far-Field	94
		6.3.2 Middle-Field	95
		6.3.3 Near-Field	100
7.0	TEST CASES		101
	7.1	Geometry Code	101
	7.2	Wing Case	103
8.0	CONCLUSIONS AND RECOMMENDATIONS		111
9.0	REFERENCES		112
10.0	APPENDICES		
	APPENDIX A:	Biquadratic Interpolation	113
	APPENDIX B:	Numerical Integration for Doublet Influence Coefficient	118
	APPENDIX C:	Linear Vorticity Influence Coefficient in Two Dimensions	123
	APPENDIX D:	Neumann Boundary Condition Applied to a Surface Doublet Model	125
	APPENDIX E:	Streamline Calculation Routine	128
	APPENDIX F:	Vortex Segment Influence Coefficient	131

LIST OF FIGURES

Figure	Title	Page
1	Chordwise Pressure Distribution on a Wing with Deflected Flaps Calculated by the Quadrilateral Vortex-Lattice Method with Rigid Wake (Ref. 4)	3
2	Detailed Pressure Surveys Near the Leading Edge of a GA(W)-1 Airfoil Calculated by the Symmetrical Singularities Method	
	(a) Survey Along the Surface	5
	(b) Surveys Above and Parallel to the Surface . .	7
3	Comparison of Pressure Distributions on a Joukowski Airfoil at 10^0 Incidence	10
4	Detailed Pressure Calculations Near Leading Edge of a Joukowski Airfoil. Symmetrical Singularities Method with Local Treatment of Logarithmic Term (2.3.2)	12
5	Corner Panel Models	
	(a) Control Points on Panels	14
	(b) Control Points on Surface	14
6	Detailed Pressure Calculations Near Leading Edge of a Joukowski Airfoil. Symmetrical Singularities Method With Corner Panel Model (2.3.4)	15
7	Effect of Control Point Location on Pressures Calculated at Control Points Near the Leading Edge of the Joukowski Airfoil ($\alpha = 10^0$).	17
8	Subpanel Scheme for Two-Dimensional Flow (2.3.5)	18
9	Close-Approach Regions and Near-Field Regions for the Symmetrical Singularities Method	19

LIST OF FIGURES (Continued)

Figure	Title	Page
10	Treatment of the Surface Doublet Distribution	
	(a) Interpolation Through Panel Doublet Values to Obtain Subpanel Values	23
	(b) Local Quadratic Representation for Evaluating Vorticity	24
11	Symmetrical and Antisymmetrical Parts of the Surface Doublet Distribution	27
12	Calculations of a Joukowski Airfoil in Presence of a Vortex	
	(a) Streamlines	29
	(b) Surface Pressure Distribution	30
13	Comparison of Calculated and Exact Solutions for a CLARK-Y Airfoil in Presence of a Vortex and Sink	
	(a) Streamlines	33
	(b) Surface Pressure Distribution	34
14	Flow Chart for the Potential Flow Calculation in the Modified Code	37
15	Section Through Subpanel Scheme for the Three-Dimensional Case	39
16	Examples of Components and Patches on a High-Lift Configuration	41
17	Preliminary Guidelines for Patch Shapes	42
18	Three Examples of Arbitrary Neighbor Realtionships	43
19	Initial Wake Arrangement	45
20	Component Transformation	49
21	Sections Defining Patch Surface	51

LIST OF FIGURES (Continued)

Figure	Title	Page
22	Patch Conventions	52
23	Section Transformation Into C.C.S.	55
24	Basic Point Input Options 1 Through 4	56
25	Chordwise Regions on a Section	59
26	Spacing Options 0, 1 and 2 in the A.P.R. . . .	61
27	Spanwise Regions on a Patch	63
28	Automatic Patch Generator	
	(a) Flat-Edge Patch (KURV = 0)	68
	(b) Patch with Semicircular (KURV = 1) or Semi-Elliptical (KURV > 1) Sections	68
	(c) Patch Generated from Four Strings of Copied Points (KURV Negative)	70
29	General Character of Paneling Offered by the A.P.R.	
	(a) Simple Sections	73
	(b) General Sections	73
30	Panel or Subpanel Geometry	74
31	Arrangement of Subpanels on a Panel (3 x 3 Scheme Shown)	77
32	Panel Neighbor Information	79
33	Panel Neighbors Across Patch Edges	80
34	Extremes of Subpanel Usage	
	(a) Panel Size Constant	82
	(b) Subpanel Size Constant	82
35	Basic Wake Points Define Initial Wake Streamwise Geometry	85

LIST OF FIGURES (Continued)

Figure	Title	Page
36	Wake Relaxation	88
37	Two-Way Biquadratic Interpolation for Subpanel Doublet Values	
	(a) Local 4 x 4 Panel System	90
	(b) The Panel's 25-Panel Set	90
38	Augmented Patch Scheme for Doublet Interpolation	93
39	Evaluation of Vorticity Value and Gradient on a Panel	
	(a) Information from Panel Neighbors	96
	(b) Panel Vorticity Components	96
40	Basic Linear Vorticity Model (γ_x Component) . .	98
41	Tests for the Geometry Code	
	(a) Wing Planform Indicating the Patches of Panels on Three Components	102
	(b) General View of Panels	104
	(c) Panels and Subpanels on the Tip Patch (Patch 7)	105
	(d) Panels and Subpanels on Flap (Patches 10 and 11 Only)	106
	(e) Panels and Subpanels on Edge of Flap Cutout on Wing (Patch 8)	107
42	Rectangular Wing Pressure Distribution	
	(a) Chordwise Distribution at .125 Semispan . .	108
	(b) Spanwise Distributions at x = .0086c and .889c	110

1.0 INTRODUCTION

At present it is possible to compute the flow over simple wings and wings with full-span high-lift devices up to incipient flow separation using a viscous/potential flow iteration method (Ref. 1). The computer code, VIP3D, which performs this analysis, was developed by Analytical Methods, Inc. while under contract† to the large-scale Aerodynamics Branch at the NASA Ames Research Center. The program is designed as a special purpose tool for the analysis of high-lift wing configurations.

Under a follow-on to the contract, the potential flow part of the computer code has been modified to allow the method to be applied to problems that are more representative of the high-lift configurations encountered on today's aircraft. The primary objectives were to allow part-span high-lift devices and to improve the modeling of close interference, such as exists between a surface and a vortex wake.

The modified potential flow code and preceding exploratory work are described in this report. The new objectives required the removal of the close-approach problem associated with practical potential flow codes; this problem and ways of treating it are examined in Section 2.0. A doublet subpanel technique which resulted from the investigation in two-dimensional flow is described in Section 3.0, together with some test cases. The extension of this technique for the VIP3D code and the modified geometry routines are discussed in general terms in Section 4.0, while Section 5.0 includes details of the geometry package. The latter has undergone extensive modification to conform with the new singularity model and also to deal with the more general configurations. Section 6.0 describes the treatment of the surface doublet distribution. Some preliminary tests of the modified parts of the code are described in Section 7.0 The general layout of the VIP3D program, and in particular the viscous routines, remain as described in Reference 1.

---

†Contract NAS2-8788.

2.0 THE CLOSE-APPROACH PROBLEM AND ITS TREATMENT

2.1 Occurrence of the Close-Approach Problem

Viscous effects and the requirement of a force-free wake introduce strong non-linear effects into the calculation of the flow about high-lift configurations. The method of Reference 1 is a practical approach to calculating such flows using a viscous/potential flow iteration, but the force-free wake requirements are only partially satisfied since the wake relaxation is limited to vertical displacements.

The new objectives for more general configurations and part-span high-lift devices make it imperative that the full wake relaxation and roll-up be included (Refs. 2 and 3). It is important not only to obtain the correct wake location relative to downstream components in a multi-element configuration, but also to get correct force-free orientation as each wake leaves a wake-shedding element carrying moderate to high lift levels. If the wake is not force-free as it leaves the surface, then surface pressures can be affected; for example, a cross-over between upper and lower surface pressures can be calculated near the wing tip trailing edge when using a flat, chordwise wake. Figure 1 (from Ref. 4) shows an extreme example of this crossover effect with a fixed wake in a high-lift calculation and emphasizes the need for a fully relaxed wake.

Fully relaxed wake calculations on high-lift configurations can lead to situations where free vortex sheets pass very close to the lifting surfaces, and this can result in a breakdown of the surface singularity method. This CLOSE-APPROACH problem was the reason behind the restriction to vertical relaxation in the method of Reference 1.

The failure of surface singularity methods in a close-approach situation arises because of practical reasons: the airfoil geometry and flow distribution have to be approximated and the boundary conditions can be applied only at a finite

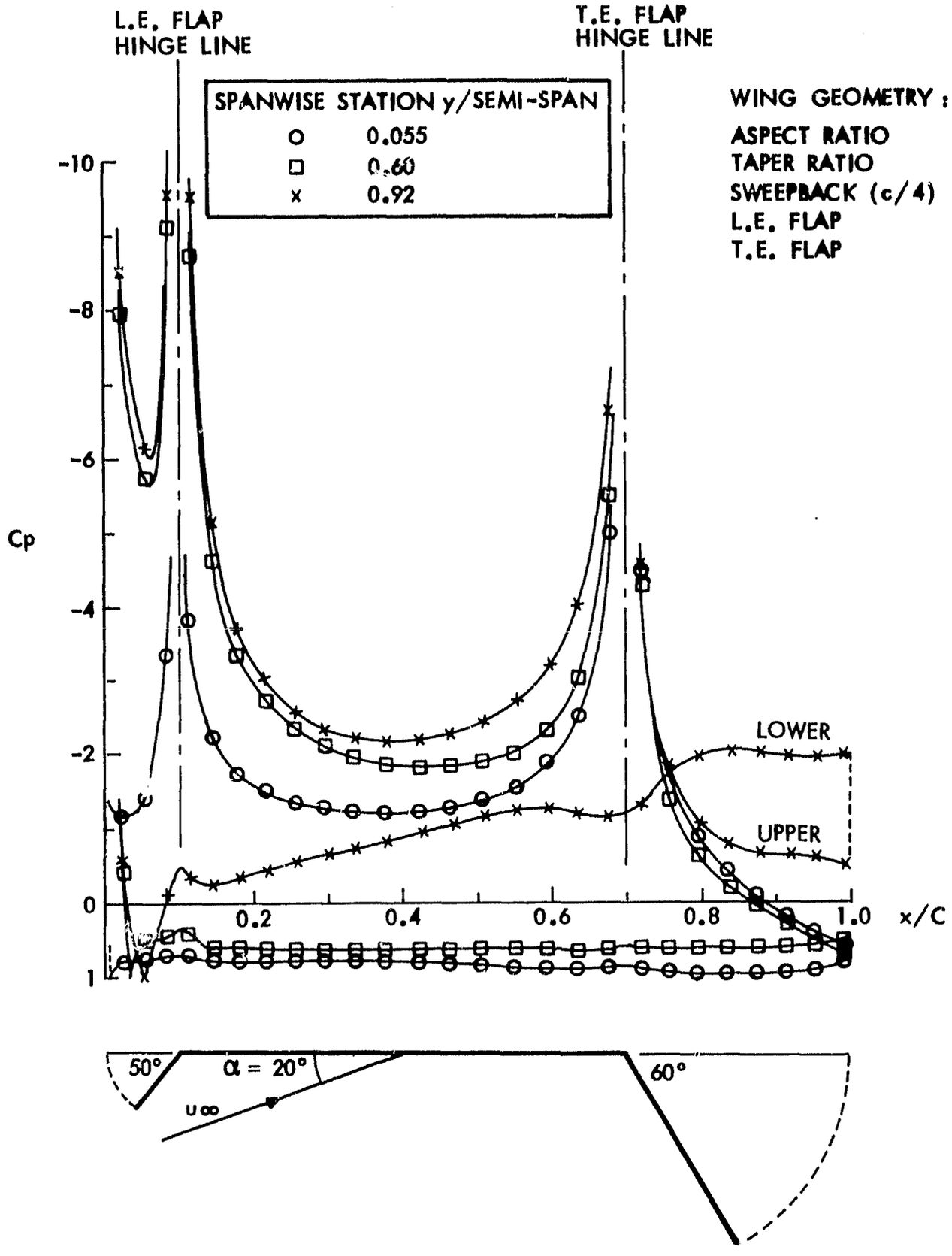

Figure 1. Chordwise Pressure Distributions on a Wing with Deflected Flaps Calculated by the Quadrilateral Vortex-Lattice Method with Rigid Wake (Ref. 4).

number of points. Between the boundary condition points, the flow is unconstrained, and so the detailed flow distribution in the model generally has local distortions. These flow distortions can influence the relaxed-wake calculations in two ways:

(i) Flow distortions associated with the free vortex sheets can influence the boundary conditions on the surface, and hence affect the singularity solution.

(ii) Flow distortions associated with the fixed surfaces can influence the calculated location of the relaxed wake--sometimes even causing penetration at the fixed surfaces.

The severity of the problem increases with circulation level, and is particularly bad in regions of high curvature and high pressure gradient. The close-approach problem--which is present to a varying degree in all existing surface singularity methods--can be alleviated (usually at the expense of more computing effort) by increasing the number of control points (i.e., panels) and/or going to higher-order models.

The extent of the close-approach region (i.e., the region in which flow distortions are significant) was investigated in Reference 5 for discrete singularities. It was established that the close-approach problem persists to a distance of about one panel size away from the discretized sheet. An extension of that investigation was conducted in the present work for the case of a distributed singularity model; namely, the symmetrical singularity method (Ref. 6), employing piecewise linear vorticity and a constant source on flat panels. The symmetrical singularity concept minimizes singularity strengths (Ref. 6), and hence minimizes the flow distortions; even so, large pressure deviations were calculated in a detailed analytic survey of surface pressures near the leading edge of a GA(W)-1 airfoil at 20° incidence, Figure 2(a). The location of panel edges is identified and a smooth line passing through control point

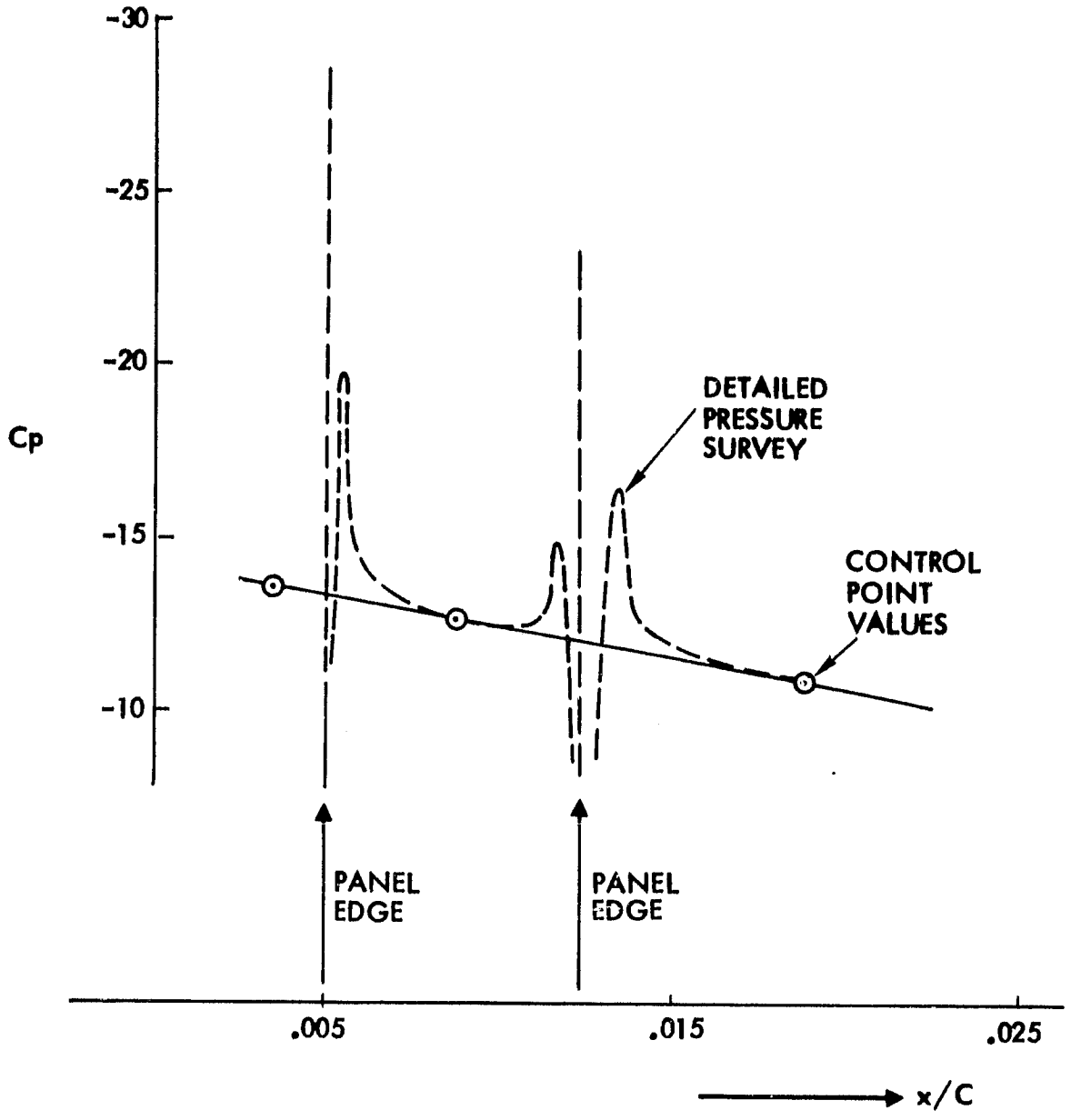

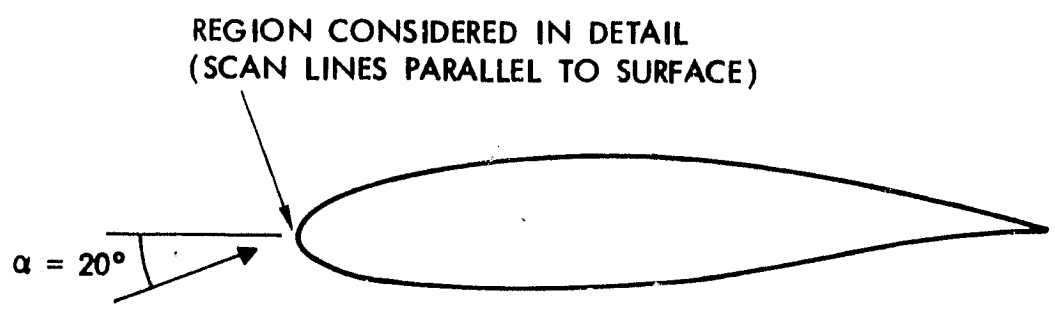

(a) SURVEY ALONG THE SURFACE

Figure 2. Detailed Pressure Surveys Near the Leading Edge of a GA(W)-1 Airfoil Calculated by the Symmetrical Singularities Method.

values emphasizes the extent of the region in which the close-approach problem is significant for this model.

Figure 2(b) shows two additional pressure surveys taken above and parallel to the surface at heights corresponding to approximately a quarter- and a half-panel size. As the pressure survey moves away from the surface, the extreme distortions at the panel edges quickly reduce to small "bumps" in the detailed distribution. (With increasing distance from the inclined surface, these bumps appear to move sideways in the x-wise plot because the corner disturbance propagates normal to the surface.) Bearing in mind that the situation shown is particularly extreme (the real flow would have separated), it would seem feasible for the close-approach problem area to be held within a half panel size for this particular model. Even so, some local treatment would be necessary to restore a smooth pressure distribution close to the surface.

An investigation of ways of removing the close-approach problem is outlined in the following subsections. This investigation considered alternative singularity models in addition to various close-approach techniques applicable to existing models, because the symmetrical singularity panel model considered above is not directly extendable to the three-dimensional case without some deterioration in its close-approach characteristics. Although most of the evaluations were performed in the two-dimensional case, the form of each model for three-dimensional flow was the major consideration throughout the investigation.

2.2 Singularity Model

Good close-approach properties in a surface singularity model require continuous and smooth representations of the surface geometry and flow distribution. These requirements conflict with the properties of practical singularity models, most of which are based on panels over which a piecewise analytic integration is performed to evaluate influence coefficients.

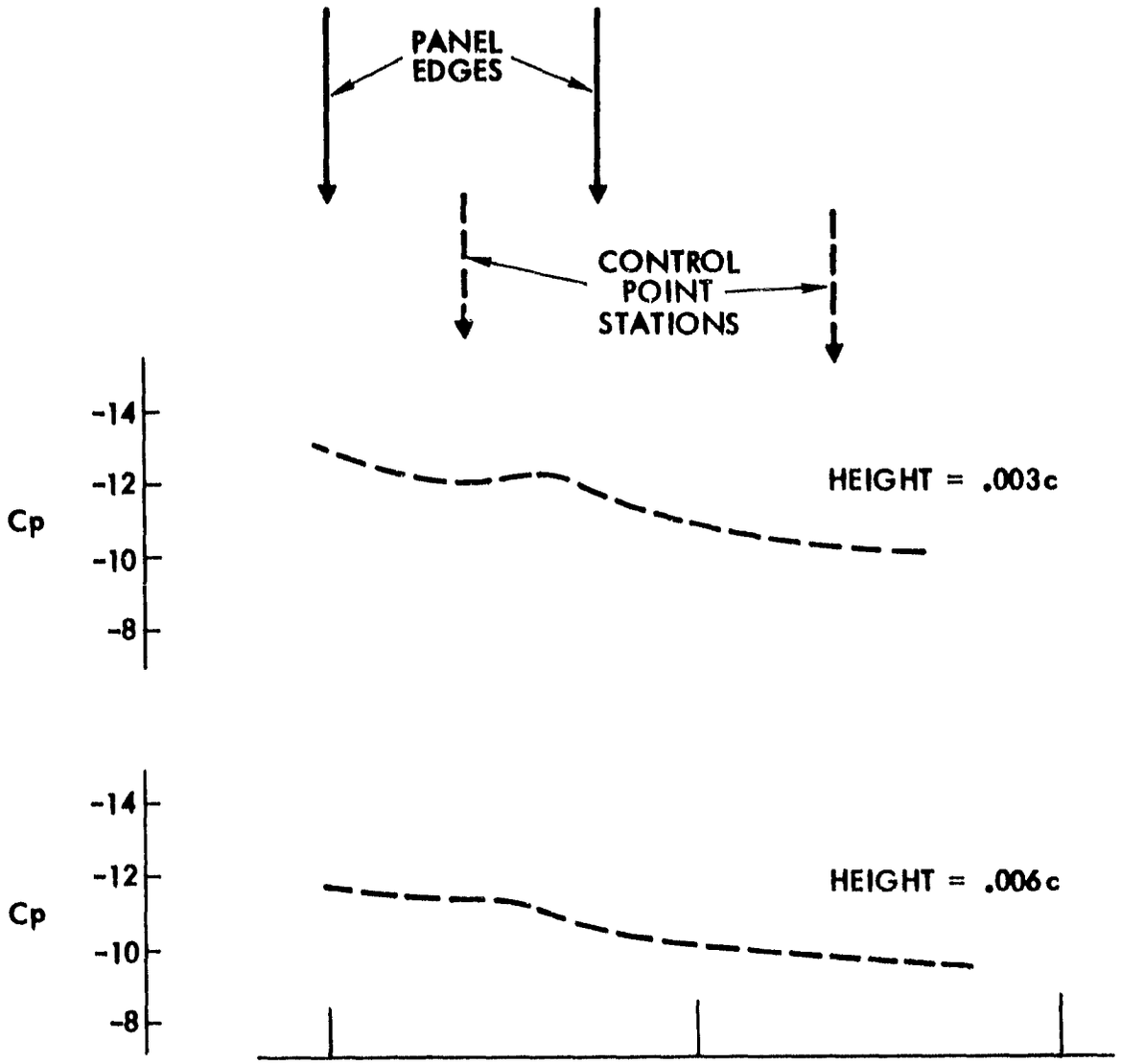

(b) SURVEYS ABOVE AND PARALLEL TO THE SURFACE

Figure 2. Concluded.

Panels are usually flat, but higher-order effects due to surface curvature and smooth singularity distributions may be approximated using a series expansion in the integrand. Generally the close-approach problem is present to a varying degree in all these methods making it necessary to couple them with some close-approach technique to accomplish the present objectives.

An alternative to piecewise analytic integration uses a numerical integration scheme based on a continuous singularity distribution over the curved surface. Such a method has no close-approach problem concerning the representation of the surface geometry and singularity distributions, but it does have a problem in evaluating the local singularity contribution when calculating velocities close to the surface.

To examine a numerical integration approach a pilot code was assembled based on a surface doublet distribution. A smooth doublet distribution is the most convenient singularity model for the three-dimensional lifting case because it automatically satisfies the requiremnt of continuity in the vorticity distribution (vorticity being the gradient of the doublet distribution). The doublet distribution and the surface geometry were represented using the biquadratic expression (Appendix A). The numerical integration scheme used the Romberg method coupled with Richardson's extrapolation technique (Appendix B). It will be recalled that this method is based on the trapezoidal rule integration, but, by continuously doubling the number of strips, the error value can be controlled and the computing effort minimized.

The main problem associated with numerical integration over a doublet sheet is the evaluation of the local contribution near the velocity calculatior point. It arises from a unique behavior of the doublet integrand which first goes to a large positive value and then to a large negative value as the velocity calculation point is approached, see Appendix B. To make the numerical scheme more effective in the pilot code, various

transformations were applied in a number of regions based on the behavior of the integrand (Appendix B). The Romberg integration scheme became very effective with this treatment and gave accurate solutions of the two-dimensional airfoil problem with execution times comparable with piecewise analytic methods. A three-dimensional version, however, was not as effective. Although exact agreement was obtained in comparison with a method using linear vorticity panels for several velocity scan lines approaching the surface, the overall computing time for the numerical scheme was an order of magnitude higher than for the analytic scheme. Even though it seemed feasible to reduce computing effort further by "fine tuning" the transformation schemes, it was clear that considerable development time would be needed to make the numerical scheme a practical and fail-safe method for the general three-dimensional configurations envisaged. Effort was thereafter concentrated on investigating close-approach techniques that are applicable to existing singularity models. The various techniques considered are described in the next subsection.

2.3 Close-Approach Techniques

There are several close-approach techniques which can be applied to existing singularity models to obtain smooth pressure calculations between control points. Techniques considered in the present work are described below. Details of some of the evaluations are included for the calculated surface pressures near the leading edge of a Joukowski airfoil at 10^{o} incidence; the overall pressure distribution calculated by the symmetrical singularities method (Ref. 6) is given in Figure 3.

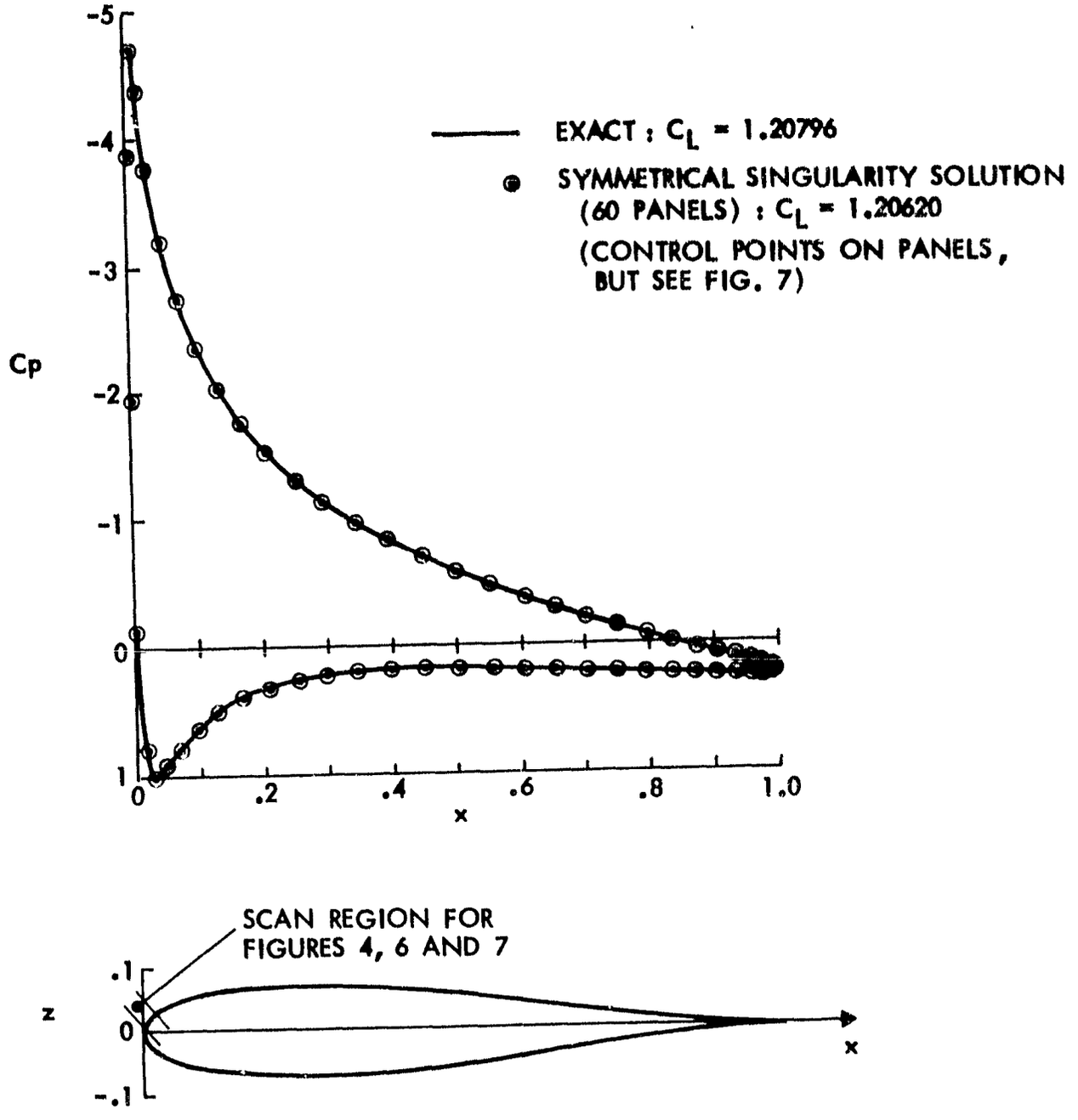

Figure 3. Comparison of Pressure Distributions on a Joukowski Airfoil at 10° Incidence.

2.3.1 Interpolation

A technique that has been used in the past interpolates between the control point values to obtain intermediate surface pressures. Likewise, off-body pressures may be obtained by interpolating between "good" values calculated outside the close-approach region--such a technique has been used successfully even with discrete singularity models.

Clearly, interpolation is a reasonable technique to apply to attached flow single-airfoil problems (e.g., Figure 3), especially if the interpolation is performed in terms of surface distance rather than x or z; however, in the case of multiple-element high-lift calculations, situations exist where interpolation is not applicable. For example, there are no "good" values where the close-approach regions of a free wake and a fixed surface overlap. Higher panel density may alleviate the problem, but would increase the number of unknowns and--if computer storage would allow such an increase--would be more expensive to run.

2.3.2 Treatment of the Panel-Edge Singularity

The main culprit behind the local flow distortions is a logarithmic term which can become singular at each panel edge. Under certain conditions the logarithmic singularity terms from two adjacent panel edges cancel; e.g., when the surface slope and singularity value are continuous from panel to panel. For the more general case, an interpolation formula was examined in which the induced velocity influence coefficients from two neighboring panels were combined linearly according to the location of the calculation point within the close-approach region. Results from calculations based on a limiting close-approach distance of a quarter panel size from the corner point are presented in Figure 4. Although considerable improvement is indicated over the basic solution, the results are not acceptable for the present objectives. Further

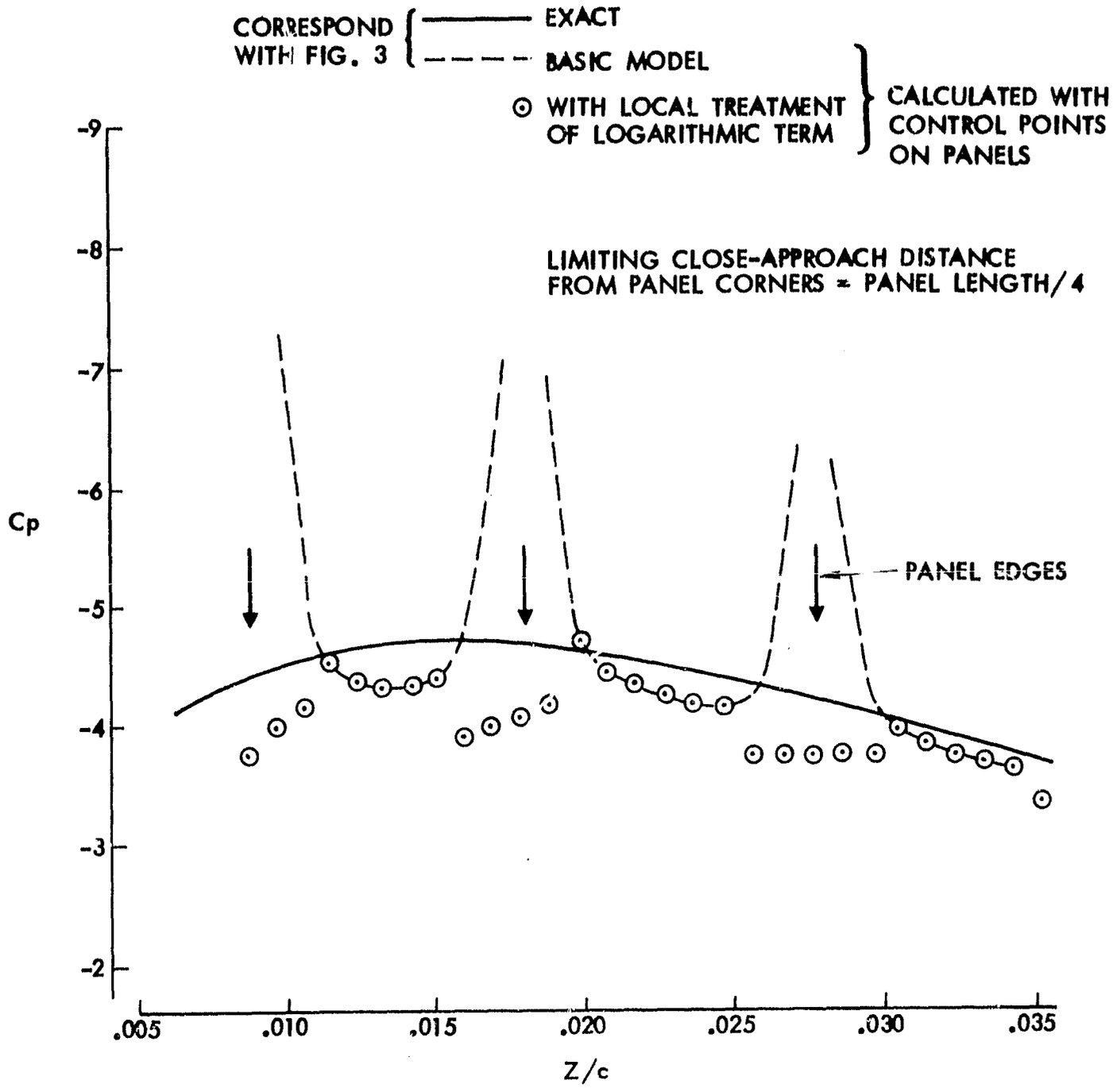

Figure 4. Detailed Pressure Calculations Near Leading Edge of a Joukowski Airfoil. Symmetrical Singularities Method with Local Treatment of Logarithmic Term (2.3.2).

development of this technique is possible, but any further complication from the model evaluated could get very cumbersome in the general three-dimensional case.

2.3.3 Internal Singularities

Earlier investigations (Ref. 5) of discrete singularities in two-dimensional flow lead to a "submerged singularity" technique (Ref. 7) in which the close-approach problem region was enclosed within the airfoil contour by placing the singularity sheet the appropriate distance below the surface. This submerged distance was minimized by applying the subvortex technique (Ref. 5) as well. (In fact, the internal singularities technique is best applied in combination with another close-approach technique--in this way the interior singularity surface can be more closely related to the airfoil surface and this aids accuracy.) This internal singularity technique gives a very smooth pressure distribution (Ref. 7) and is applicable to simple wings in the three-dimensional case, but it may be difficult to apply to general three-dimensional configurations.

2.3.4 Corner Panels

In this technique the two panels adjacent to a close-approach velocity calculation are temporarily replaced by three panels. The middle panel of the temporary set straddles the corner between the two control points (Figure 5(a)), and the other two are the remaining halves of the replaced panels. The singularity values for the temporary panels are obtained by interpolation through the basic panel values.

Again, this technique removed the "spikes" in the detailed pressure distribution, Figure 6, but the resulting distribution is not sufficiently smooth; kinks occur at the points where the corner panel scheme takes over from the basic panels. (The limiting close-approach distance was a quarter panel size in this case.)

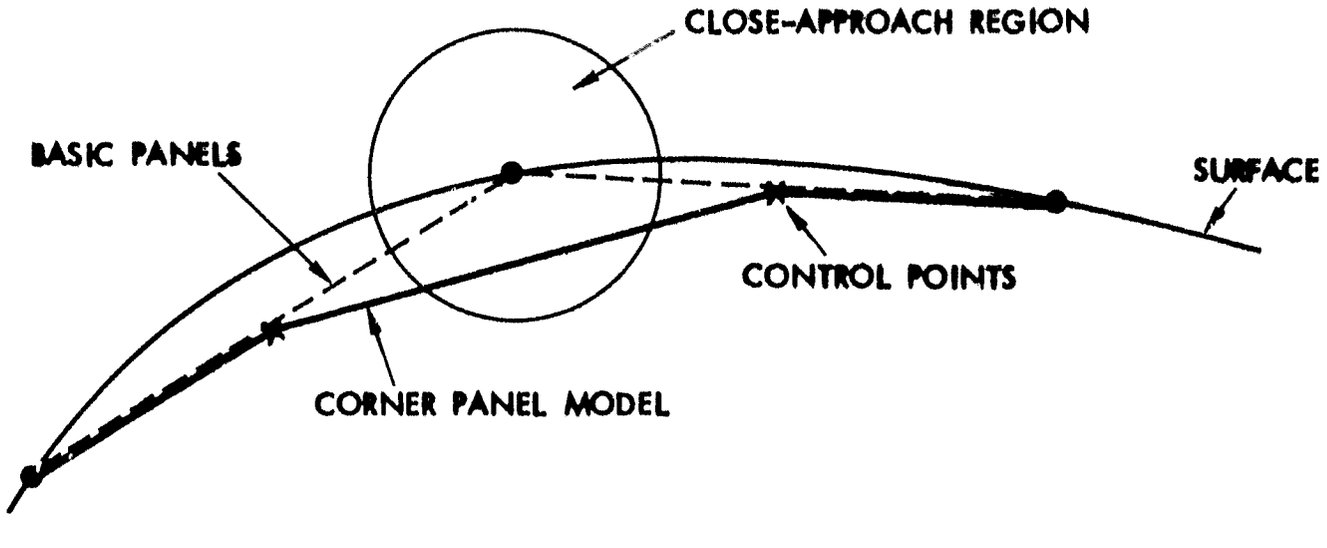

(a) CONTROL POINTS ON PANELS

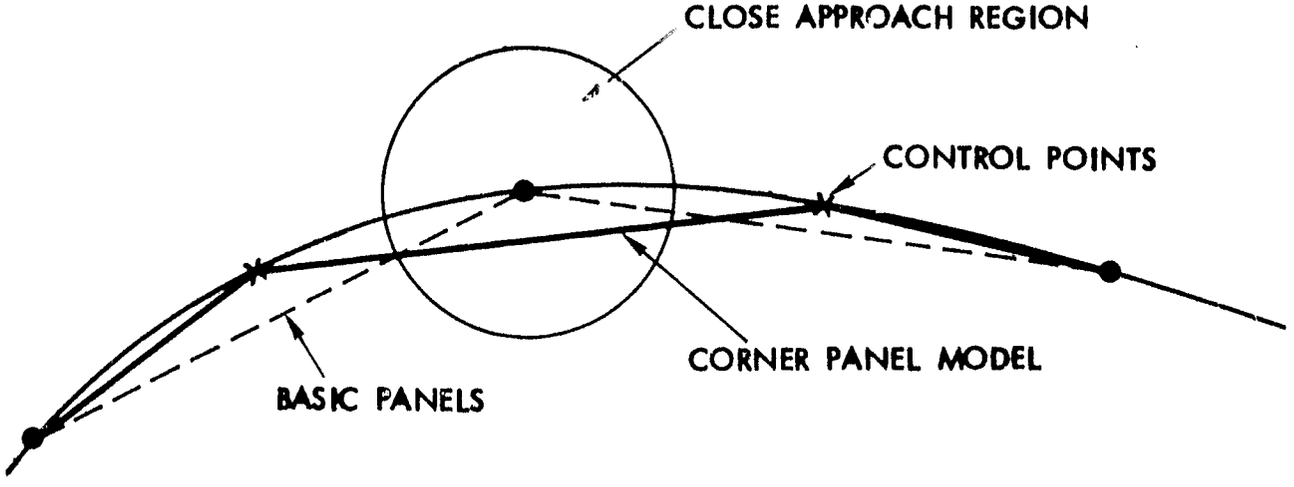

(b) CONTROL POINTS ON SURFACE

Figure 5. Corner Panel Models.

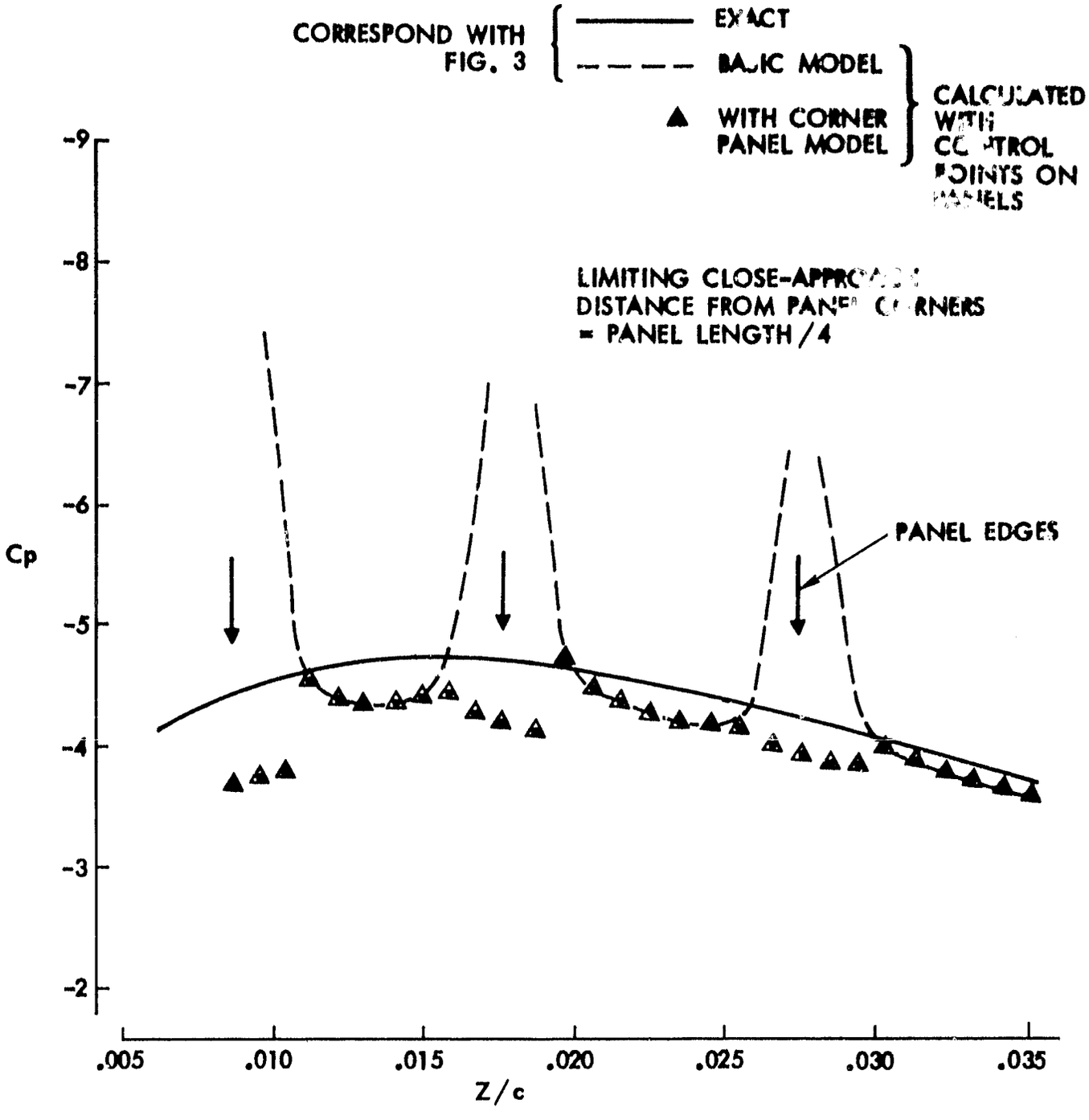

Figure 6. Detailed Pressure Calculations Near Leaing Edge of a Joukowski Airoil. Symmetrical Singularities Method with Corner Panel Model (2.3.4).

It will be observed in Figure 6 (and in Figure 4) that the control station values are not in close agreement with the exact solution. Accuracy was later restored by placing the control points on the airfoil surface rather than on the panel centers, Figure 7. The corresponding corner panel model, Figure 5(b) was then re-evaluated, but, the detailed pressure distribution still had kinks at the changeover stations. Clearly, to remove these kinks would require the changeover point from one panel scheme to the other to be moved further away from the velocity calculation point, i.e., the limiting close-approach distance must be increased. This consideration lead to the more general technique described below and based on a number of subpanels.

2.3.5 Subpanel Technique

In this technique, each panel which contains the velocity calculation point within a certain NEAR-FIELD RADIUS from its control point is divided into a number of subpanels, Figure 8. Subpanel corner points are obtained by interpolation on the airfoil surface and singularity values by interpolation through the panel values. When accumulating panel velocity contributions at a given point, immediately a panel detects the point is within its near-field radius a perpendicular is dropped from the point to the surface. The projected point becomes the center of a subpanel, the size of which is related to the height of the velocity point above the surface, Figure 8. Other subpanels are constructed with size increasing with distance from the point until all the near-field panels are modified. (Note: this way of distributing the subpanels was later changed for the three-dimensional case, see 4.2.)

The region covered by the near-field radius is necessarily larger than the close-approach region, Figure 9, because the velocity distribution induced by the temporary subpanel set does not match that of the basic panel until some distance away

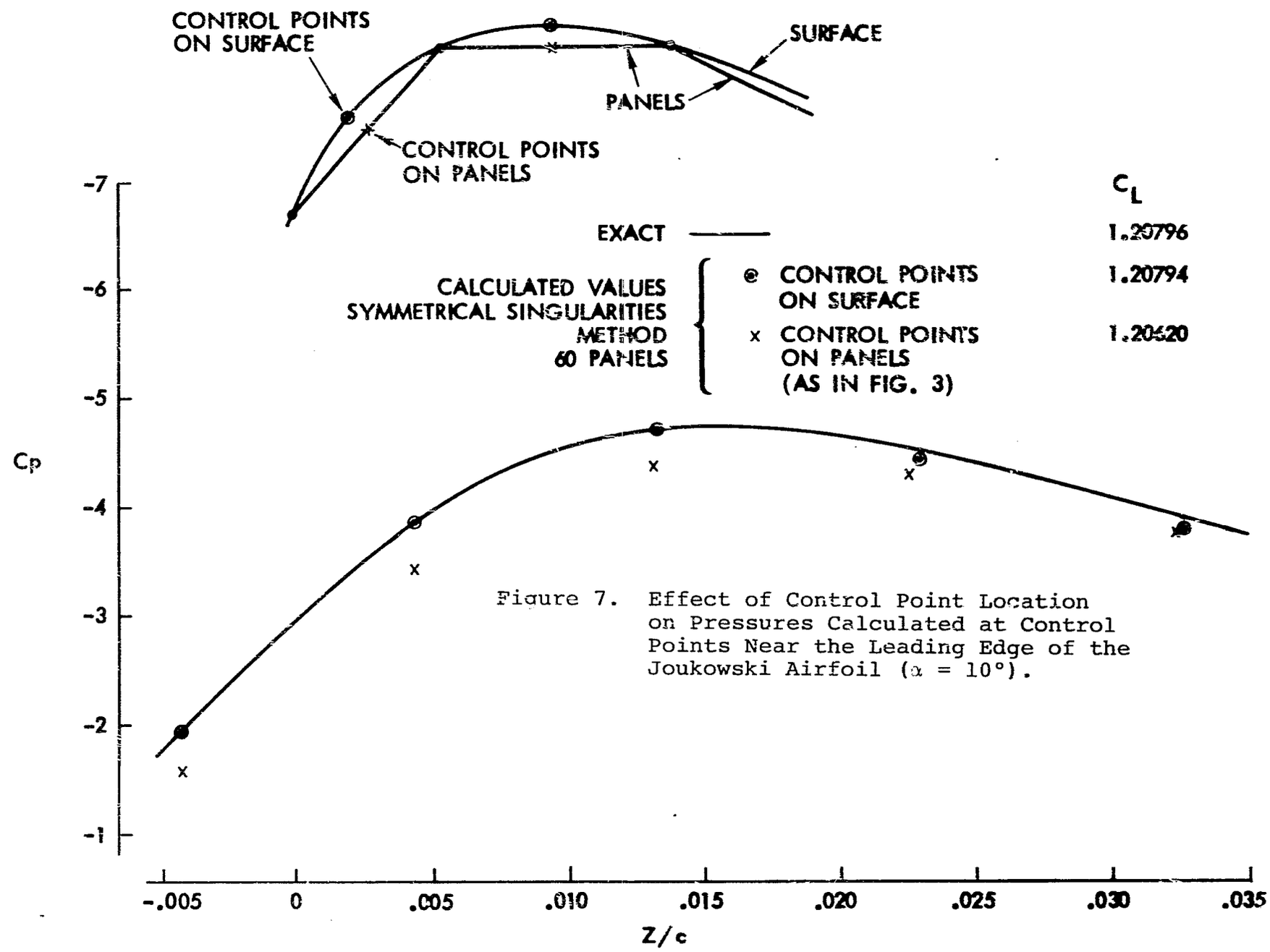

Figure 7. Effect of Control Point Location on Pressures Calculated at Control Points Near the Leading Edge of the Joukowski Airfoil ($\alpha = 10°$).

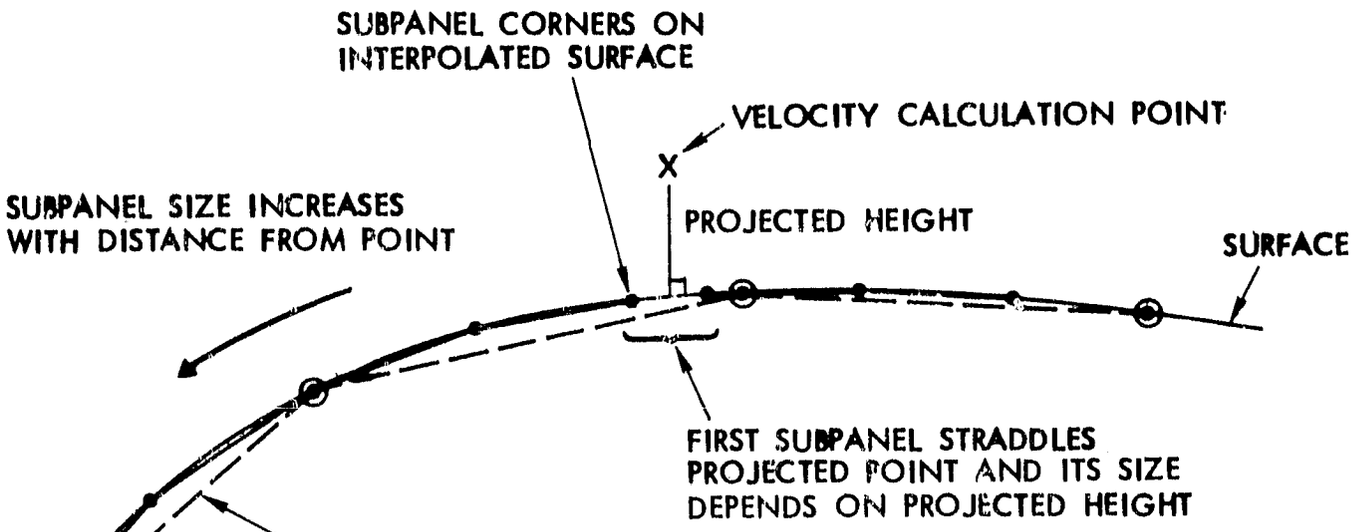

Figure 8. Subpanel Scheme for Two-Dimensional Flow (2.3.5).

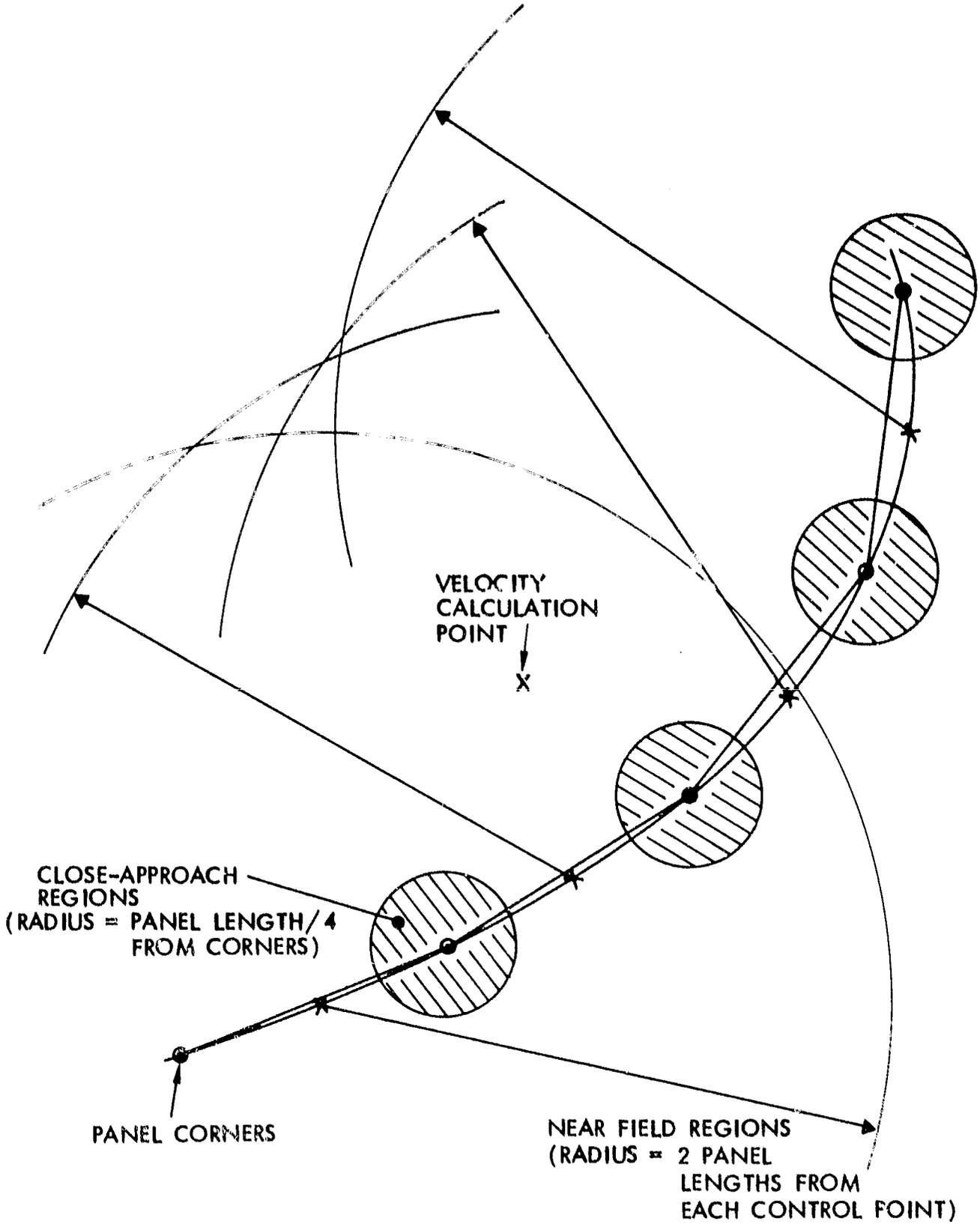

Figure 9. Close-Approach Regions and Near-Field Regions for the Symmetrical Singularities Method.

(e.g., see Figure 5 in Ref. 5). Thus, when one panel is represented by subpanels, several neighboring panels must be similarly treated, otherwise significant "jumps" occur in the calculated velocity distribution as we pass over the near-field boundary of each panel (e.g., as observed in Figures 4 and 6). These jumps can be made as small as we please by increasing the near-field radius.

Using the near-field radius as the criterion for generating a subpanel set rather than the close-approach distance can result in unnecessary use of subpanels. For example, the calculation point in Figure 9 is inside the near-field radius of several panels yet is outside the close-approach regions. Clearly, the subpanel model is superfluous in such a situation, but individual panels would not be "certain" of that fact unless the geometric relationship between the point and all the panels was tested at the beginning. Since such a test would duplicate the evaluation of some of the geometric quantities in the panel influence coefficients calculation, it was decided to adopt the panel-by-panel, near-field radius test and accept the occasional "overkill" situation illustrated in Figure 9.

For convenience, the near-field radius is expressed as a factor applied to each panel length. In this way the factor has one input value for the entire calculation, yet the local near-field radius varies according to the size of each panel.

While the subpanel technique is an extension of the corner panel technique, it is also a higher-order form of the subvortex technique described in Reference 5. With this technique, velocity calculation at any arbitrary point on the surface or in the flow field never experiences a panel corner problem since the generated subpanels are always in the ideal relationship with the calculation point. The number of subpanels required for the near-field calculations appears to be very small. For example, in the case of a point on the surface, the <u>total</u> number of

influence coefficients evaluated (panels plus subpanels) is usually of the order of five more than the number of basic panels representing the airfoil. The subpanel pilot code was initially based on the symmetrical singularities model (Ref. 6); i.e., panels of linear vorticity and constant source. This was later converted to a doublet model which is described in the next section.

3.0 DOUBLET SUBPANEL TECHNIQUE

3.1 Singularity Model

Before evaluating the subpanel technique in more detail in the two-dimensional flow case, the singularity model was changed to a surface doublet distribution to facilitate extension to the three-dimensional case. For the purpose of evaluating doublet values at subpanel centers, the doublet distribution is described by a biquadratic interpolation curve (Appendix A) passing through known values at panel control points, Figure 10(a). Thus, for each subpanel, the central doublet value is obtained in terms of four local panel doublet values, μ_i:

$$\mu = \sum_{i=1}^{4} \mu_i G_i \tag{1}$$

The biquadratic multipliers, G_i, are evaluated at the subpanel center and are functions only of surface distances (Appendix A).

The linear vorticity influence coefficient routine for panels or subpanels is retained from the earlier code (see Appendix C), but the vorticity is now evaluated as the gradient of the doublet distribution with respect to surface distance. Clearly, the vorticity value could be obtained by differentiating the biquadratic expression directly (Appendix A), but such treatment of high-order curves is not always reliable. An alternative approach adopted here and based on a local quadratic curve passing through three subpanel doublet values, Figure 10 (b), makes use of the fact that the panel doublet values have been augmented by the biquadratic interpolation for subpanel values; that is, the vorticity value at the middle subpanel is

$$\gamma_M = -\partial\mu/\partial s = (\mu_A S_2/S_1 - \mu_C S_1/S_2)/(S_1 + S_2)$$

$$+ \mu_M(S_1 - S_2)/S_1/S_2 \tag{2}$$

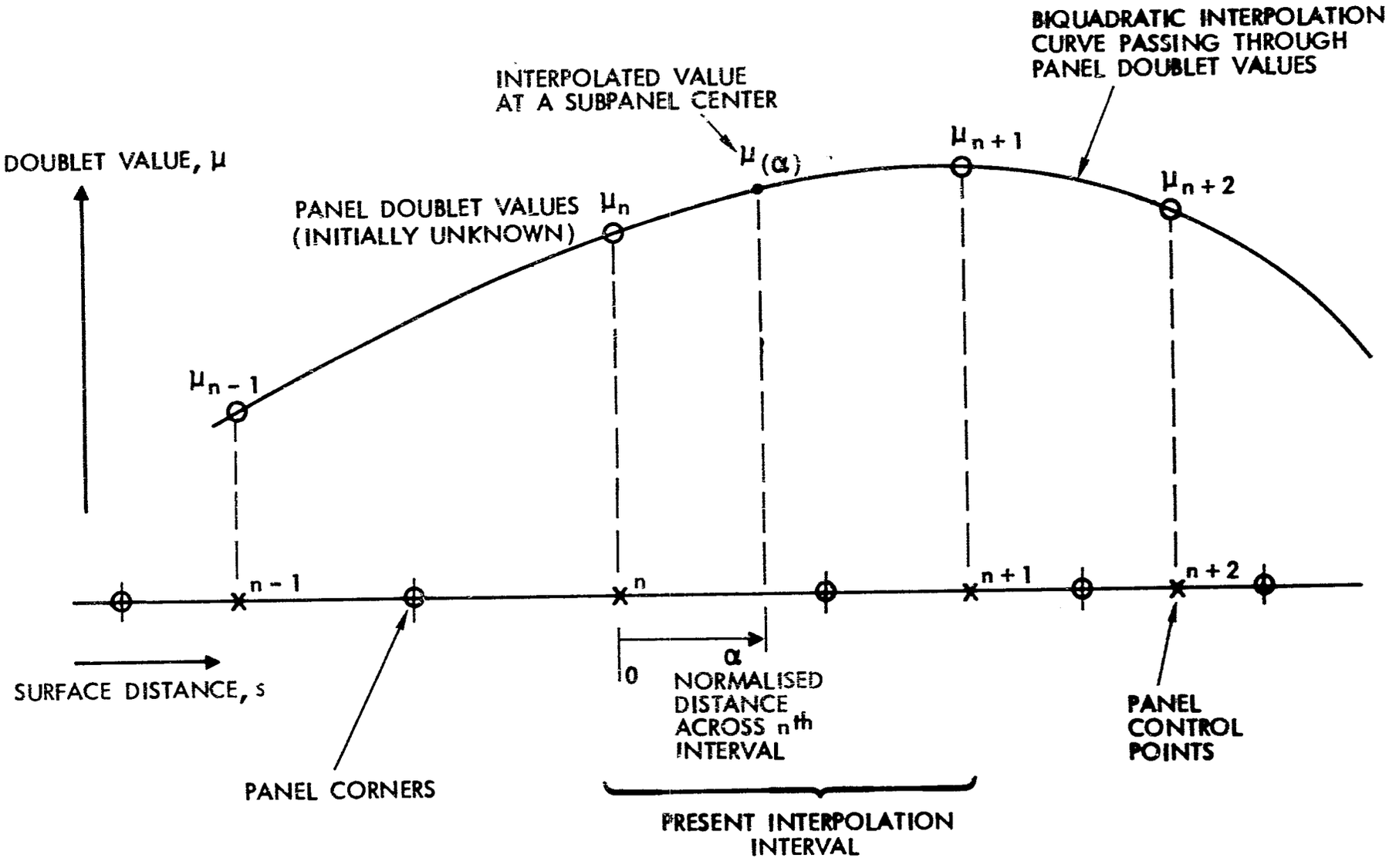

(a) INTERPOLATION THROUGH PANEL DOUBLET VALUES TO OBTAIN SUBPANEL VALUES

Figure 10. Treatment of the Surface Doublet Distribution.

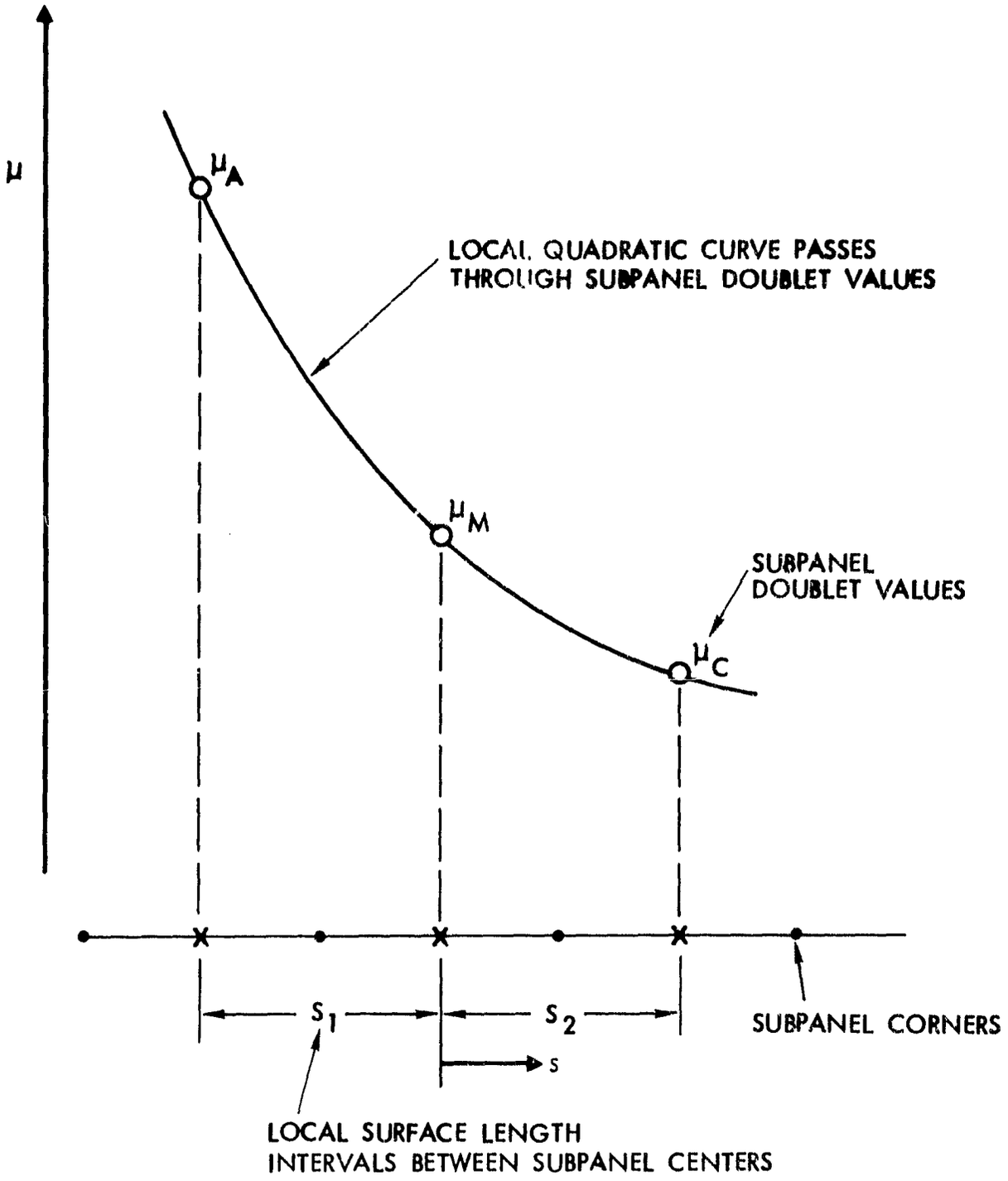

(b) LOCAL QUADRATIC REPRESENTATION FOR EVALUATING VORTICITY

Figure 10. Concluded.

and the vorticity gradient is

$$\gamma'_M = -\partial^2\mu/\partial s^2 = 2\left\{\mu_M/S_1S_2 - (\mu_A/S_1 + \mu_C/S_2)/(S_1 + S_2)\right\} \quad (3)$$

Since each subpanel doublet value (viz., μ_A, μ_M, μ_C) is known in terms of a set of four local panel values, Eqn. (1), then the linear vorticity influence coefficients (Appendix C) for subpanels can be immediately expressed in terms of panel doublet values.

3.2 Boundary Condition

With a smooth doublet distribution on (and with doublet axes normal to) a closed surface there are two equivalent ways of applying the exterior tangential flow boundary condition: (i) the exterior Neumann boundary condition in which the normal velocity component is set to zero, and (ii) the interior Dirichlet boundary condition in which the interior velocity potential is set to a constant (e.g., 0).

The Neumann boundary condition when applied to a surface doublet or vorticity distribution is weak in the region approaching the airfoil trailing edge. This often leads to local deviations in the solution. The problem does not occur for the alternative interior boundary condition, and so from this standpoint, the latter boundary condition is to be preferred. In addition, since the Dirichlet form works with a scalar quantity (velocity potential) rather than a velocity vector, computing effort and storage requirements are minimized. However, with this approach, the surface velocities are obtained from the gradient of the velocity potential and this might introduce inaccuracies in the general three-dimensional case. At this time, therefore, and because the VIP3D program is set up for it, the Neumann boundary condition is used here. The possibility of changing to the interior boundary condition will be kept in mind for

a future modification subject to the availability of a reliable way of obtaining the surface velocities in the general case.

Use of the Neumann boundary condition requires that the ill-conditioning be alleviated in the equations leading to the solution of the panel doublet values. The cause of the problem can be narrowed down to a certain part of the doublet distribution; by considering a typical doublet distribution on the surface of a lifting airfoil we can identify symmetrical and antisymmetrical parts with respect to surface distance from the trailing edge, Figure 11. The symmetrical part can be associated with the airfoil thickness or displacement effect, while the antisymmetrical part is closely related to the circulation. Because the normal velocity component is continuous, passing through the doublet sheet, it can be shown (see Apendix D) that the Neumann boundary condition equations for control points near the trailing edge are ill-conditioned only for the solution of the symmetrical part. It will be recalled that when the surface pressures from the doublet solution become inaccurate near the trailing edge, it is usually observed that the pressure difference between upper and lower surfaces (i.e., the circulation or antisymmetric effect) is correct.

In the symmetrical singularities method (Ref. 6), the antisymmetrical doublet distribution is represented by a symmetrical vorticity distribution (being the gradient of the doublet distribution) while the symmetrical doublet distribution influence is represented by a symmetrical source distribution. Both the source and vorticity components are solved using the same number of boundary condition equations as there are panels by applying the symmetry constraints. In an earlier code (Ref. 7), the symmetrical source distribution was actually applied at the beginning as a simple function of the rate of change of thickness. The applied source influence when combined with the onset flow was found to be adequate in stabilizing the doublet solution. In the present work, the presence of the source singularity is

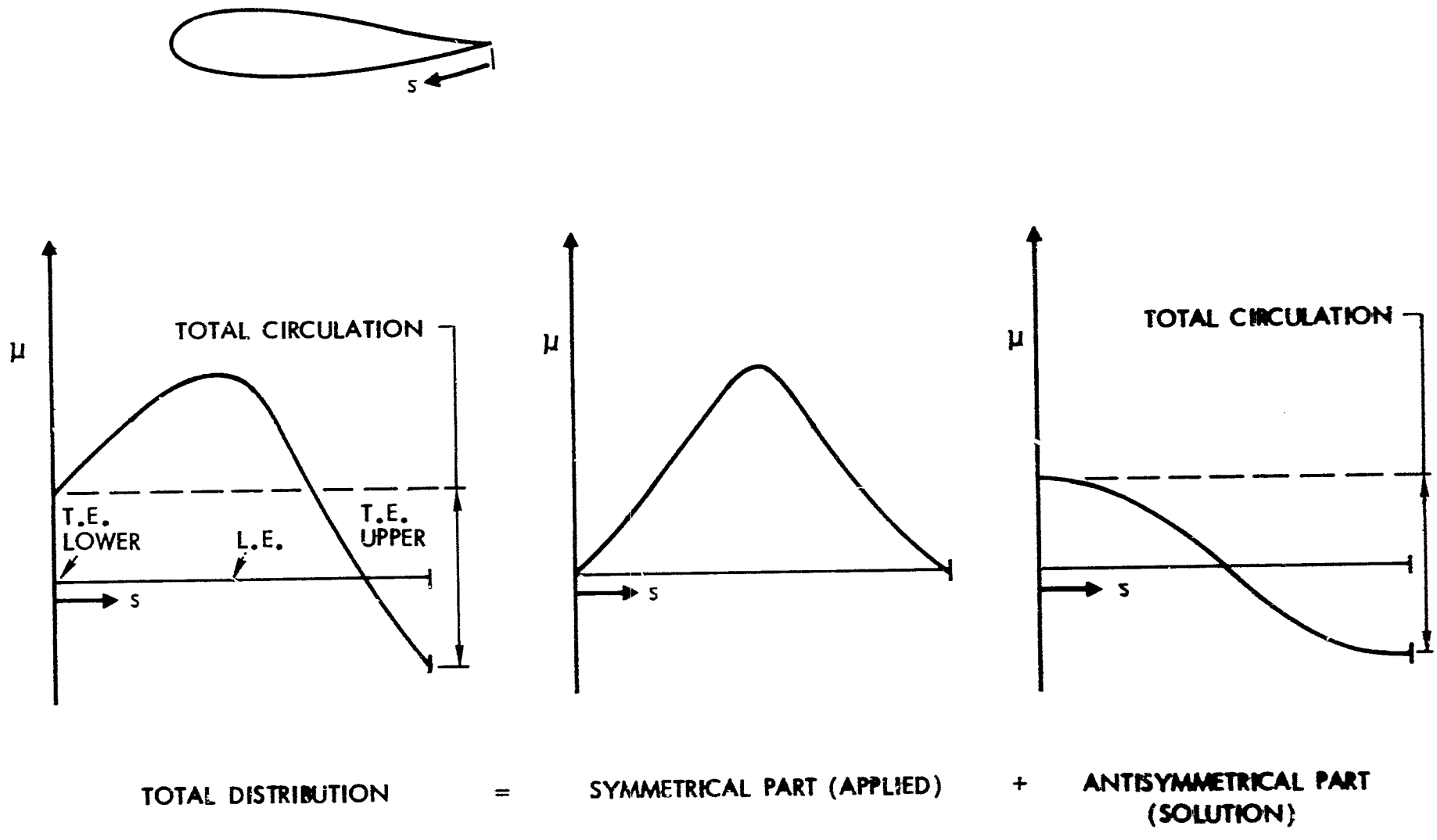

Figure 11. Symmetrical and Antisymmetrical Parts of the Surface Doublet Distribution.

undesirable; it is more convenient to work with the total doublet distribution for the purpose of shedding circulation from free edges, such as flap edges, wing tip, etc. To maintain a stable solution with the Neumann boundary condition, therefore, an approximate symmetrical doublet distribution is applied (by the program) at the beginning based on the flow about a symmetrical Karman-Trefftz airfoil at zero lift. The Karman Trefftz section is constructed having the same trailing-edge angle and cross-section area as the actual airfoil. In this way the solution part of the doublet distribution is concerned primarily with the (antisymmetric) circulation component, but has small adjustments because the applied symmetrical component is not exact for that particular airfoil. (The solution part could be reduced even further by simply setting the Karman-Trefftz section at the appropriate angle of attack--rather than zero--when evaluating the applied doublet distribution.)

3.3 Test Cases

As a searching test of the subpanel technique, a vortex/surface interaction calculation was chosen in which a prescribed vortex was positioned close to a Joukowski airfoil. The vortex location was $x = .15c$, $z = -.125c$, and its strength was $.2\pi$. The vortex flow was combined with an $\alpha = 10^0$ onset flow. Thirty panels were used in a cosine spacing, and the near-field radius factor was set to 3.

The ability of the subpaneling scheme to provide smooth velocity calculations anywhere is very apparent in Figure 12(a), which shows calculated streamlines. The streamline calculation method is one developed during the course of the work (Appendix E). Three starting points were selected as shown in Figure 12 (b). The forward point gives a streamline that on the upstream part passes very close to the leading edge, and in the downstream part climbs over the vortex before dropping to the airfoil surface which it follows very closely back to the trailing

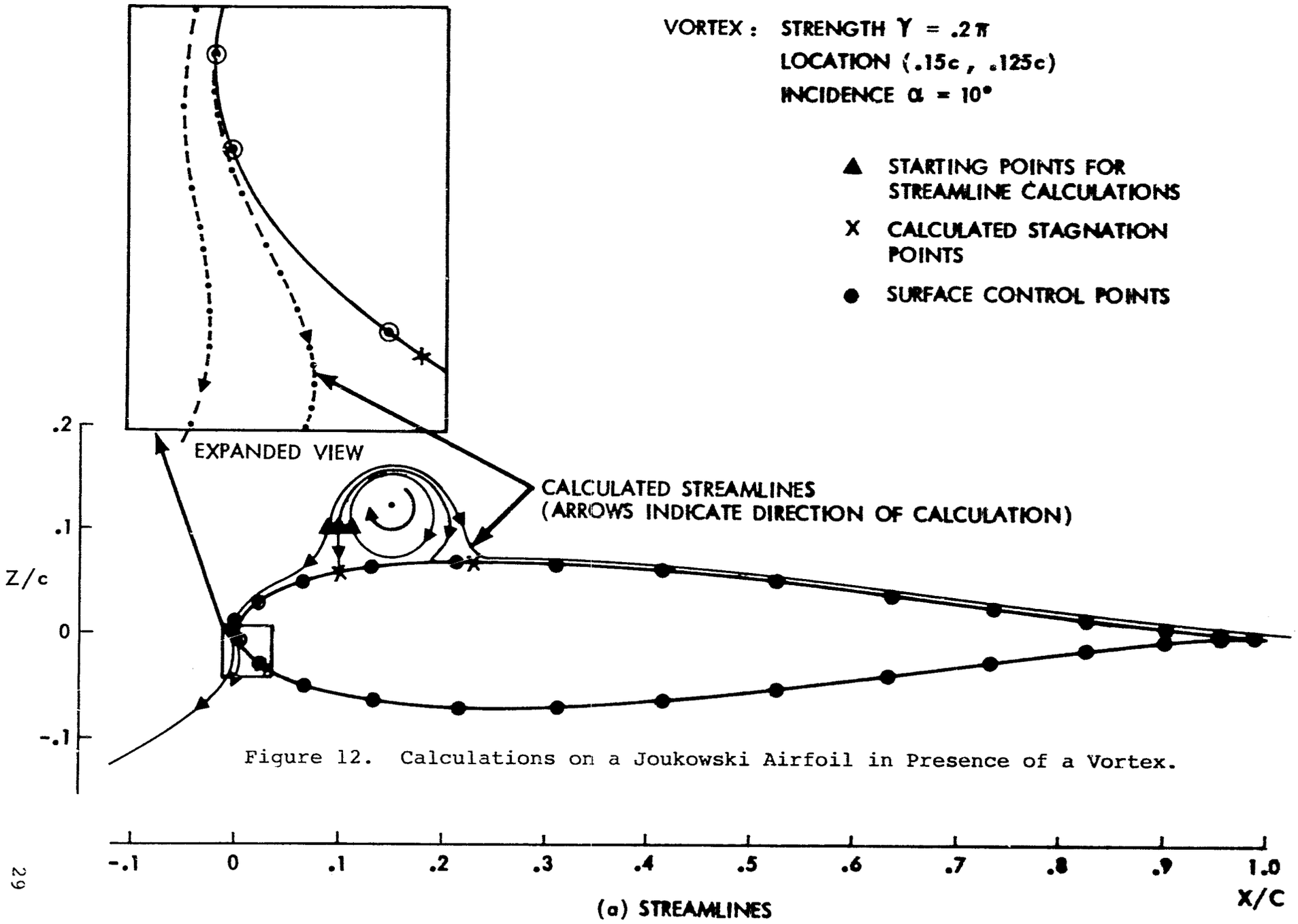

Figure 12. Calculations on a Joukowski Airfoil in Presence of a Vortex.

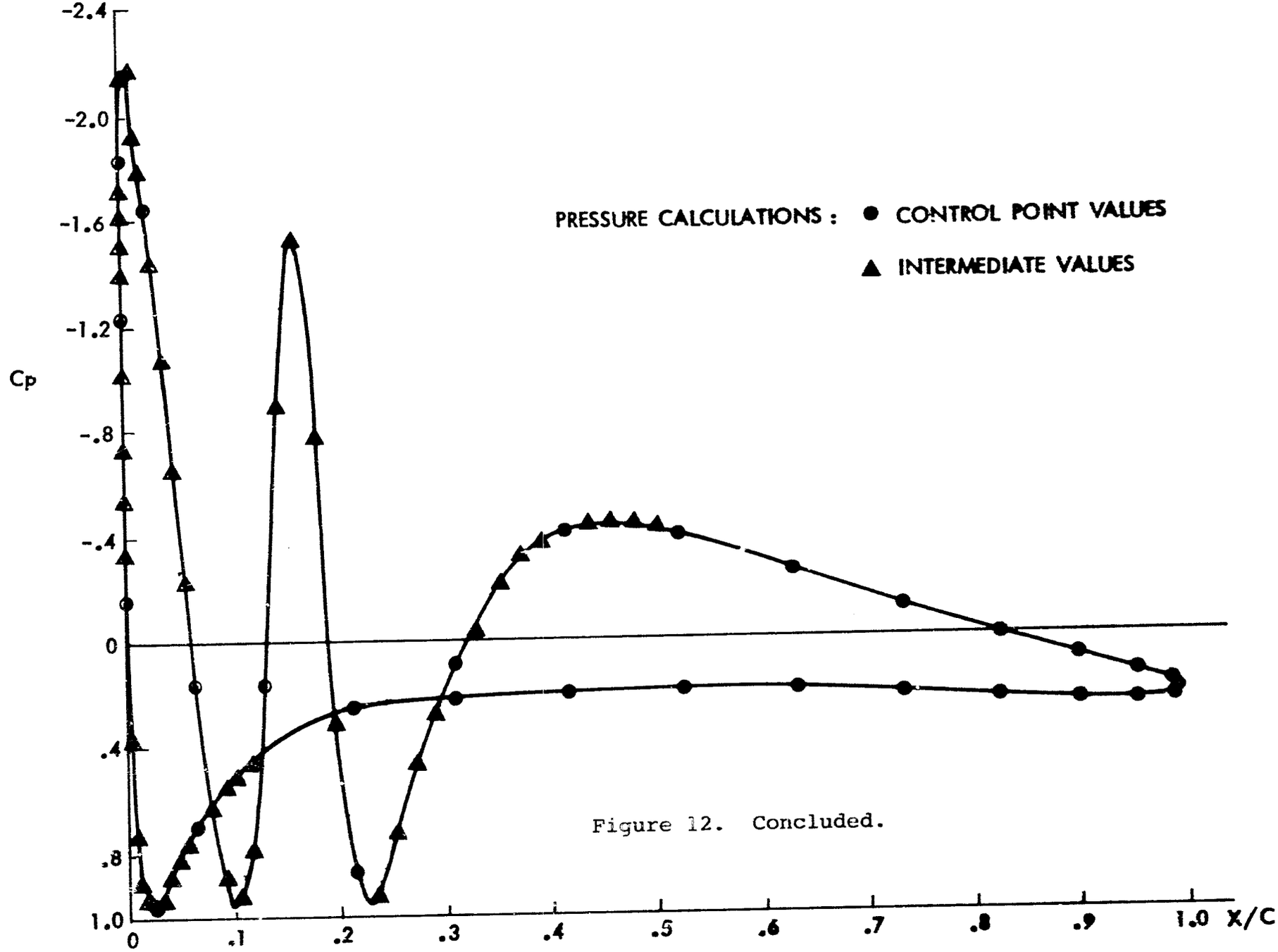

Figure 12. Concluded.

(b) SURFACE PRESSURE DISTRIBUTION

edge. Details of this streamline (and the second streamline) in the leading-edge region are given in the inset in Figure 12 (a). The first streamline passes very close to the surface, well within the spacing of the control points. The line is very smooth, even though the velocity calculations have been performed at a number of "arbitrary" positions. The second streamline is clearly very close to the stagnation streamline and essentially follows the surface with one or two minor oscillations. As the calculation proceeds from the starting point, this second streamline hits the airfoil very steeply, and yet quickly takes up the surface direction, a very searching test for both the streamline calculation procedure and the velocity calculation routine. On the downstream side, this second streamline follows the surface back to the trailing edge.

The third streamline forms a closed loop round the vortex and does several turns (total streamline length specified is 2.5 chords) before accumulating errors eventually allow it to escape downstream along the airfoil surface.

The surface pressure distribution corresponding to this calculation is shown in Figure 12(b). Intermediate velocity calculations are indicated by triangles to distinguish them from the basic control-point values. These additional calculations, made possible by the subpaneling technique, clearly define the details of the three suction peaks and three stagnation points. The control point values in some of these areas would have been inadequate--particularly in defining the suction peak located beneath the vortex. Clearly, the interpolation technique (2.3.1) would have been incapable of constructing these details given only the panel control point values. An exact solution for this type of problem has been provided by Dr. V.J. Rossow at NASA Ames Research Center (Ref. 8). The solution is obtained by a transformation technique and gave the results for a CLARK-Y section.

Figure 13(a) compares the exact and calculated streamlines for a vortex and sink. The sink, which is coincident with the vortex, provides the necessary stabilizing force to keep the vortex in equilibrium in the exact analysis. The sink influence was included in the pilot code for this calculation. The streamline calculations (using the procedure described in Appendix E) show very close agreement with the exact lines. Figure 13(b) shows the close agreement between the calculated and exact pressure distributions for this case. The calculated pressures are at arbitrary stations (i.e., not necessarily at control points) and closely represent the multiple stagnation point and peak suction features.

These calculations clearly demonstrate the effectiveness of the subpanel technique in a problem situation that is pertinent to the multi-element high-lift configuration analysis; viz., vortex/surface interaction. The main features of the technique are summarized below.

(i) Subpanels offer a closer representation of curved surfaces and smooth singularity distributions than is possible with practical panel densities.

(ii) Subpanels give the effect of higher panel density without increasing the number of unknowns.

(iii) Subpanels give a "higher-order effect", yet maintain simple influence coefficient expressions.

(iv) A panel's subpanel set is used only when a velocity calculation is performed within a small near-field radius from the panel's center (e.g., within three panel sizes away). This minimizes computing effort.

(v) Smooth velocity calculations are obtained with reasonable panel density, even in the case of the vortex/surface interference problem. Features of the interference pressure field are closely represented even

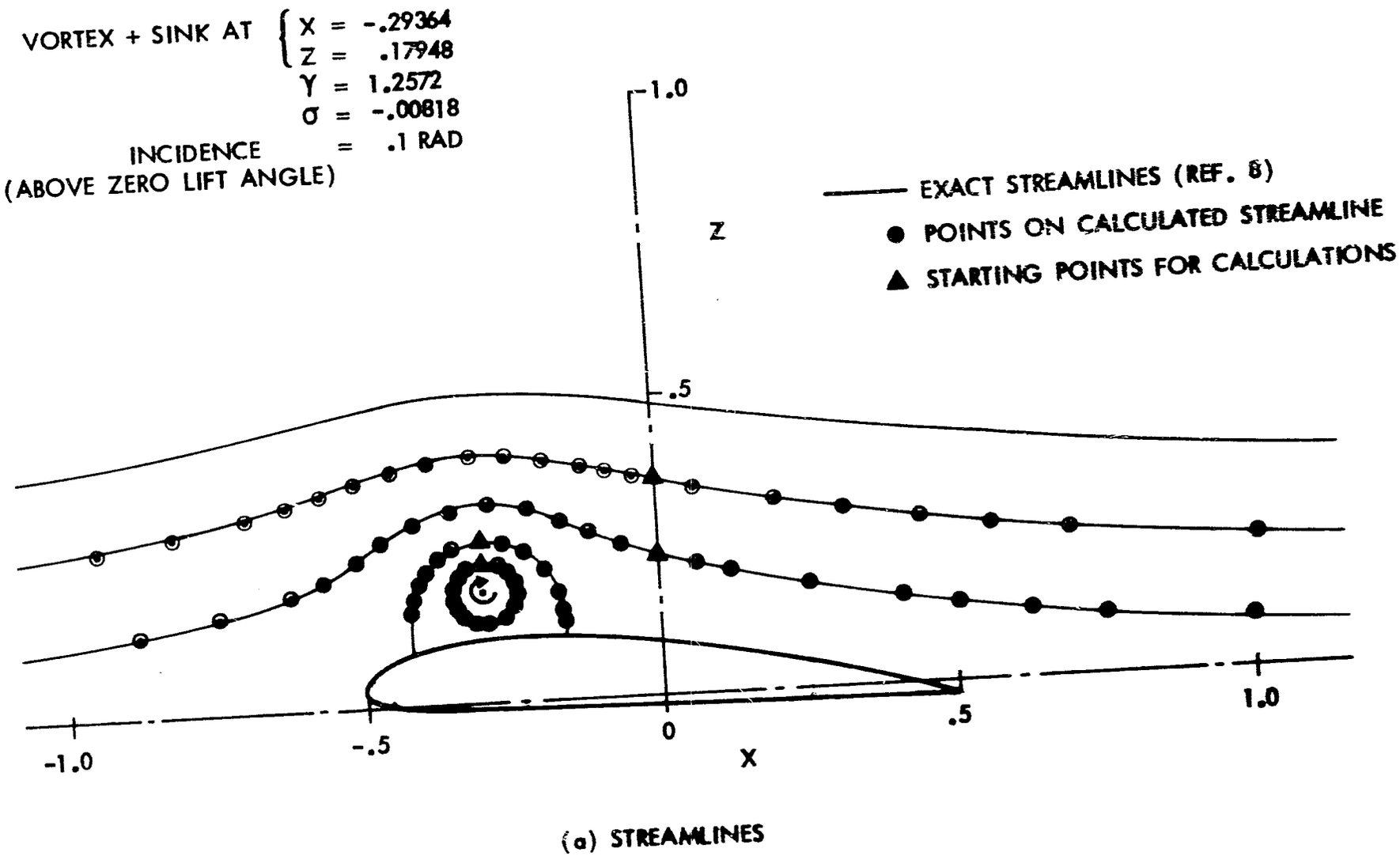

(a) STREAMLINES

Figure 13. Comparison of Calculated and Exact Solutions for a CLARK-Y Airfoil in Presence of a Vortex and Sink.

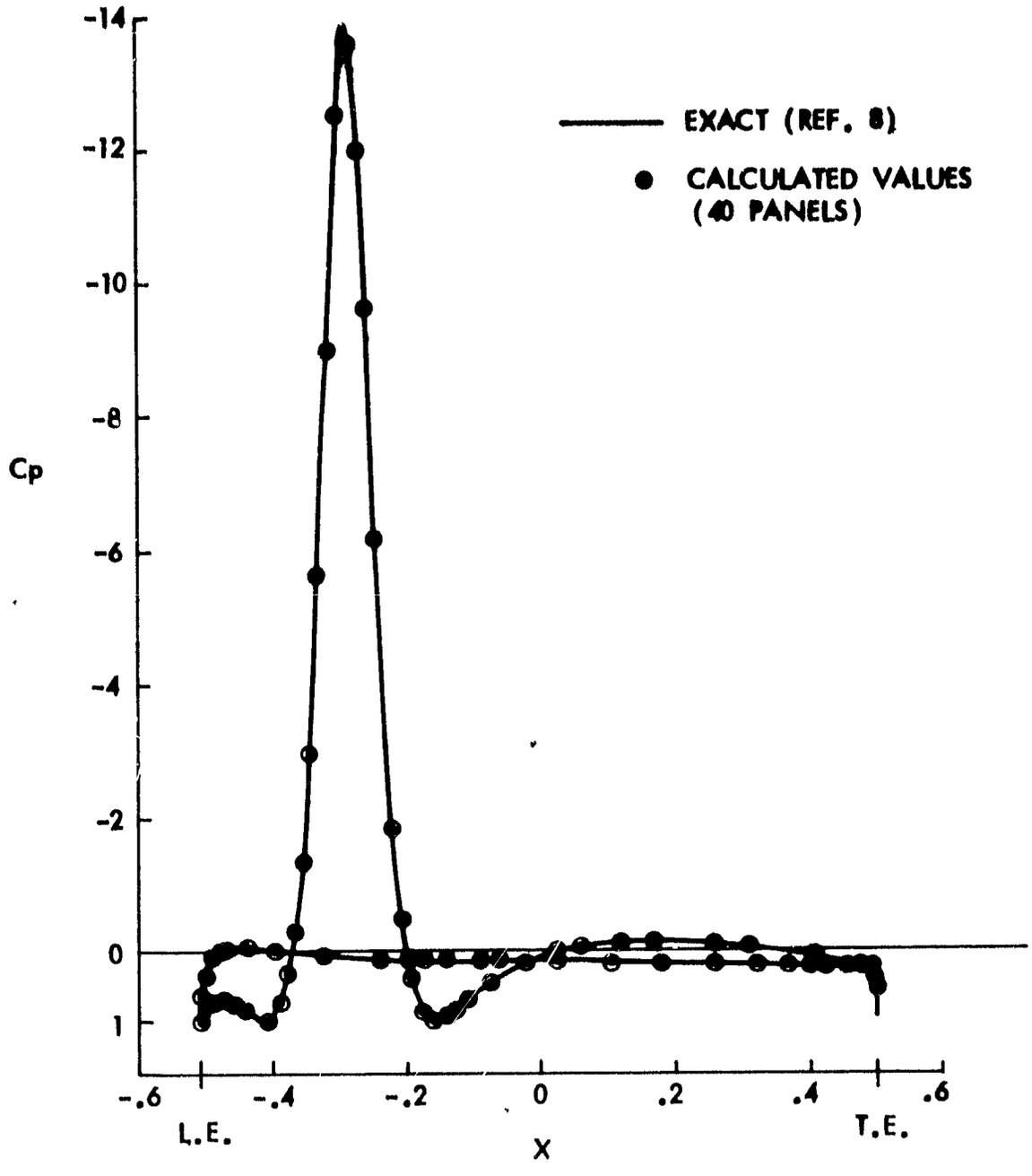

(b) SURFACE PRESSURE DISTRIBUTION

Figure 13. Concluded.

though the control points have not been specially located relative to the vortex position.

4.0 OVERVIEW OF THE VIP3D CODE MODIFICATIONS

4.1 General

The new work concerns only the WBOLAY part of the overlay structure in the VIP3D program (Ref. 1); boundary layer routines are unaffected. The potential flow routines--including the geometry package--have been modified and new routines added in accordance with the new objectives and the new singularity model. The flow chart for the initial calculations covering the geometry specification and potential flow solution is shown in Figure 14.

The program modifications and new capability are described in general terms in the following subsections. Details of the new work are given separately in later sections.

4.2 Geometric Model

The geometry routines in VIP3D have been extended to satisfy the new objectives concerning more general configurations and also to be compatible with the new close-approach singularity model. For these purposes--and also as a convenience to the user--a configuration is now broken down into more parts than before. In descending order of size, these parts include assemblies, components, patches and wakes, panels and, finally, subpanels. The nature and purpose of each of these parts is discussed in the following paragraphs, but not necessarily in the same order as in the list above.

The program may be applied to a configuration having a number of COMPONENTS; e.g., wing, slat, flap. A component is the smallest part of a configuration for which integrated load and moment information is given in the program output. Neglecting at this time the effects of structural attachments such as between a slat and wing, components are normally regarded as separate parts of the configuration, but this need not be so. As a user convenience, the surface of a configuration may be continuous from component to component, thus allowing integrated forces

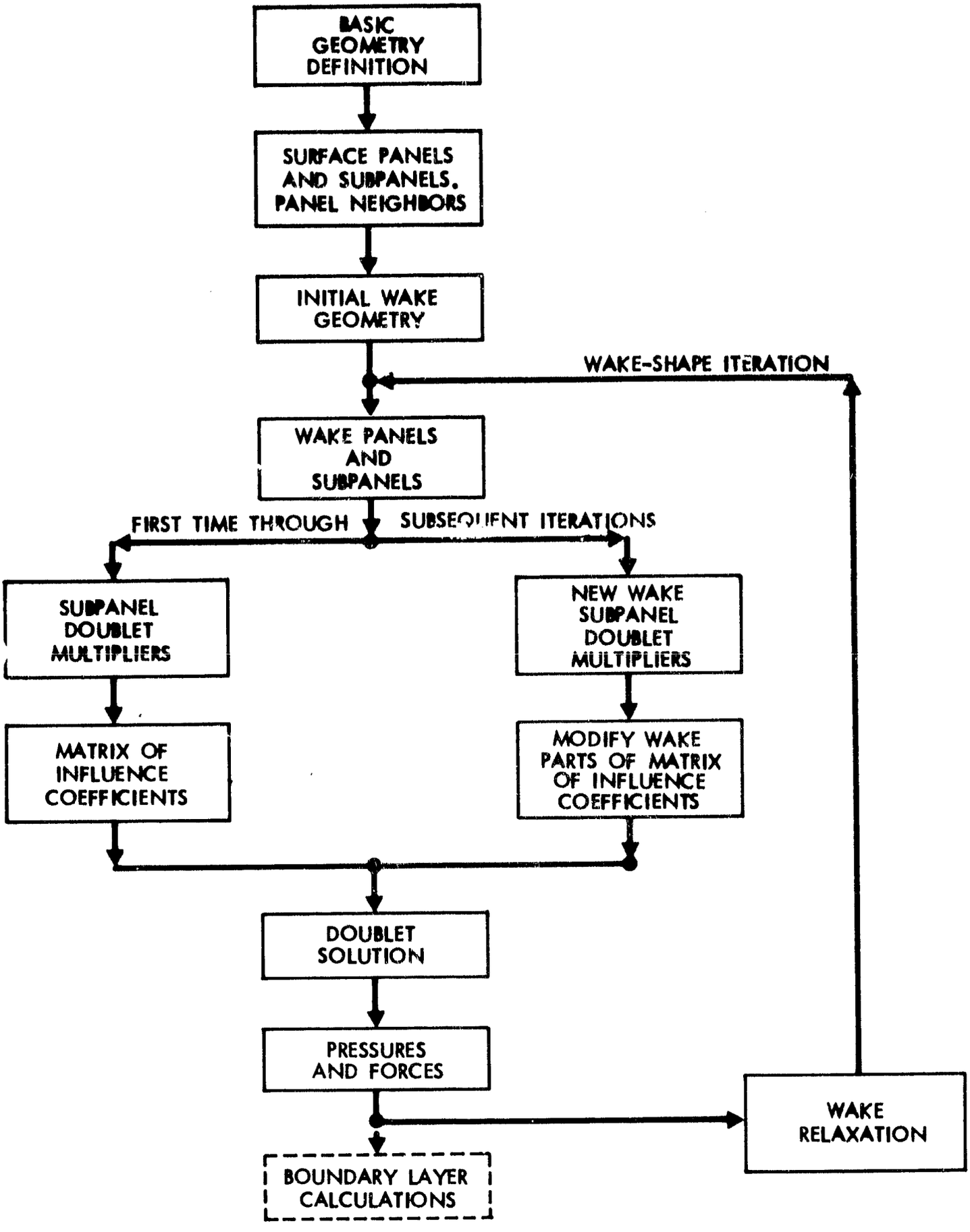

Figure 14. Flow Chart for the Potential Flow Calculations in the Modified Code.

and moments to be evaluated for just part of a wing or for a winglet, for example. Contiguous components are collected together into ASSEMBLIES within the program to allow the doublet distribution to be described continuously over the connected surfaces.

As in the earlier code, the basic unit representing the surface of each component is the PANEL. Panels have four straight sides, but one of the sides may be of zero length. In the new code each panel may be subdivided into SUBPANELS for the purpose of near-field calculations. The subpanel scheme differs from that described earlier in 2.3.5 by having a fixed subpanel set formed and stored for each panel at the beginning of the analysis. This change was made because a complete regeneration of subpanels for each near-field velocity calculation, while practical in the two-dimensional case--the computing effort being relatively small--could become unacceptable in the three-dimensional case where the calculations are more involved.

Figure 15 shows a section through the new subpanel scheme for comparison with the earlier model in Figure 8. The subpanels, which are generated automatically within the code, form a "square" array within each panel with an odd number per side. This arrangement ensures the central subpanel of a set falls in the middle of the panel; the center point and unit normal vector of this subpanel are then adopted by the panel for its control point geometry. This treatment places the panel's control point very close to the surface rather than on the panel; the advantage of this was observed earlier in Figure 7. The subpanel sides are straight but the corners lie on the interpolated surface represented by a two-way biquadratic scheme. Compared with the panel model, therefore, the subpanel set represents surface curvature more closely.

New routines installed in the code to interpolate and differentiate the surface doublet distribution require information concerning neighboring panels. Similar information is required when redistributing the boundary layer displacement source values

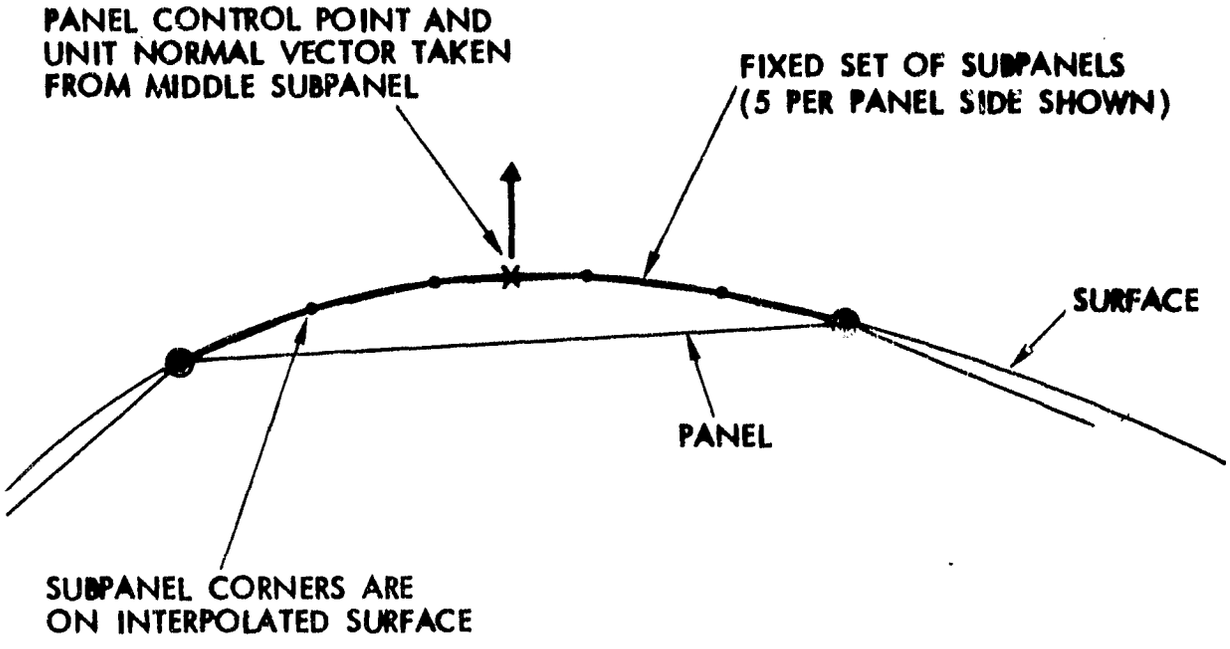

Figure 15. Section through Subpanel Scheme for Three-Dimensional Case.

at the panel centers, and may be anticipated for the future in connection with surface streamline calculations. The most efficient way to locate neighboring panels is to arrange the panels in a "rectangular" grid of rows and columns (i.e., equal number of panels in each column). Such an arrangement, however, lacks versatility when considering general configurations. A compromise has been reached in the new code by the use of PATCHES of panels, each patch having a rectangular array of panels. Awkwardly shaped components may be represented by several patches, whereas simple shapes, for example, the entire main surface of a swept tapered wing, may require just one patch. Figure 16 shows a typical breakdown of a high-lift configuration into components and patches. Parts A, B, C and D are typical patches on Component 2. The main surfaces of components 1 and 3 may be formed by single patches; additional patches may be used to cover the open ends (shaded).

The developed (i.e., "opened out") shape of a patch should be roughly four-sided to keep panel shapes and distributions reasonably regular. This does not exclude the presence of kinks in any or all of the patch sides, but kink angles should not be large (the upper limit has not been established, but for the time being 60^0 should be regarded as a large kink angle). One side or two opposite sides of a patch may be reduced to zero length provided the overall patch shape is reasonably regular. Figure 17 gives some basic guidelines for acceptable patch shapes.

The versatility of the patch scheme is ensured by allowing arbitrary relationships to occur between neighboring edge panels across patch joints, Figure 18. Automatic procedures (described later in 5.4.3) have been developed in the code to select "preferred" neighbors from edge panels on neighboring patches. Only edge panels on patches within the same assembly of components are considered as possible neighbor candidates. (This distinction is necessary in the automatic procedure to avoid the possibility

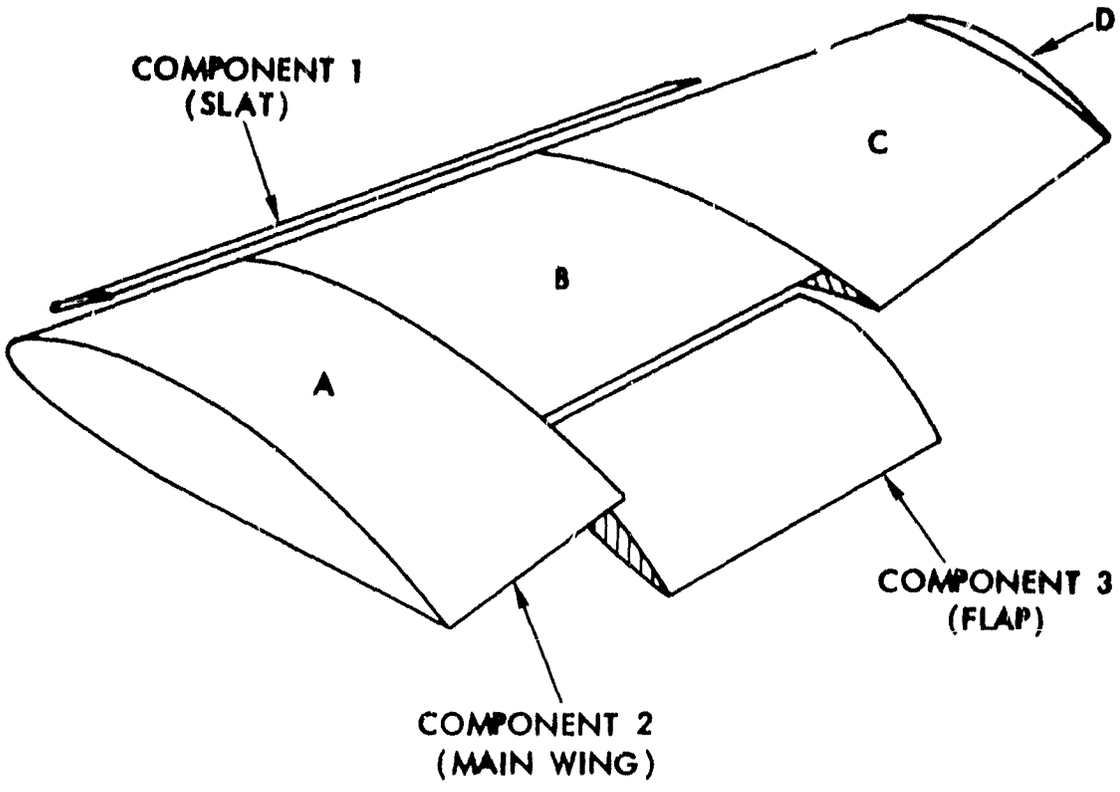

Figure 16. Examples of Components and Patches on a High-Lift Configuration.

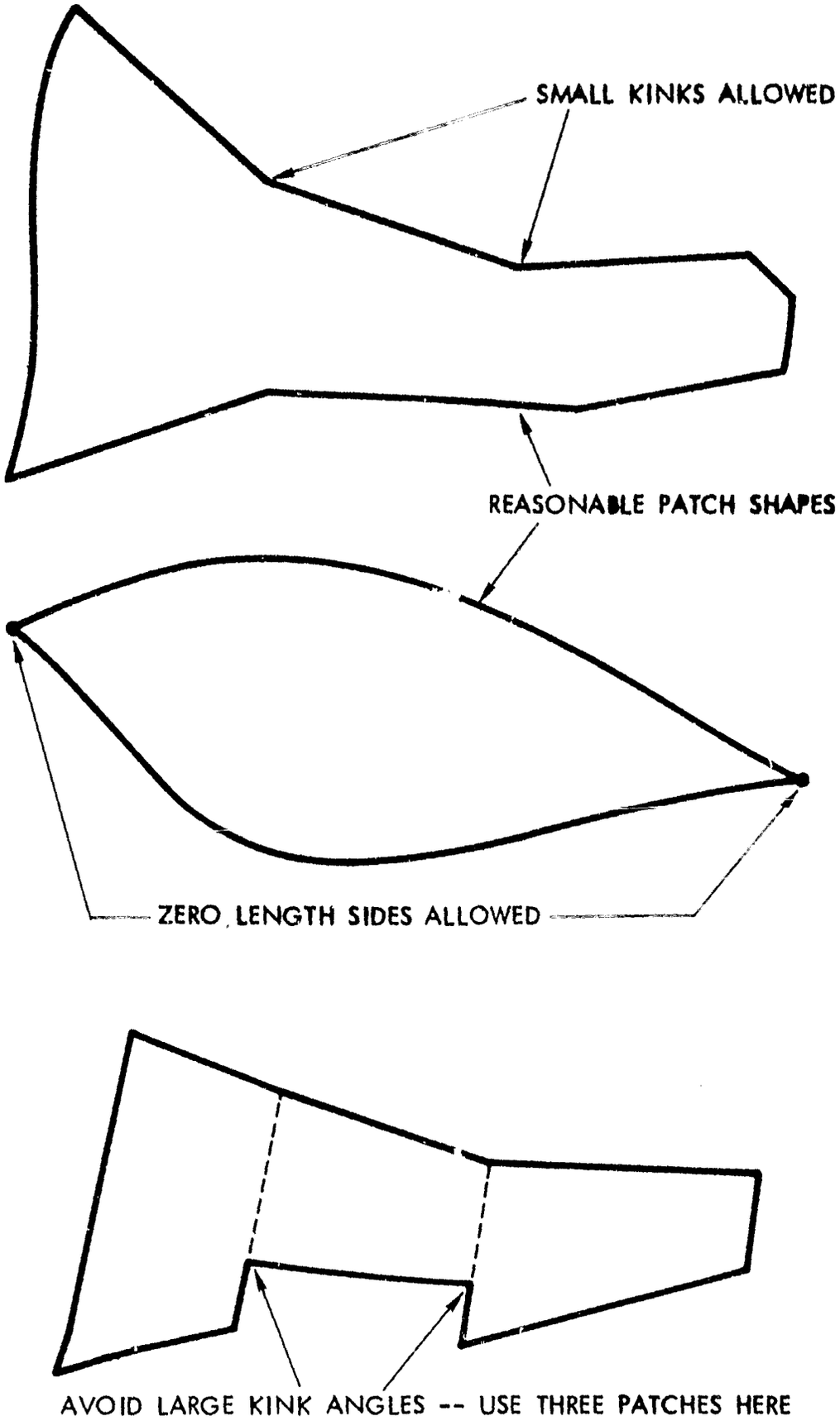

Figure 17. Preliminary Guidelines for Patch Shapes.

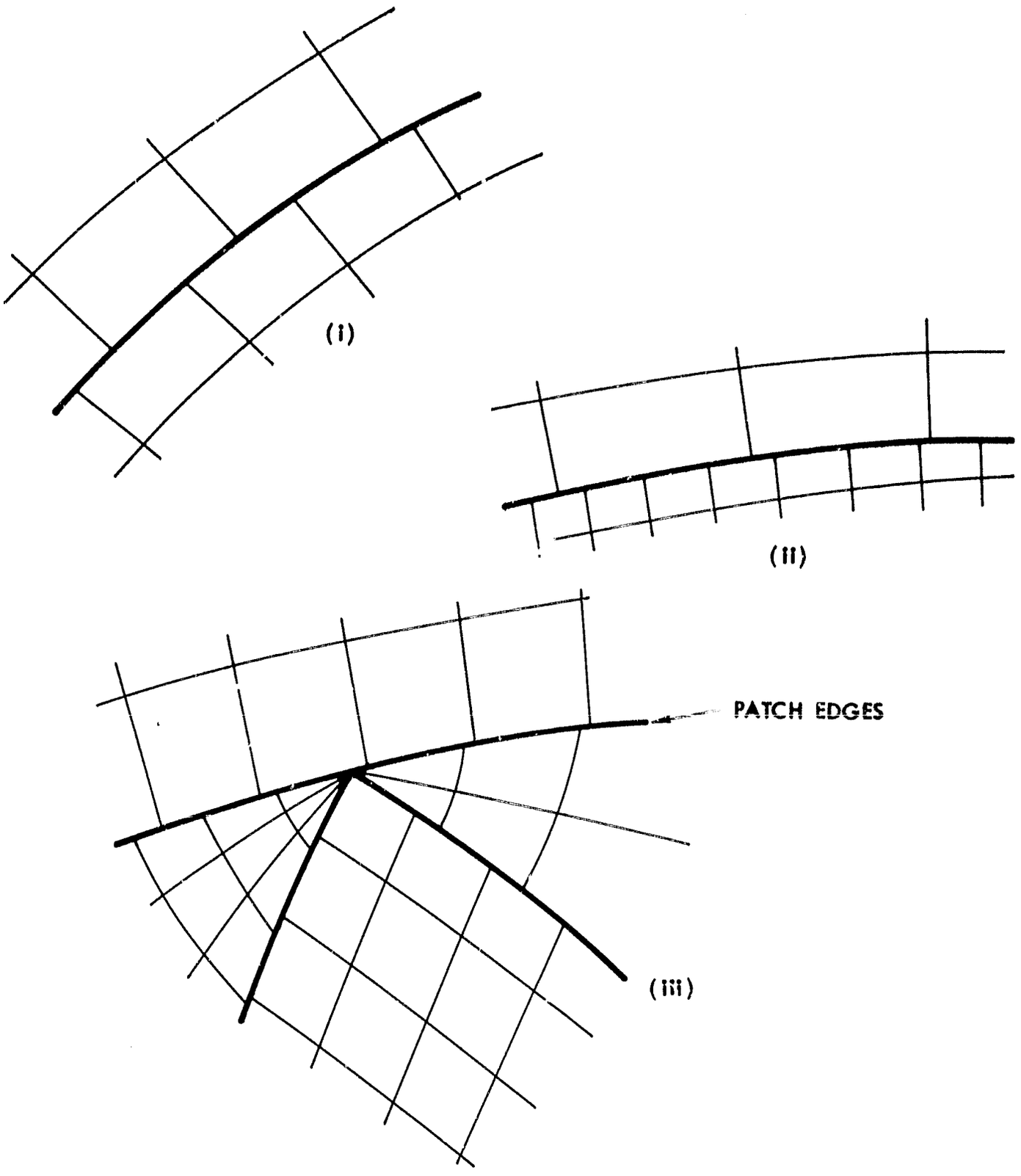

Figure 18. Three Examples of Arbitrary Neighbor Relationships Allowed Between Panels on Adjacent Patches.

of, say, a slat panel being selected as a preferred neighbor to a wing panel.)

A number of factors contribute to the usability of the patch scheme; in particular, options are provided for automatic paneling and also for automatic patch generation in special situations, e.g., wing tip. These options, which are described later in Section 5, are activated by setting a few integer flags in the input deck; they offer a very convenient mode of operation for a minimum of data preparation. These options are provided without sacrificing the basic simplicity of the input format.

The surface doublet distribution passes continuously onto WAKES representing the shed vorticity sheets from each component. Initial wake geometries are generated within the program following a small amount of user input. This information is needed to form an initial representation of the often complicated wake arrangements seen at part-span flap cutouts and edge separations.

Each wake is in two parts; a near- and far-wake. The near-wake starts at the wake shedding line on the component and extends downstream a short distance beyond the end of the configuration. The near-wake, which is similar to a patch, has panels and, for close-interference calculations, subpanels (Figure 19).

The far-wake model extends from the end of the near-wake back to downstream infinity and is represented by semi-infinite vortices (i.e., a piecewise constant doublet model). These vortices are attached to wake panel corners at the end of the near-wake. The far-wake requires no detailed representation since it is remote from the regions of interest.

The simple wake shape iteration in the earlier code allowed vertical movements only. The new singularity model has lifted that restriction so the new wake shape iteration, which involves the potential flow code only, now allows full roll-up in the near-wake.

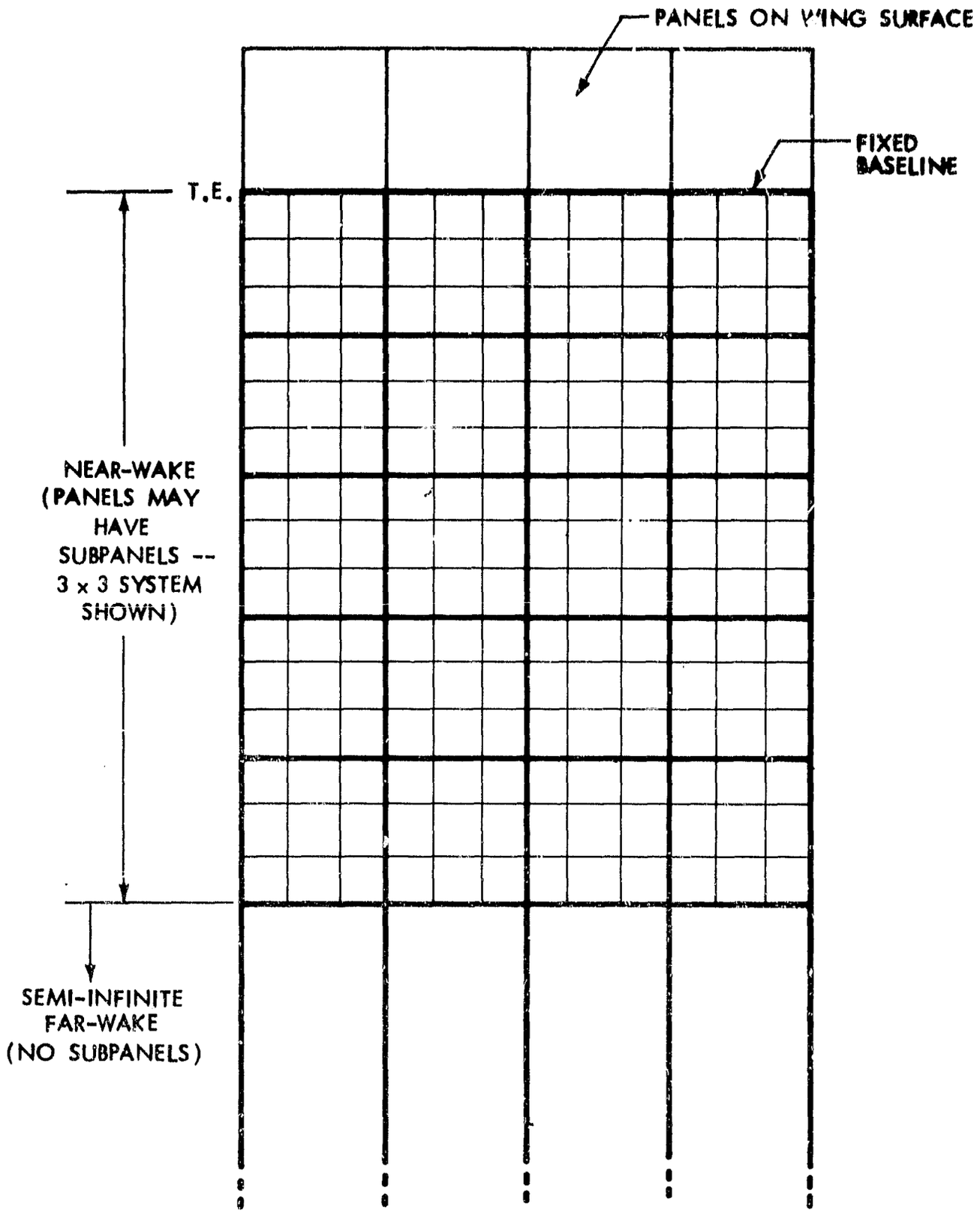

Figure 19. Initial Wake Arrangement.

4.3 Singularity Model

The piecewise constant source and vorticity model in the VIP3D program has been replaced by a continuous surface doublet distribution incorporating the three-dimensional forms of the subpanel close-approach technique. With the fixed subpanel sets of this latest technique (4.2) it is possible for a calculation point to approach the edge of a subpanel. The interpolation technique described in 2.3.1 is therefore coupled with the scheme using velocities calculated above local subpanel centers. Interpolation within the subpanel system is acceptable because the associated close-approach problem area is considerably smaller than that for the basic panel system.

Each subpanel is associated with a two-part doublet value located at its center point; the applied symmetrical part is evaluated at the beginning (3.2) according to the local chordwise geometry, while the solution part is initially described in terms of biquadratic interpolation multipliers applied to a local set of panel doublet values. These multipliers are evaluated from a two-way biquadratic interpolation scheme passing through panel doublet values (solution part) located at control points where the surface boundary condition is applied. The panel's applied doublet part is provided by the middle subpanel in its set.

The total doublet value (applied plus solution) occurring at the trailing edge is passed onto the wake panels. The resultant doublet value (i.e., between upper and lower surfaces at the trailing edge) is held constant in the streamwise direction for each column of wake panels.

4.4 Solution Procedure

The solution procedure in VIP3D remains essentially unchanged except that we now solve for panel doublet values. The matrix routine, therefore, calls a new influence coefficient

procedure (described later in 6.3). When the doublet solution is obtained, it is immediately combined with the applied doublet values prior to the pressure distribution calculations.

5.0 GEOMETRY ROUTINES

This section describes the way the modified geometry routines treat the various parts of the configuration. Details are included to emphasize the versatility of the new routines. The discussion is user-oriented to help in applying the new capability to general configurations.

The reference coordinate system used in the original code is maintained here but is now referred to as the general coordinate system, or G.C.S., to distinguish it from two other reference systems, namely, the component coordinate system, or C.C.S., and the section coordinate system, or S.C.S. These other systems are described in this section and are provided as a user convenience for specifying the geometry of a configuration.

5.1 Components

When defining the surface geometry of a configuration, each component may be described in its own local coordinate system for convenience. This also allows components to be relocated at a later date with minor changes to the input deck, for example, a slotted flap may be moved to a different setting.

The component specification starts with the appropriate transformation information which converts from the component coordinate system (referred to as C.C.S.) to the general coordinate system (referred to as G.C.S.). This information includes (i) the translation vector, (CTX, CTY, CTZ), which is simply the origin of the C.C.S. expressed in the G.C.S., (ii) the scaling factor, and (iii) the rotation angle, θ, about a hinge line vector, $\underline{h}$, Figure 20. Provision is made for the user to specify two points on a general hinge line vector (in the C.C.S.), otherwise the y-axis in the C.C.S. is used. Both the scaling and the rotation are applied in the C.C.S. prior to the translation. This component transformation is performed at the end of the geometry input routine, i.e., after the basic geometry of the complete configuration is assembled.

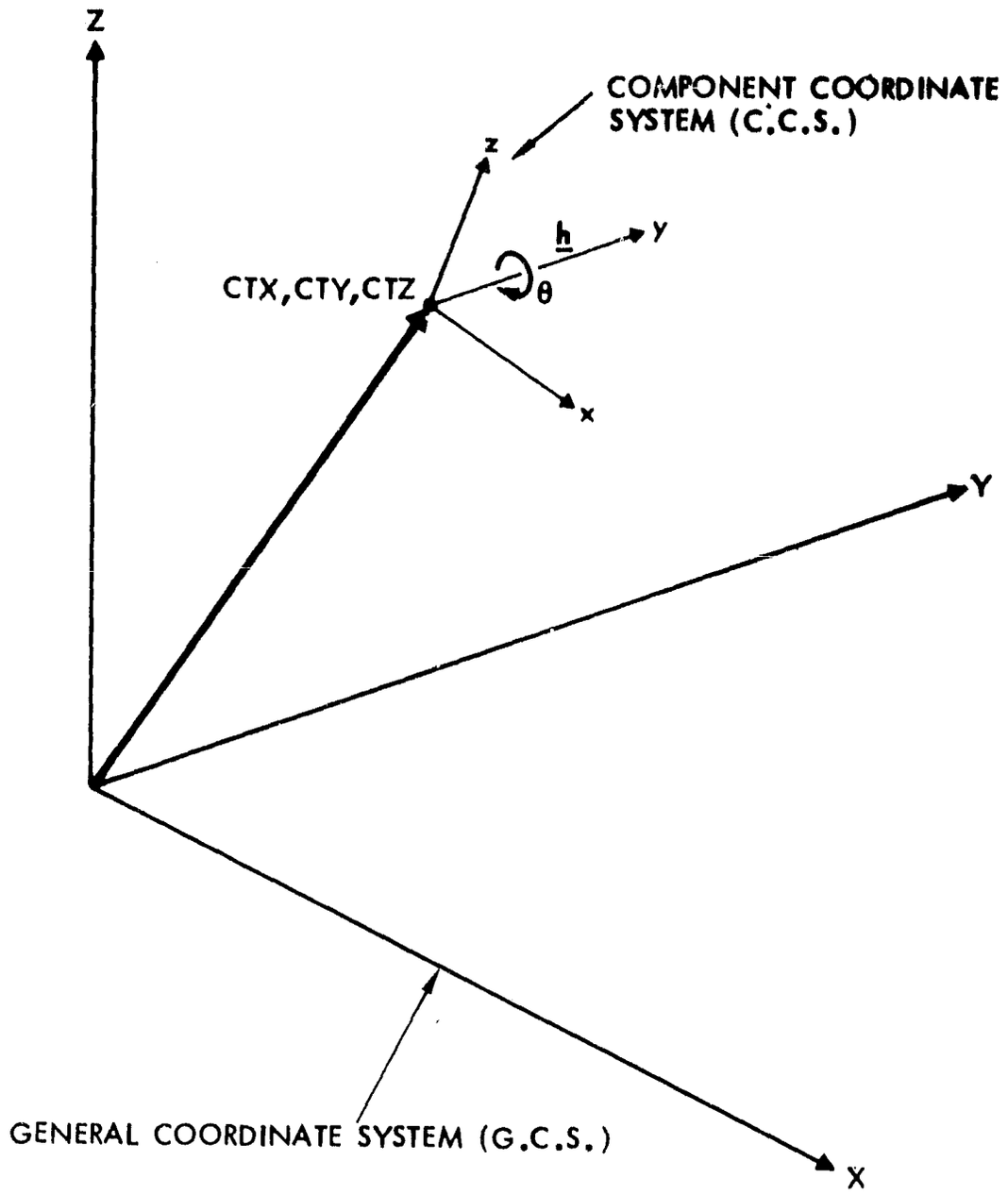

Figure 20. Component Transformation.

5.2 Patches

5.2.1 Convention

We have seen (4.2) that a patch is basically a four-sided shape when developed or "opened out". It must always be regarded as such, even if one of the sides or two opposite sides are made zero or if some of the sides have kinks. In the following discussions patches will often be regarded as rectangular--this is purely a convenience for discussing relationships and is not a shape restriction. Our view of the patch will always be from the outside, i.e., looking onto the surface from a point in the flow field.

For convenience, a patch is defined in terms of a "chordwise" and a "spanwise" direction, Figure 21. These directions are analogous to the conventional wing layout, but, in the patch context these directions are not restricted to the x and y directions, respectively. For example, on a patch representing the wing tip, the "spanwise" direction will probably be in the wing chordwise direction and the "chordwise" direction will be vertical.

Patch geometry is defined using chordwise lines called SECTIONS. (These are described later in 5.2.2.) A set of sections distributed spanwise across a patch defines the patch surface. The convention adopted here is that points defining a section shape proceed from top to bottom, Figure 21. (In the case where a patch represents the main surface of a wing, this convention causes the points defining each section to proceed from the trailing edge lower surface and finish at the trailing edge upper surface, i.e., as in the original program.) In our view of the patch, the order of the sections always proceeds in the positive spanwise direction; however, for user convenience, we allow the spanwise direction to proceed either from left to right or vice versa, Figure 22. As we shall see later (5.4.3), it is important that the program distinguishes

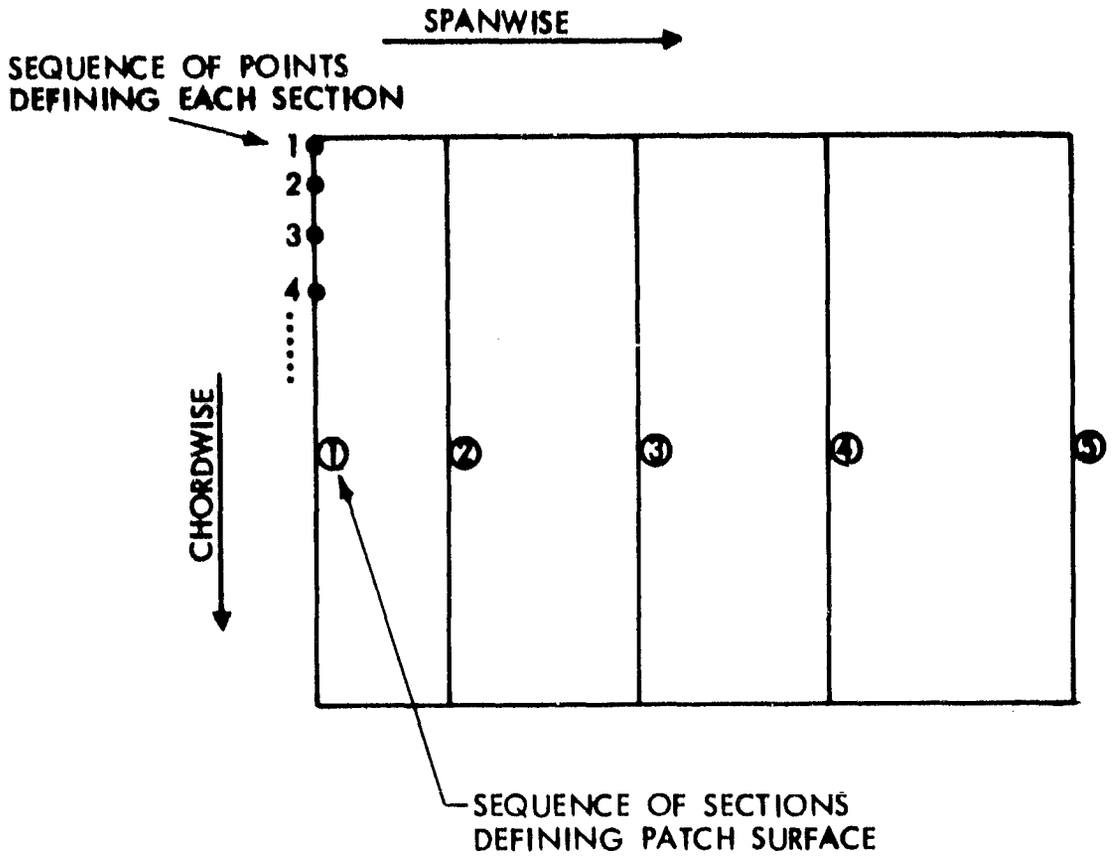

Figure 21. Sections Defining Patch Surface.

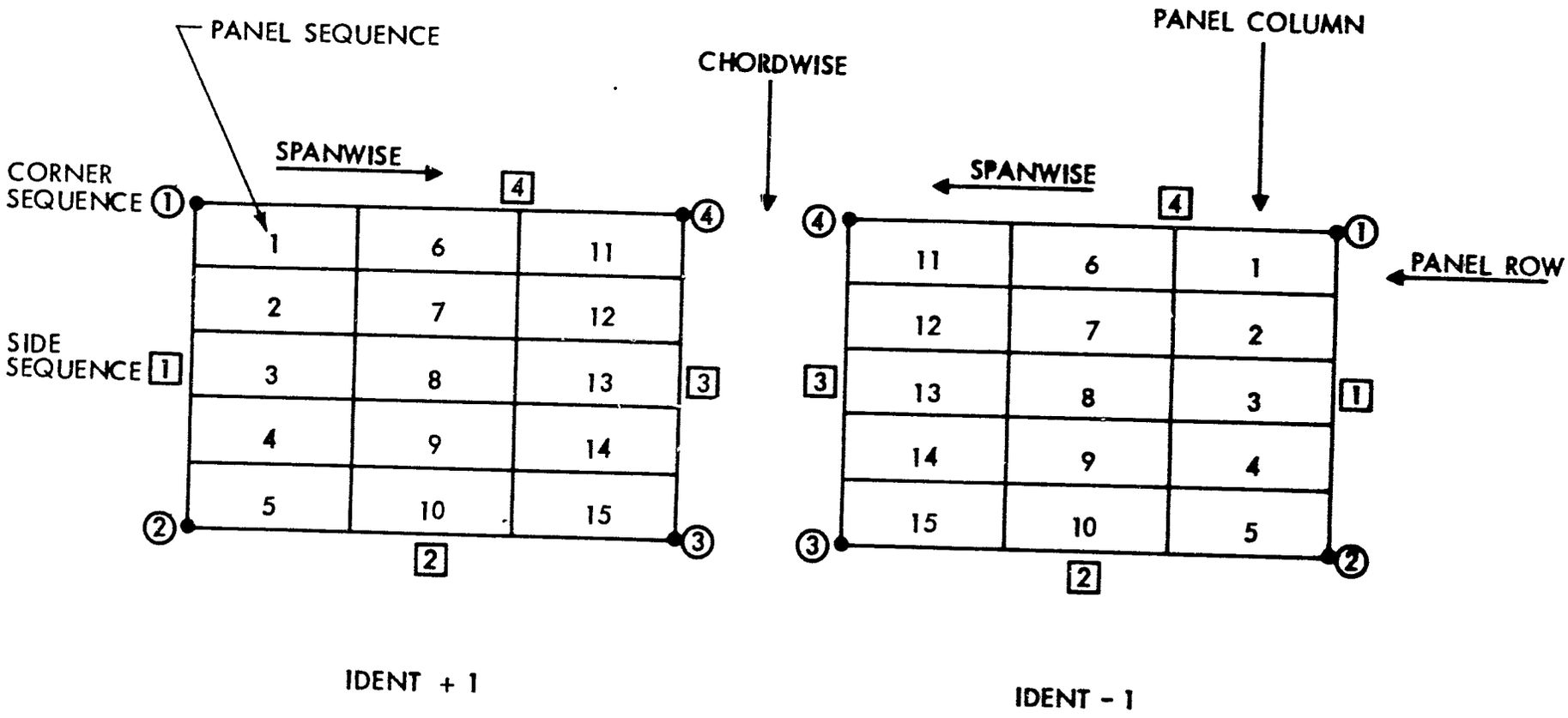

Figure 22. Patch Conventions.

between the two possibilities so we set a patch IDENT parameter to +1 if the spanwise direction is selected from left to right (i.e., root to tip in the wing convention) or -1 if the direction is right to left.

For the purpose of automatically connecting panels from one patch to another, it is important to identify patch sides. The convention adopted here is that the first and last sections defining a patch correspond to sides 1 and 3, respectively, while the patch top and bottom correspond to sides 4 and 2, respectively. With this convention, the order of the sides is anti-clockwise when IDENT is +1 and clockwise when IDENT is -1, Figure 22. The order of the corner points follows the same sequence as the sides, starting with 1 at the top of side 1.

Panels and subpanels take the same side and corner point convention as their parent patch. For convenience, the panels are referred to in ROWS--which run spanwise--and COLUMNS--which run chordwise, Figure 22. Panel arrangements within a patch are referred to by ROWS X COLUMNS.

5.2.2 Sections

Each section of a patch may be defined in its own local coordinate system, referred to as the section coordinate system, or S.C.S. The user provides the necessary information to transform from the S.C.S. into the C.C.S. at the beginning of each section. This transformation is performed immediately a section's geometric description is complete. This transformation is separate from that described earlier in 5.1 in which the complete component is converted into the G.C.S. (at which stage the S.C.S. geometry is discarded). This double transformation--both levels of which are optional--offers useful flexibility when preparing the input data. One particular advantage is that the geometric relationships--especially the rotations--are kept reasonably simple without sacrificing generality.

The information required to transform from the S.C.S. into the C.C.S. (see Figure 23) consists of: (i) the translation vector, (STX, STY, STZ), which is the position vector of the S.C.S. origin expressed in the C.C.S. coordinates; (ii) a scaling factor (default 1.0) which is applied in the S.C.S.; (iii) the rotation angle (θ, degrees) about the y-axis of the S.C.S.; and (iv) the angle (ϕ, degrees) in the C.C.S. x-y plane, between the projection of the S.C.S. x-axis and the C.C.S. x-axis.

The contour line of each section is defined by a set of BASIC POINTS, (BX, BY, BZ). These points may be used directly as panel corner points, i.e., MANUAL PANELING, in which case the user must take care over the number of input points. Alternatively, an AUTOMATIC PANELING ROUTINE, or A.P.R. (described in 5.4.1) may be activated which interpolates through the basic points to form a new set of points corresponding to panel and subpanel corner points. (Note, this is just a temporary set as the user may opt to use the A.P.R. in the spanwise direction as well, in which case the section points do not necessarily line up with panel edges.) Subpanel points are always obtained by interpolation whether or not the A.P.R. has been activated.

No matter which paneling option has been selected, basic points should be reasonably dense in regions of high curvature, such as near the wing leading edge.

Several options have been provided for defining the basic points and these, in combination with the two-stage transformation described above, provide great flexibility when preparing the input. The options may be exercised at the section level so the input form may be changed from section to section. The options available at this time are described below and are controlled by the value of INPUT. INPUT values of 1 through 4 are illustrated in Figure 24 together with instances for their use.

INPUT values of 1, 2 and 3 are used when a section lies in one of the reference planes of the chosen S.C.S.; in these cases we have a constant coordinate, x, y, or z, respectively.

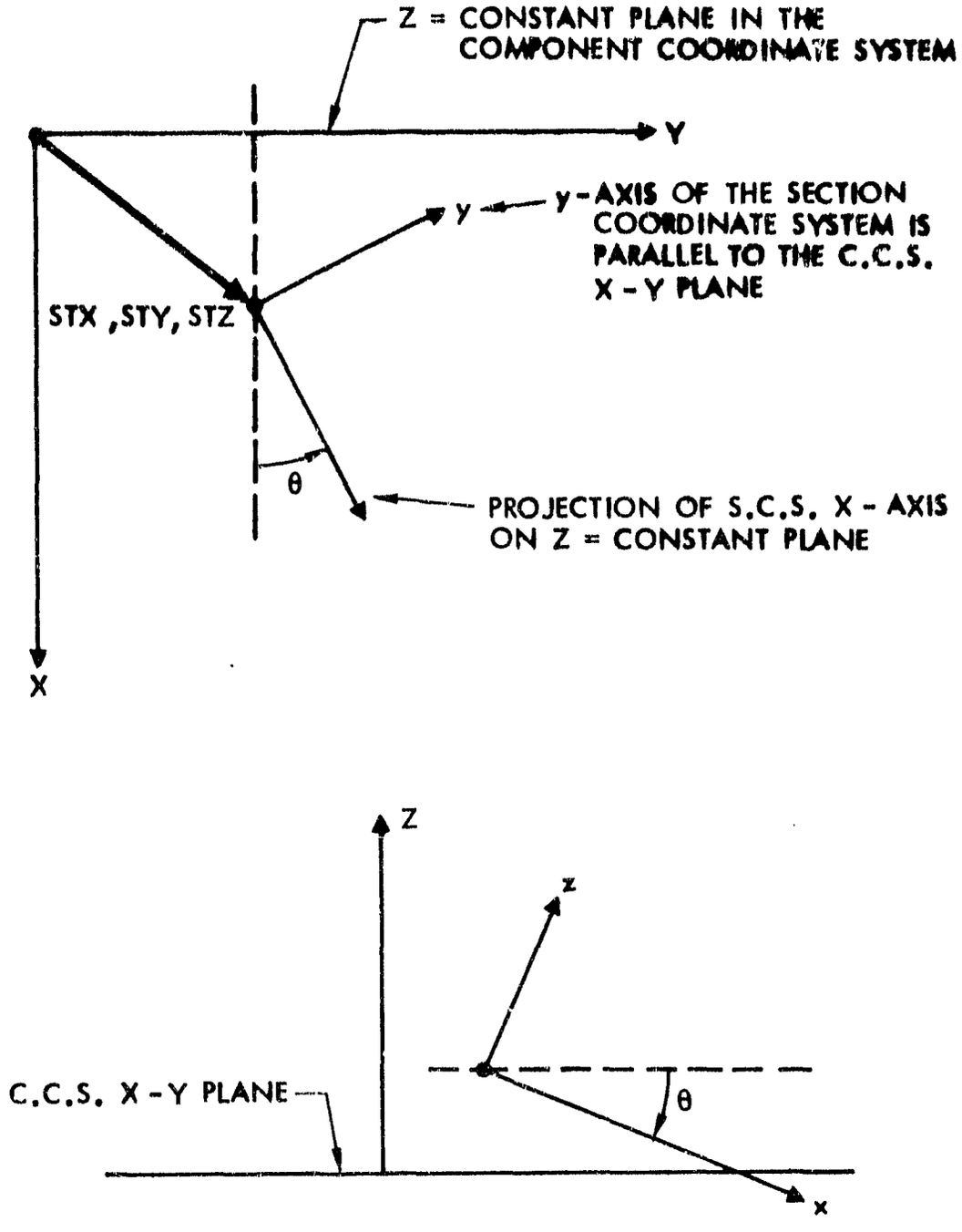

Figure 23. Section Transformation Into C.C.S.

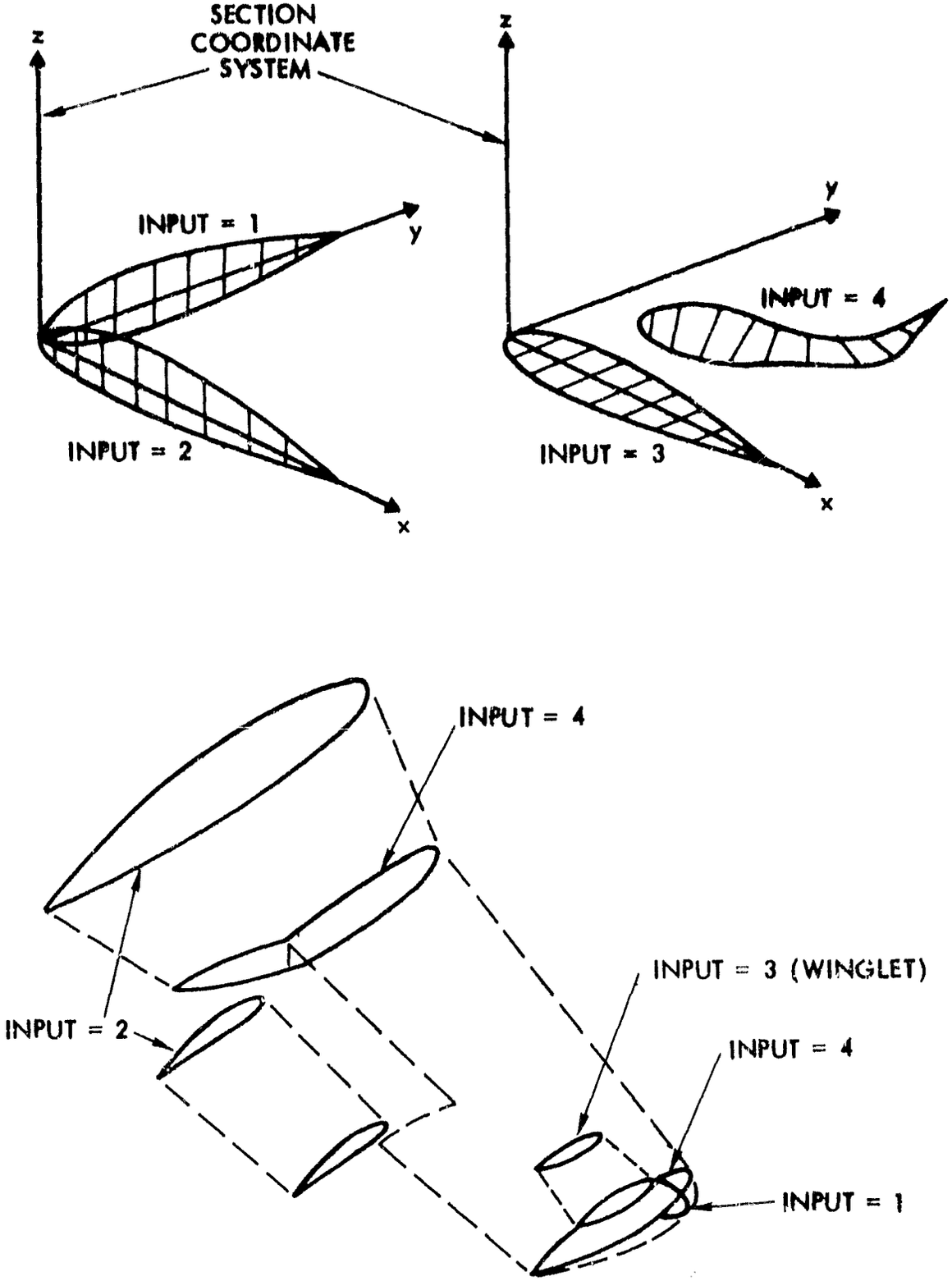

Figure 24. Basic Point Input Options 1 Through 4.

With one coordinate fixed we need input only two coordinates for each basic point, e.g., y and z when INPUT = 1. Provision is made to specify a third quantity to give a local adjustment to the "constant" coordinate, e.g., when using INPUT = 2 we may specify x, z and δy. Usually the δ-quantity is left blank (i.e., 0). The basic value for the constant coordinate is zero until the section points are transformed into the C.C.S., so the value of that coordinate in the C.C.S. must be provided in the transformation information.

INPUT value of 4, which requires all three components of each basic point position vector, is used when defining a completely arbitrary section shape.

INPUT values greater than 4 are provided and access a NACA four-digit equation to automatically generate a symmetrical section, the thickness/chord ratio having value INPUT/100 (i.e., there is a lower thickness limit of .05c). This option was originally used to check out the geometry routines but it has been left installed as a possible future convenience--other equations could be substituted easily. The coordinates are generated in the INPUT = 2 format, i.e., x, z with y = 0.

Zero or negative INPUT values allow the present section's basic points to be copied over completely from any previously defined section. The section number is (-INPUT) except when INPUT = 0; the latter copies over the points from the section just completed. The section number specified is the absolute number from the beginning of the input and includes other copied sections as well as sections which may have been generated automatically. If the section counting becomes complicated, alternative ways of copying are available as described later in 5.3.1. The basic points are copied from the S.C.S. set (i.e., as originally specified) and are then transformed to the present C.C.S. according to the new section's transformation information.

5.2.3 Chordwise Regions

The basic points defining a section may be assembled in a number of CHORDWISE REGIONS for the purpose of controlling the panel density and distribution on that section. In addition, the option on manual or automatic paneling is selected at the chordwise region level, allowing the user to switch from one to another within each section wherever he chooses. Chordwise regions are used only as an input convenience and are discarded in the program as soon as the surface paneling is complete.

A chordwise region must end on a basic point called a NODE POINT, Figure 25. A NODE CARD, containing the chordwise region paneling information (see below), inserted after a basic point in the input deck identifies that point as the end of a chordwise region. Node points are usually placed at "problem" areas where large velocity gradients are expected to occur, e.g., flap hinge line, leading edge, close-interference regions, but the user can place them wherever he wishes to change from one panel scheme to another. Four types of node point are provided at this time and are described below.

The information on a NODE CARD consists of just three integers.

(i) NODEC identifies the node point and its type.

(ii) NPANC is the number of panels to be generated by the A.P.R. in the chordwise region just completed--a zero value gives manual paneling.

(iii) ISPAC controls the form of the distribution in the automatic paneling mode and is inactive in the manual paneling mode.

(The C on the end of each quantity distinguishes the chordwise from the corresponding spanwise quantities, which end in S, 5.2.4.)

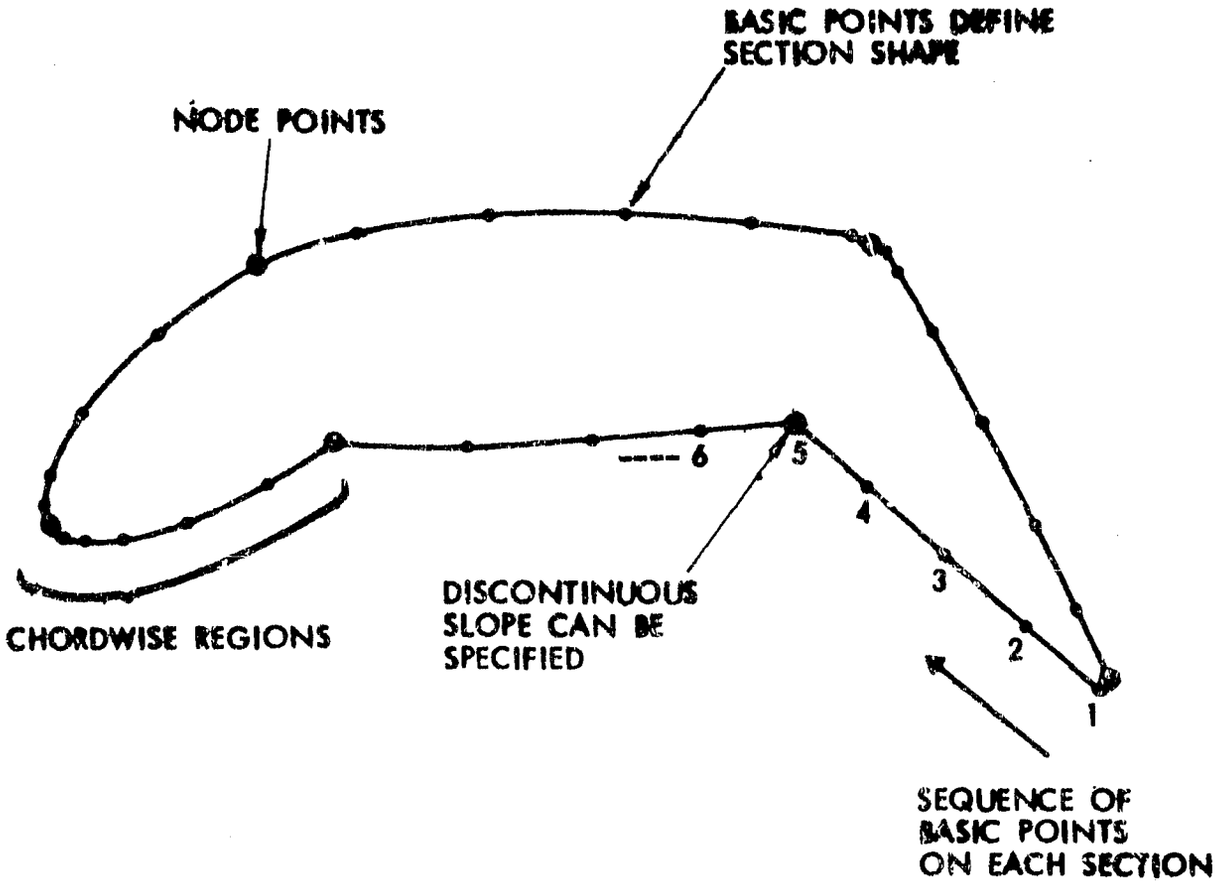

Figure 25. Chordwise Regions on a Section.

NODEC values of 1 or 2 specify the end of a chordwise region with, respectively, continuous or discontinuous surface slope onto the next chordwise region. These values are, therefore, used only on regions ending in the interior of a section. The last point on a section is specified by NODEC = 3 and is the only node point that must always be specified even if manual paneling has been selected. Negative NODEC values are also permitted and initiate a special copying routine described in 5.3.1.

Four panel spacing options are provided in the A.P.R. The action of ISPAC values of 0, 1 and 2 is illustrated in Figure 26 and is based on the cosine distribution giving increased panel density towards, respectively, the beginning and end, the beginning only, or the end only, of the region. Equal spacing throughout the region is provided by ISPAC = 3. Coupled with the flexibility offered by the choice of chordwise region location, these spacing options have proved adequate so far; however, other options could easily be added should the need arise later, e.g., one based on increments in integrated surface curvature, or on increments in doublet value from a preliminary two-dimensional solution for the section.

Clearly, node cards provide the user with an extremely versatile paneling tool. With one card deck of basic points defining the configuration geometry, he can, from run to run, change the form of the paneling simply by changing two integer values on each node card. Not only that, he can also move node cards within the deck (but not the node cards at section ends) or remove some or add new ones from run to run. This allows the user to concentrate his paneling in areas of interest, leaving other areas more sparsely paneled. It thereby provides a very effective use of the limited number of panels available, yet, on a subsequent run a few small changes to the node cards allow the emphasis to be switched to another area without having to punch a new basic geometry card deck.

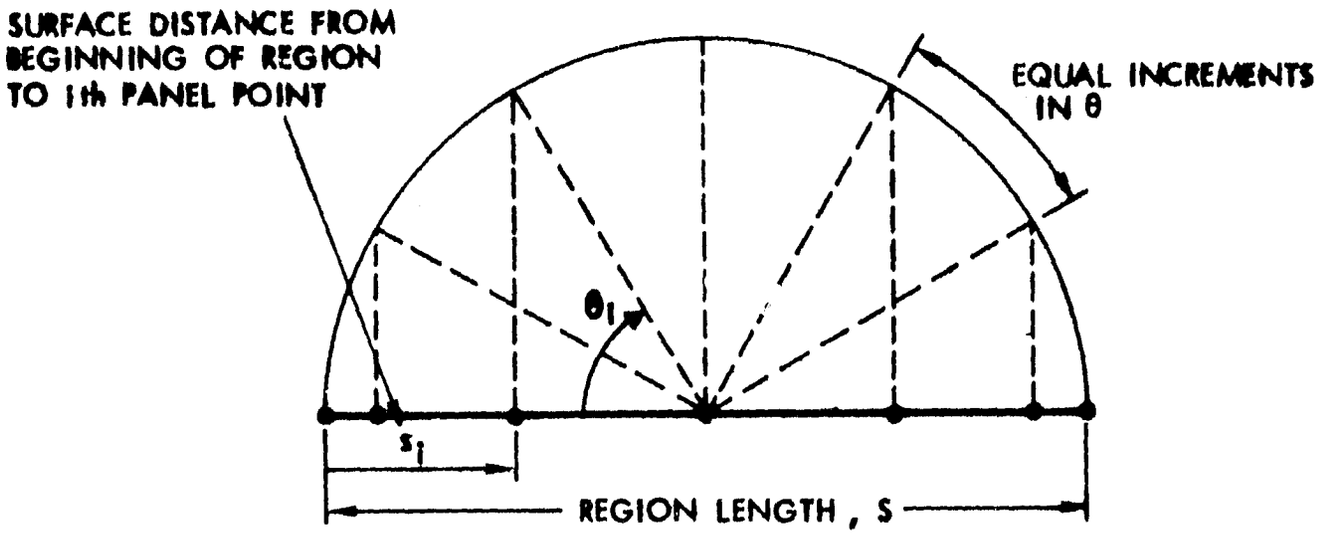

$s_i = S(1 - COS(\theta_i))/Z$

WHERE $\theta_i = (I - 1)\pi/N$ AND N IS THE NUMBER OF INTERVALS REQUIRED

(a) ISPAC = 0

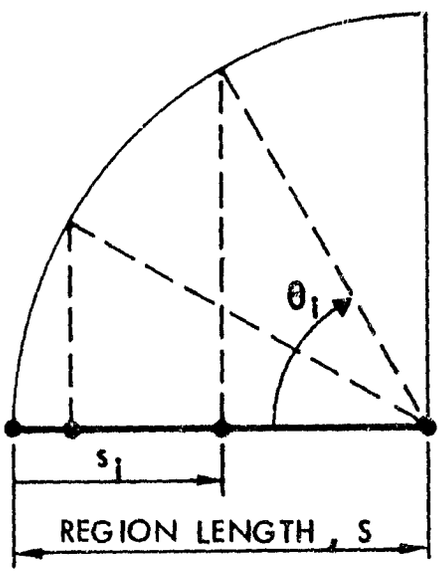

$s_i = S(1 - COS(\theta_i))$

WHERE $\theta_i = (i - 1)\pi/2N$

(b) ISPAC = 1

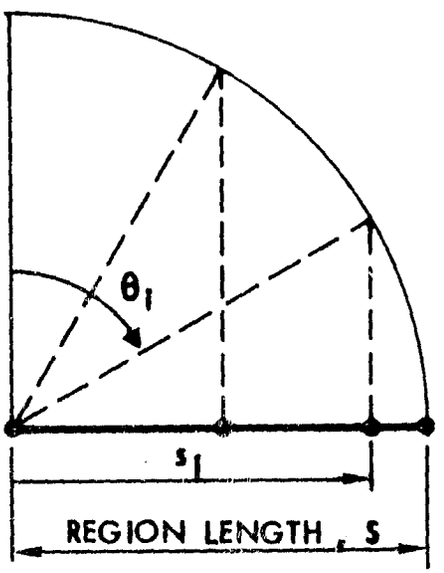

$s_i = S\ SIN(\theta_i)$

WHERE $\theta_i = (i - 1)\pi/2N$

(c) ISPAC = 2

Figure 26. Spacing Options 0, 1 and 2 in the A.P.R.

There is just one important ground rule for the use of node cards; the total number of panels (automatic and/or manual) on each section of a patch must be the same. The total is, in fact, the number of panel rows, NROW, for that patch. The program monitors the number of panels on each section and the calculations are terminated with an error message should the user make a mistake. Provided this ground rule is satisfied, it is not necessary for the panel distribution to be the same from section to section--in other words, the number of chordwise regions and their node information can vary from section to section. The significance of this will be illustrated in 5.4.1.

5.2.4 Spanwise Regions

Sections defined within each patch may be assembled in a number of SPANWISE REGIONS for the purpose of controlling panel density and spacing in the spanwise direction. In forming spanwise regions, sections defined by the user take on a similar role to that of basic points in the chordwise regions. Although the options available for the spanwise regions are essentially the same as described for the chordwise regions in 5.2.3, the two are applied completely independently; for example, the user may request automatic paneling in the chordwise direction and manual in the spanwise direction. As in the case of chordwise regions, spanwise regions are used only as an input convenience and are discarded once the paneling is complete.

Spanwise regions must end at user-defined sections, called NODE SECTIONS, Figure 27. These usually coincide with kinks in the spanwise direction on the patch planform, but the user can place one whenever he wishes to change the form of the paneling or to change between manual and automatic paneling in the spanwise direction. For convenience, the spanwise node information is included on the section card together with the section transformation information (5.2.2). The function of the spanwise region node quantities, NODES, NPANS, ISPAS--distinguished from

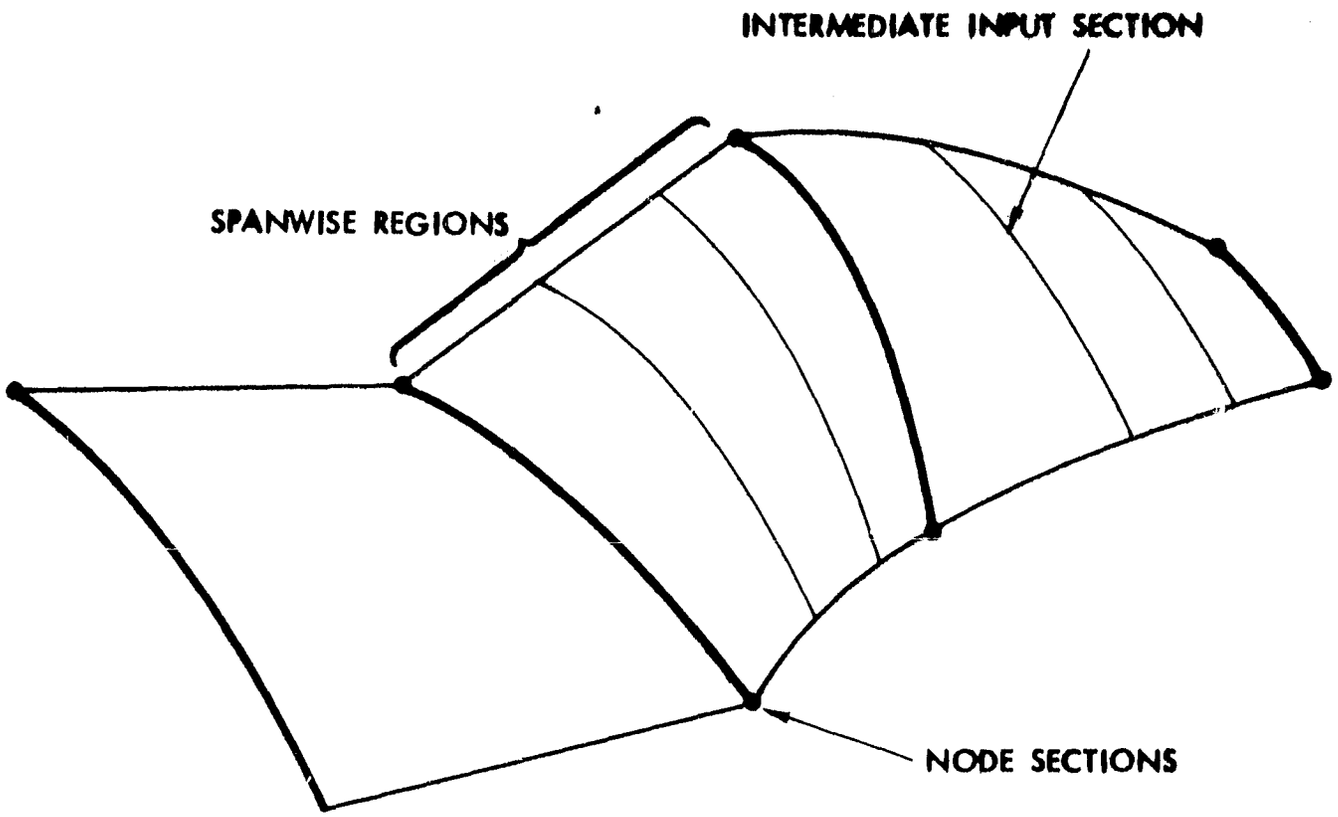

Figure 27. Spanwise Regions on a Patch.

the corresponding chordwise quantities by ending in S--follows closely the description in 5.2.3. NODES, however, must be set to zero (blank) on the first section of a patch and on all intermediate input sections that are not node sections. (NPANS and ISPAS are then inactive.) The last section on a patch is identified by a NODES value of 3, 4 or 5; 4 is used if the patch is the last one on a component and 5 is used if the patch is the last one on the configuration, in which case the present section completes the basic description of surface geometry.

The total number of panels defined (manually or automatically) across each patch in the spanwise direction is monitored by the program and becomes the number of panel columns, NCOL, for that patch. In view of the ease of generating panels, the code also monitors the running total of panels, and if a limit is exceeded, the calculation terminates with an appropriate error message. The limit is set internally by the storage capacity, but the user is given the opportunity to override that value with his own estimate of the total he intends to use for that case. In the event of an input error, this will avoid the inadvertent and expensive use of, say, 1,000 panels when the user intended using only 100.

5.3 Special Routines

The geometry routines described above may be applied for the complete configuration; however, special routines have been provided to reduce user input and, in particular, to avoid duplicating information already supplied. These routines, which are described below, are optional.

5.3.1 Copying Routine

We have already seen (5.2.2) a copying facility accessible at the section input level. This copies over a complete section, including the chordwise region information, and has,

therefore, a rather limited application. More general copying routines are provided and are activated at the basic point level to copy STRINGS OF BASIC POINTS, rather than complete sections. This capability allows a new section to be assembled from parts of previously defined sections. Several strings of basic points may be assembled from a number of previously defined sections and the points selected need not follow the same direction as originally specified. Furthermore, the copied strings of points may be intermixed with strings of manually input basic points to complete the new section.

For this copying mode, the value of INPUT on the section card (5.2.2) must be in the range 1 to 4. The copying is activated by inserting a NODE CARD having a NEGATIVE sign on NODEC. This is regarded as a DUMMY node card because it does not necessarily terminate a chordwise region (see below). The negative value for NODEC determines the action at the end of the copied string of basic points. If NODEC = -1 or -2, then the last copied point becomes the end of a chordwise region on the new section and signifies, respectively, continuous or discontinuous slope onto the next chordwise region. We then continue to specify further basic points, or, by inputting another negative node card, we can copy another string of basic points, and so on. If NODEC = -3, then the last copied point in the string completes the new section.

If the user does not require a chordwise region to end at the last point in a copied string, then he sets NODEC = -4 when he initiates the copy. When the string has been copied over, the program then expects to receive further basic points to complete the chordwise region or another negative node card can be used to copy another string of points, and so on. Clearly, if NODEC = -4, then the NPANC and ISPAC values on the NODE CARD are inactive and may be left blank.

Whenever a negative node card is inserted, it must always be followed by a COPY CARD containing the following information

(four integers) defining the location of the required string of points, IPCH, ISEC, IB, LB.

IPCH is the patch number containing the required points.

ISEC is the section number relative to the start of that patch.

IB, LB are, respectively, the first and last basic point numbers (inclusive) defining the string. The numbering is relative to the start of the section ISEC.

Thus, even in a complicated configuration, it is relatively easy to specify a string of basic points.

This option offers not only an alternative to the earlier copying routine, but also a more general capability because the copying is initiated at the basic point input level, rather than at the section input level. For example, the complete copied section need form only a part of the new section, it being possible to have other basic points, both before and after the copied string. In addition to this, the ability to break the copying into strings of points allows a new distribution of chordwise regions to be selected.

One restriction must be considered when using this copy routine--the new section's value for INPUT must coincide with the INPUT values on sections from which strings of points are to be copied. This restriction has not posed a problem so far, but if it does, it would not be too difficult to remove it.

An example of the use of this copy routine will be shown in the test case in 7.1.

5.3.2 Automatic Patch Generator

Patches covering tip edges, flap edges, cutouts, etc. can be input by the user as ordinary patches, but this can get tedious. Optional automatic procedures have been installed which simplify this input by generating a complete patch within the

code. This AUTOMATIC PATCH GENERATOR, or A.P.G., is initiated at the patch input level by inserting a non-zero value for parameter, MAKE, on the patch data card. The value of MAKE identifies the patch number on the edge of which a closing patch is to be generated. The sign of MAKE determines whether the new patch is on side 3 (positive) or side 1 (negative) of the basic patch.

Consider, for example, a tip-edge patch. Here we have already defined the patch representing the main surface. The end section of that patch provides the BASE SECTION from which the A.P.G. creates the new patch, Figure 28(a), according to user instructions. When the A.P.G. has been activated, the next card must contain the following:

NPANC, ISPAC, KURV, NODES, NPANS, ISPAS.

Referring to 5.2.3 and 5.2.4, the generated patch has one chordwise region with NPANC panels spaced according to the value of ISPAC. It has one spanwise region with NPANS panels spaced according to ISPAS. The value of NODES must be either 3, 4 or 5, depending on the location of the patch in the input. The function of KURV is described below.

Sections defining the new patch are created automatically from the base section coordinates. The contour of each section generated may be either a straight line ("square-cut" tip) or an ellipse, depending on the value of the quantity, KURV, supplied by the user. If KURV is 0, sets of basic points are generated on straight lines joining upper and lower points on the base section. The same number of points is created even if the interval across the base section is zero (e.g., at the leading and trailing edges), Figure 28(a).

If KURV is 1, the basic points are created on semicircles having diameter equal to the local "thickness" of the base section.

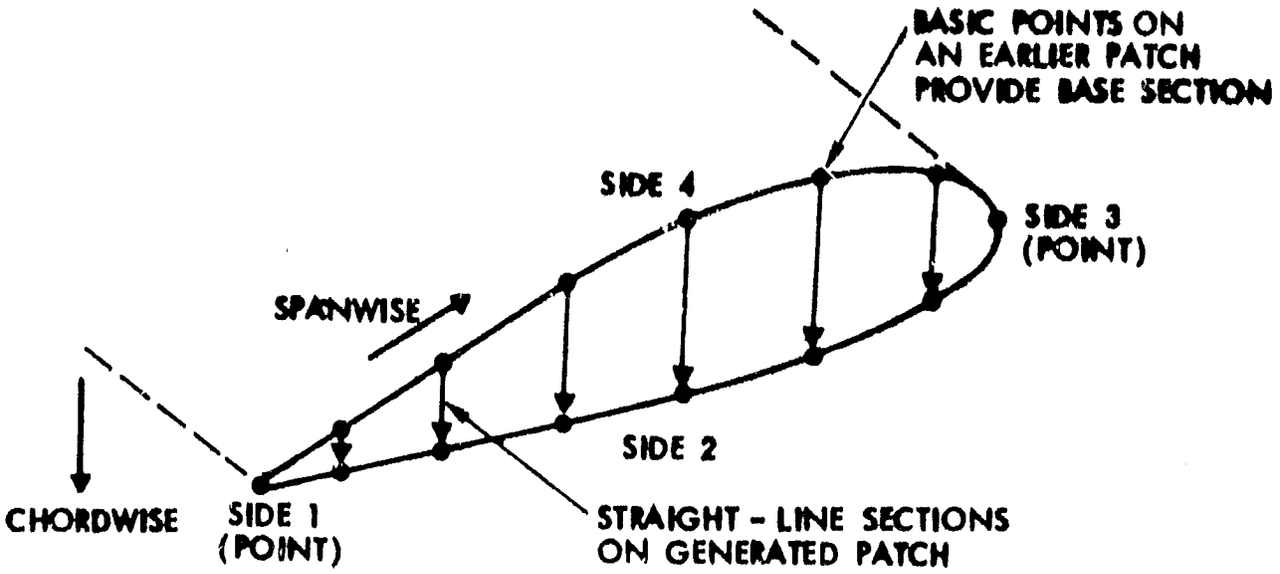

(a) FLAT EDGE PATCH (KURV = 0)

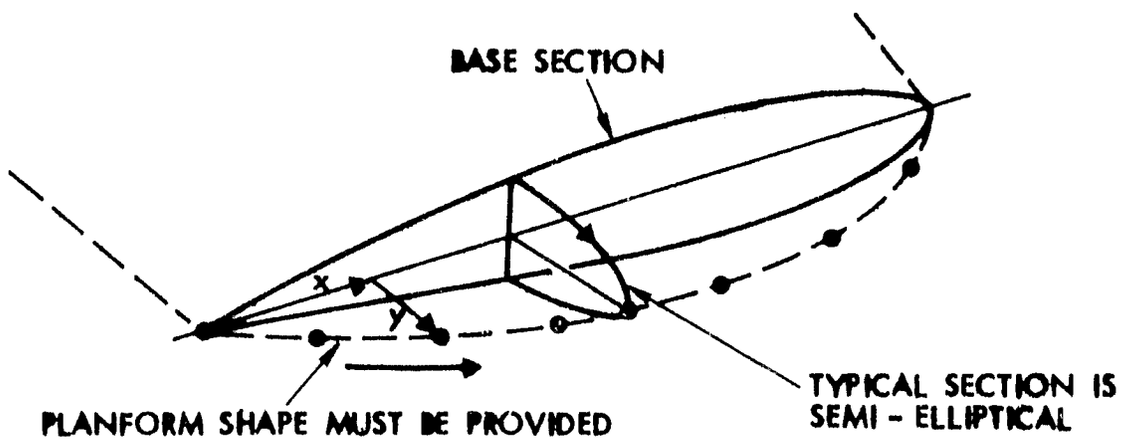

(b) PATCH WITH SEMICIRCULAR (KURV = 1)
OR SEMI - ELLIPTICAL (KURV>1) SECTIONS

Figure 28. Automatic Patch Generator.

If KURV is greater than 1, the basic points are created on semi-ellipses; the base section local thickness provides one axis, while the semi-axis is derived from additional user input. A planform shape is input using a set of coordinates, x_i, y_i, $i = 1$, KURV, defined in a convenient local coordinate system with origin at the trailing edge, Figure 28(b). The scale and point distribution are completely arbitrary, so the points may be conveniently measured from a planform view of the wing. The program scales the shape to fit the length of the basic section and interpolates to find the local semi-axis for each ellipse.

KURV may also take a negative value. The generated patch then uses the copying routine (5.3.1) to locate the four sides of the new patch. In this case we input for each side a copy card containing the four integers, IPCH, ISEC, IB, LB, to locate four strings of basic points on previously defined sections. The A.P.G. then joins points on side 4 to points on side 2 using straight lines, i.e., sections on the new patch. The first and last sections on the new patch are taken directly from the strings of basic points for sides 1 and 3, respectively. If the copy cards for either of these sides has been left blank, then the appropriate first or last straight line joining sides 4 and 2 become, respectively, the first or last section for the new patch. This option in the A.P.G. is useful for fitting in side openings left by flap-edge cutouts, Figure 28(c). Clearly, when KURV is negative, the value of the parameter, MAKE, is no longer important (as long as it is non-zero); however, the sign of MAKE still determines which way the patch is facing. Accordingly, we set MAKE = +1 or -1.

One final point--the A.P.G. works directly in the component coordinate system (C.C.S.) even when copying strings of points. It always generates patches with positive IDENT (5.2.1).

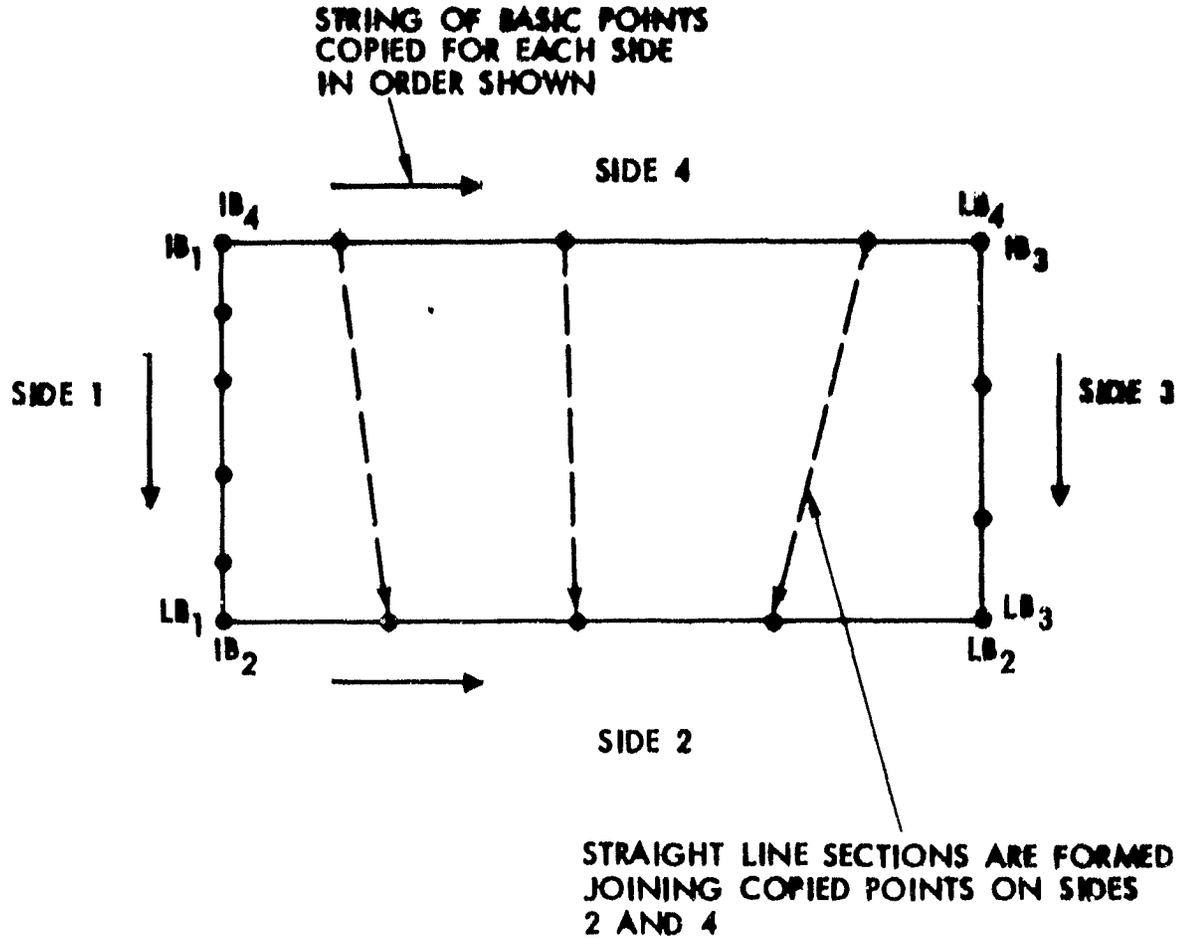

(c) PATCH GENERATED FROM FOUR STRINGS OF COPIED POINTS (KURV NEGATIVE)

Figure 28. Concluded.

5.4 Panels and Subpanels

5.4.1 Automatic Paneling Routine

When the basic geometry has been specified, the panel and subpanel corner points are assembled, patch by patch. A temporary set of chordwise points corresponding to panel and subpanel corners is first assembled on each of the defined sections. This is performed in each chordwise region in turn (5.2.3) and interpolation is used when the A.P.R. is requested (i.e., when NPANC > 0). Subpanel points are always generated by interpolation; if the A.P.R. has been requested, then the subpanel points are included as a set with the panel points. If manual paneling is being used, the subpanel spacing is based on normalized point subscript (Appendix A); this creates subpanel intervals more closely related to the changes in spacing in the user-specified panel points.

The form of the interpolation used by the A.P.R. depends on the number of basic points available in the chordwise region, including the two end points. The code augments this number by taking a basic point from a neighboring chordwise region if continuous slope has been specified onto that region (i.e., NODEC = 1 on this or the previous region). The A.P.R. takes the available set of basic points and first eliminates zero length intervals, then, depending on the number of basic points left, i.e., one, two, three or more, it uses, respectively, constant, linear, quadratic or biquadratic interpolation to generate the panel and subpanel points.

When the temporary set of chordwise points is complete for all sections on a patch, corresponding points on each section are joined by lines called SPANWISE GENERATORS. The panel and subpanel points along each spanwise generator are then assembled in a similar way to that described for the chordwise direction, but now based on the spanwise region information. The interpolation routine is now applied along each spanwise generator in each

spanwise region where the A.P.R. has been selected. The new set of (spanwise) points are actual panel and subpanel corner points from which the panel and subpanel geometry is generated.

The fact that we input just one set of spanwise region information for a patch means that the same spanwise interpolation format is used on all the spanwise generators on that patch. Thus the A.P.R. in the spanwise direction has lost generality compared with the chordwise capability; however, this loss is not serious (and to avoid it would require considerably more input). At this time, therefore, the combination of the chordwise and spanwise A.P.R. has the capability illustrated in Figure 29. The general character when using simple input sections (planar) is shown in Figure 29(a), while the availability of more general sections would allow spanwise stretching or compression in the paneling, Figure 29(b).

5.4.2 Panel and Subpanel Geometry

The four corner points, R_i, i = 1, 4, specifying either a panel or subpanel quadrilateral are in the same sequence as the corners on the parent patch, Figure 30. From these points we construct the two diagonal vectors

$$\underline{D}_1 = \underline{R}_3 - \underline{R}_1 \tag{4}$$

$$\underline{D}_2 = \underline{R}_4 - \underline{R}_2 \tag{5}$$

The vector product of these diagonals produces a vector normal to the mean plane of the quadrilateral. We thereby construct the unit normal vector:

$$\underline{n} = \left\{ \underline{D}_1 \wedge \underline{D}_2 / |\underline{D}_1 \wedge \underline{D}_2| \right\} \text{IDENT} \tag{6}$$

The value of IDENT (5.2.1) is taken from the parent patch and ensures that the unit normal is always directed outwards from the surface into the flow field. The modulus of the

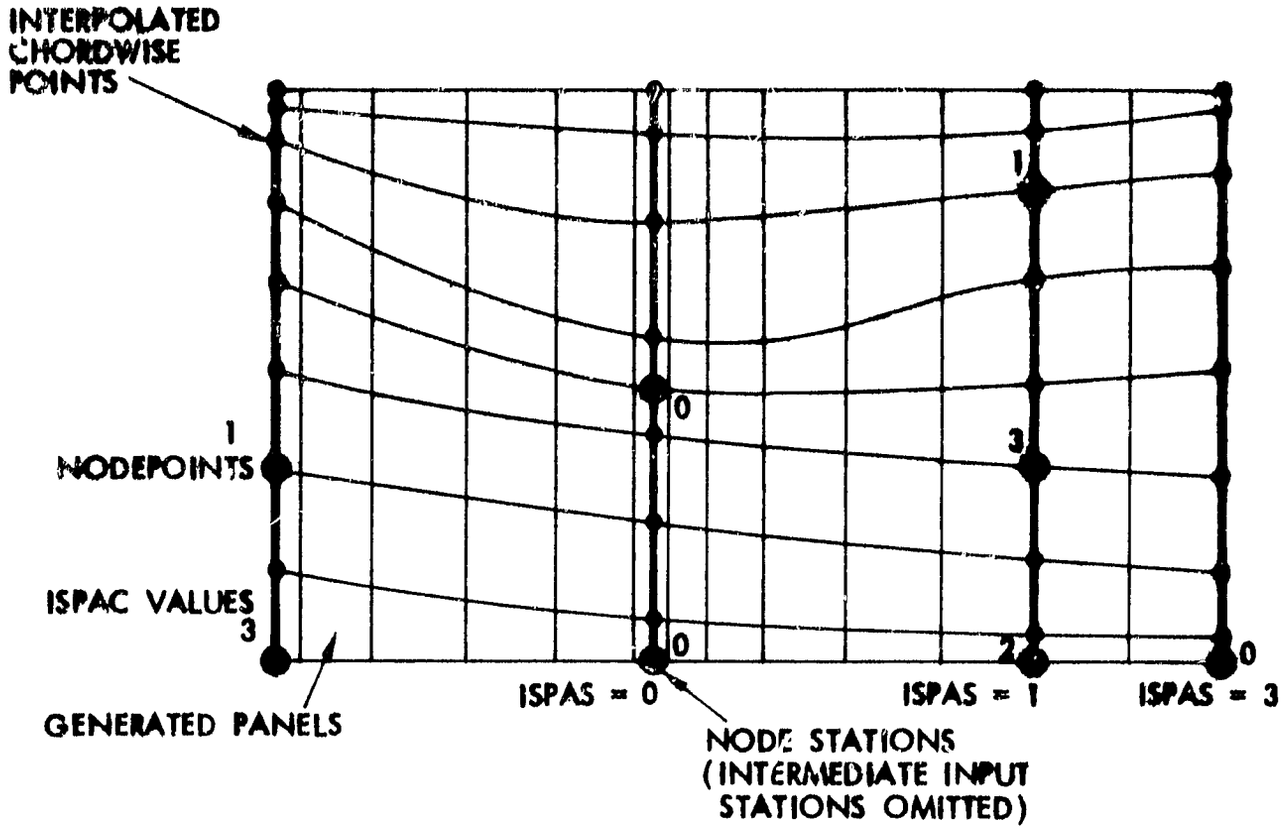

(a) SIMPLE SECTIONS

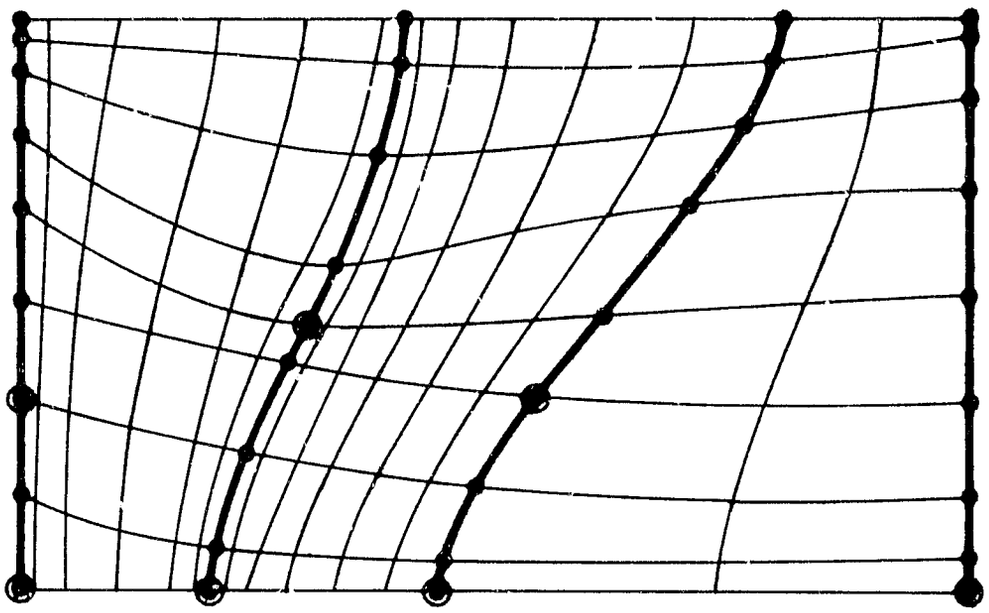

(b) GENERAL SECTIONS

Figure 29. General Character of Paneling Offered by the A.P.R.

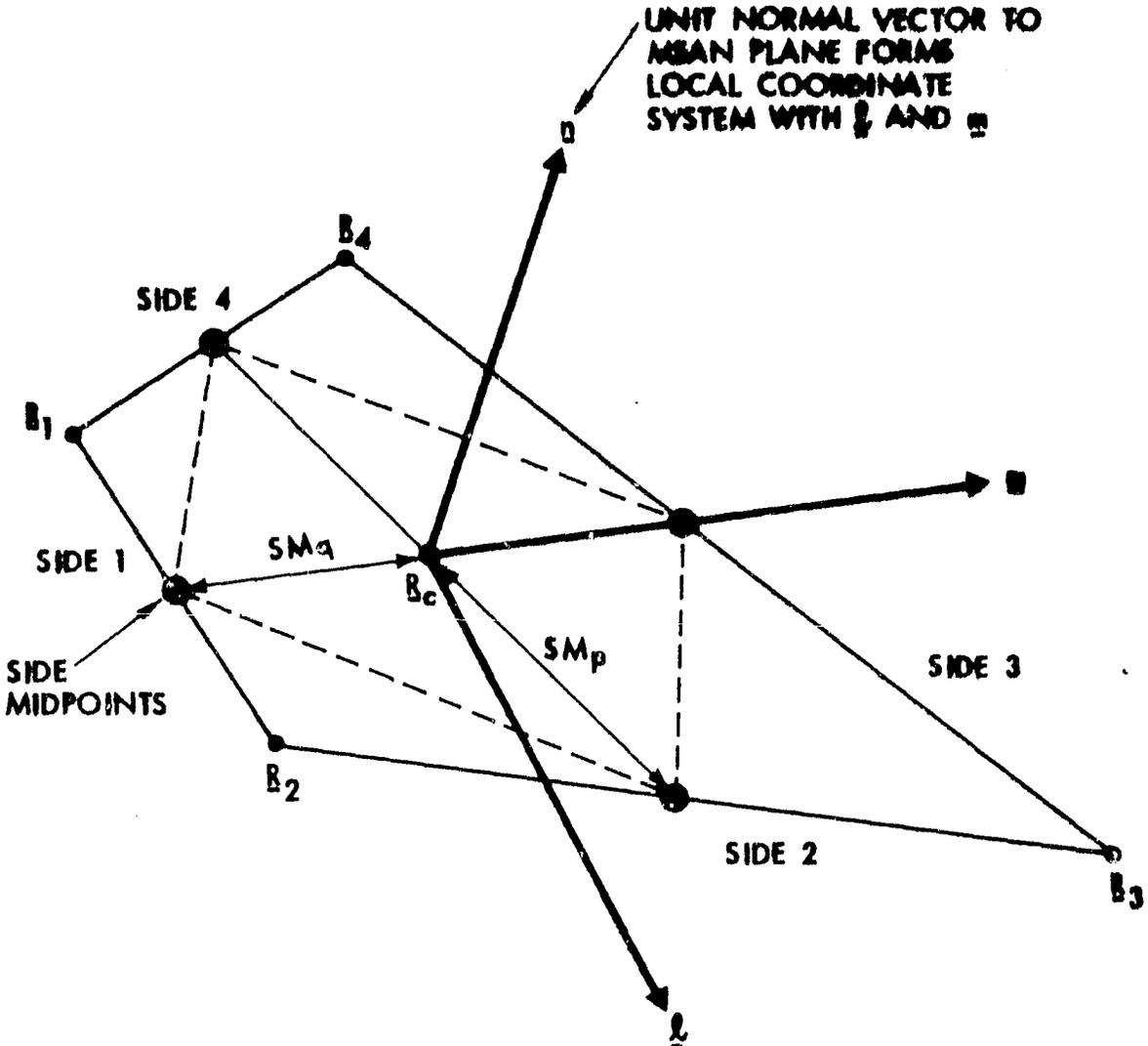

Figure 30. Panel or Subpanel Geometry.

diagonal vector product also provides the area of the quadrilateral projected onto the mean plane:

$$\text{AREA} = |\underline{D}_1 \wedge \underline{D}_2|/2 \tag{7}$$

The center point is taken as the mean of the four corner points:

$$\underline{Rc} = \left\{ \sum_{i=1}^{4} \underline{Ri} \right\} /4 \tag{8}$$

Two unit tangent vectors, $\underline{\ell}$, $\underline{m}$, are constructed, which, together with $\underline{n}$ form a right-handed orthogonal unit vector system for local coordinates. This system takes the center point, $\underline{Rc}$, as origin.

Tangent vector, $\underline{m}$, is always directed from $\underline{Rc}$ to the midpoint of side 3 of the quadrilateral, Figure 30. (This always places $\underline{m}$ in the mean plane of the quadrilateral, even if the corner points are not co-planar.) Thus,

$$\underline{m} = \left\{ \left(\underline{R}_3 + \underline{R}_4 \right)/2 - \underline{Rc} \right\} / \left| \left(\underline{R}_3 + \underline{R}_4 \right)/2 - \underline{Rc} \right| \tag{9}$$

With $\underline{m}$ and $\underline{n}$ known, we can construct $\underline{\ell}$:

$$\underline{\ell} = \underline{m} \wedge \underline{n} \tag{10}$$

Next, the projections of the four corner points onto the mean plane are expressed in terms of the local coordinate system; that is, the relative position vector of $\underline{R}_1$ from the local origin is

$$\underline{E}_1 = \underline{R}_1 - \underline{Rc} \tag{11}$$

This has components, Ex_1, Ey_1, Ez_1, say, in the local coordinate system, or $\underline{E}_1 = Ex_1\underline{\ell} + Ey_1\underline{m} + Ez_1\underline{n}$, where $Ex_1 = \underline{E}_1 \cdot \underline{\ell}$, etc.

The quantity, Ez_1, is the projection distance of the corner point from the mean plane and indicates the amount of skew of the quadrilateral from its mean plane. The magnitude of Ez_1, which is the same for all four corner points, should be kept small in relation to the size of the quadrilateral.

The quantities, Ex_i, Ey_i, $i = 1, 4$, define the flat projected panel or subpanel in the local coordinate system and are used in the influence coefficient routine.

Finally we evaluate the half median lengths, SMp, SMq, for the quadrilateral. These are (Figure 30):

$$SMp = \left| \left(\underline{R}_2 + \underline{R}_3 \right)/2 - \underline{Rc} \right| \tag{12}$$

$$SMq = \left| \left(\underline{R}_3 + \underline{R}_4 \right)/2 - \underline{Rc} \right| \tag{13}$$

These are the half-lengths of the diagonals of the parallelogram which is always formed when the midpoints of adjacent sides of a quadrilateral are joined--even if the latter's corner points are not coplanar; the parallelogram lies in the mean plane of the quadrilateral and its area is half that of the projected quadrilateral.

Within each patch, the regular arrangement of panels and subpanels causes the adjacent side midpoints of neighboring subpanels to coincide exactly. This allows the SMp and SMq lengths of subpanels to be linked, respectively, in the chordwise and spanwise direction over the patch and thereby provides a close approximation to surface distances between subpanel centers.

The geometric data evaluated above (except for $\underline{D}_1$ and $\underline{D}_2$) are stored for each panel and its subpanels as a complete set. The arrangement of subpanels within each panel is always the same, see Figure 31.

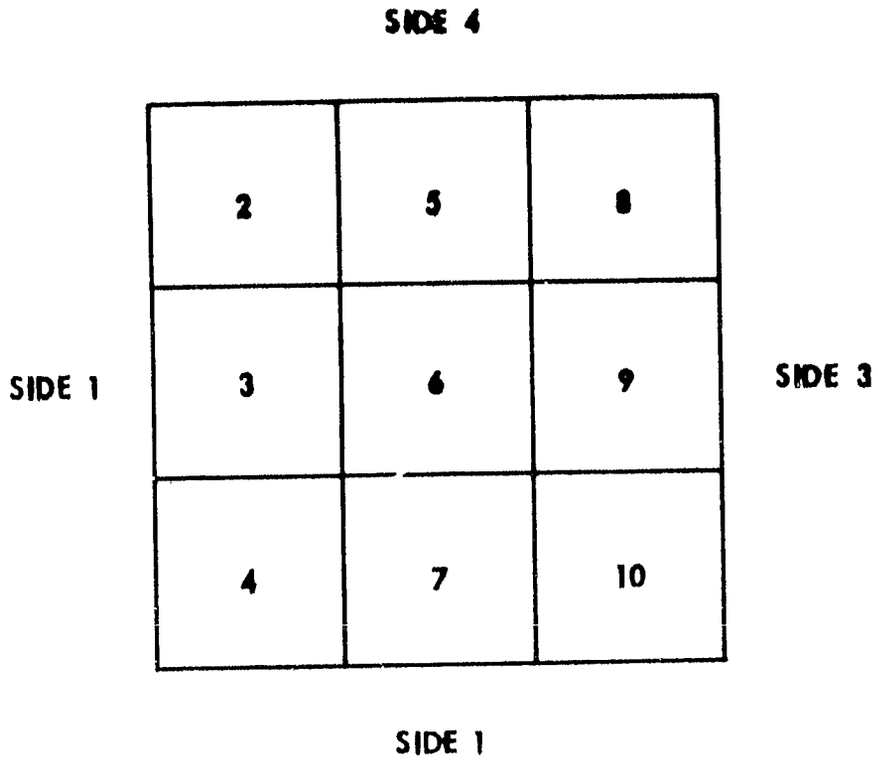

Figure 31. Arrangement of Subpanels on a Panel. (3 x 3 Scheme Shown)

5.4.3 Panel Neighbor Routine

In order that a reasonable two-way interpolation and differentiation of the surface doublet distribution can be performed, it is important that we can quickly locate for each panel the set of four neighboring panels and their orientation. Each panel, therefore, keeps an array of four neighboring panels, $NABOR_i$, i = 1,4 (in the same sequence as its sides), together with the adjacent side numbers of those panels, $NABSID_i$, i = 1, 4, Figure 32. The side number takes a negative value if the order of the sides on the neighboring panel is reversed relative to the present panel--it is useful to regard this as a change in panel POLARITY. This reversal can occur when a neighboring panel is from a patch with a different IDENT (5.2.1), or when a panel takes a reflection of itself, e.g., at the plane of symmetry.

Clearly, within the rectangular grid system of a patch locating neighbors is easy; even so, the neighbor information is still stored to form a consistent system and to avoid repetitive calculation. Across the joints between patches, however, panel neighbors are not immediately available; for example, one panel may be neighbor to several smaller panels on an adjoining patch as we saw earlier in Figure 18. An automatic procedure has, therefore, been installed in the code which scans patch side panels in a search for possible neighbors across patch joints. In this search only patches within the same assembly of components are considered. "Undesirable" neighbors are quickly eliminated on the basis of relative geometry during the assembly of a short list of possible neighbors for each side panel. From this list of candidates one PREFERRED NEIGHBOR is selected. At this time, preference is given to the panel whose control point lies closest to a normal plane constructed on the side panel, Figure 33. This plane contains the side panel's control point, unit normal vector and the side midpoint of the middle subpanel at the patch edge.

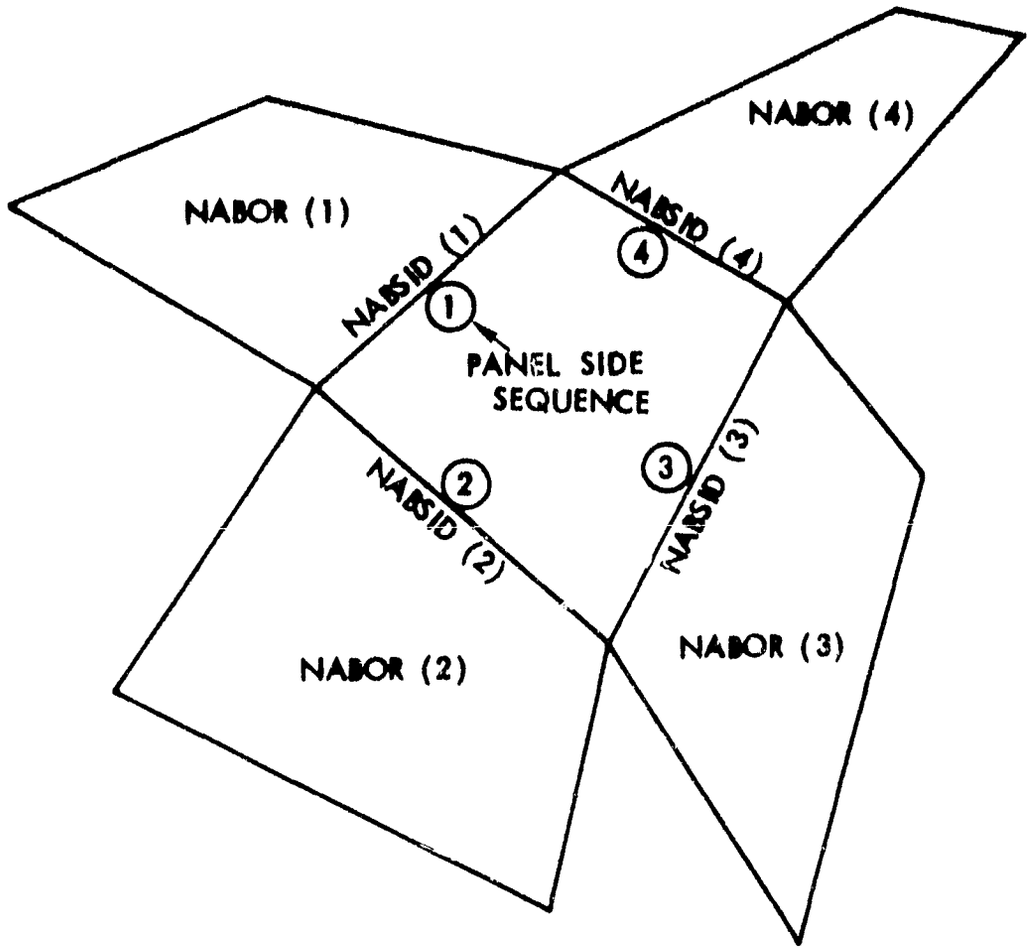

Figure 32. Panel Neighbor Information.

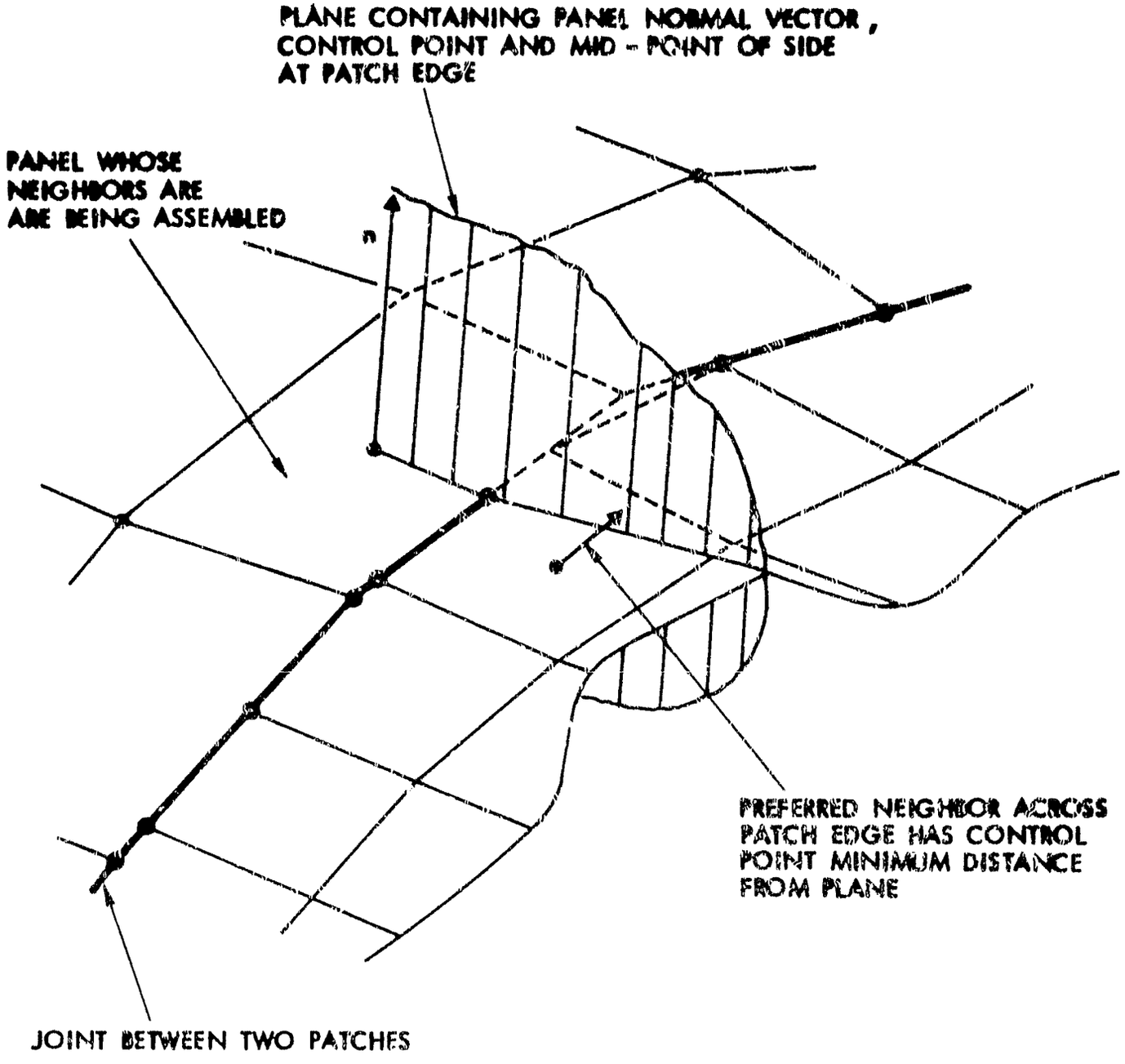

Figure 33. Panel Neighbors Across Patch Edges.

5.4.4 Subpanel Usage

Two extremes of subpanel usage are illustrated in Figure 32; on the left of the figure, panel size is fixed as subpanel density (i.e., number of subpanels per panel) is increased, while on the right, subpanel size remains constant as the density increases. For a given surface area, the former case keeps the number of panels (and, hence, unknowns) constant as the subpanel representation becomes increasingly detailed, while on the right, the number of panels decreases rapidly with increasing subpanel density. In practice, we should fall between the two, but the potential savings in the number of unknowns, examined below, indicates we should perhaps lean towards the system on the right in Figure 34.

For the purpose of evaluating the potential savings in the number of unknowns for the system on the right, we consider a surface represented by a 105 x 105 system of subpanels. We then assemble these into panels having 1 x 1, 3 x 3, 5 x 5 and 7 x 7 subpanel arrays. Table 1 compares the corresponding number of unknowns with the number of influence coefficients (panel plus subpanel) evaluated for one velocity calculation. The latter assumes ten panels have their subpanel systems accessed. The table also compares the approximate storage requirement for the subpanel doublet multipliers (see 6.1) with that for the matrix of normal influence coefficients. The table shows the rapid reduction in the number of unknowns as the subpanel density increases with the major reduction occurring for the 3 x 3 scheme, i.e., 89% compared with 96% for the 5 x 5 system. The corresponding reduction in number of influence coefficient evaluations when going from the basic panels (i.e., the 1 x 1 system) follows a similar trend; the 3 x 3 system offers an 88% reduction compared with a 94% reduction for the 5 x 5 scheme. Going to higher subpanel densities than this decreases the benefits because of the high number of subpanels involved with the assumed 10-panel near-field set.

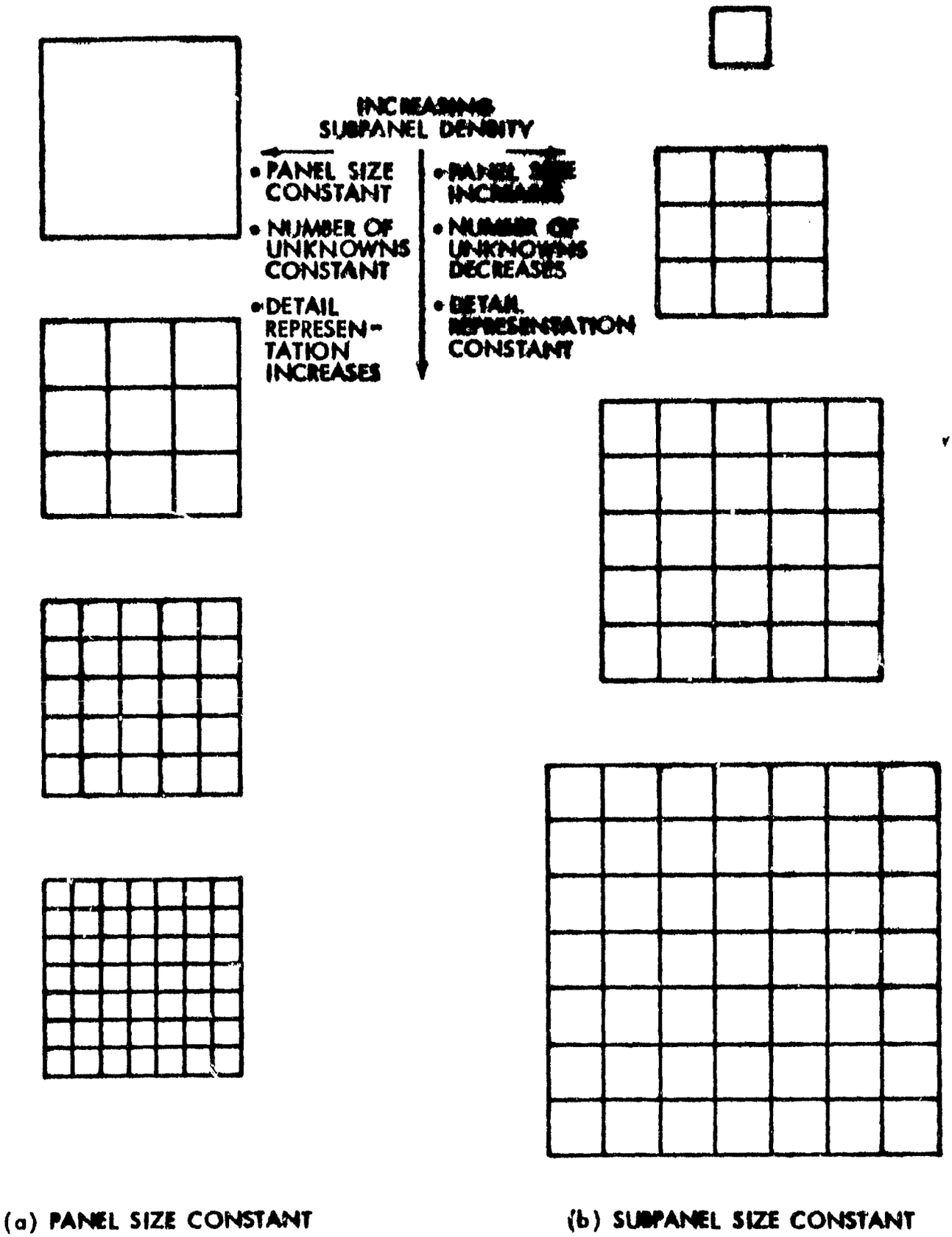

Figure 34. Extremes of Subpanel Usage.

SUBPANEL SCHEME	1 x 1 (panels only)	3 x 3	5 x 5	7 x 7
Number of Panels (Unknowns)	11,025	1,225	441	225
Number of Influence Coefficient Evaluations per Velocity Point	11,025	1,305	681	705
Approximate Storage for Subpanel Doublet Multipliers	0	99,225	127,500	140,800
Storage for Matrix of Influence Coefficients	122×10^6	1.5×10^6	192,000	50,000

TABLE I. Effect of Increasing Subpanel Density in a Basic 105 x 105 Panel Scheme Assuming the Figure 4 (b) System.

The additional storage needed for the subpanel doublet multiplier is clearly insignificant in comparison with the savings in storage for the matrix of influence coefficients.

These comparisons are based on a simplified arrangement and should be regarded only as a rough guide. Even so, there is an obvious attraction to use a 3 x 3 system and little point in going to 7 x 7 densities or higher. For this reason the new coding has an upper limit at the 5 x 5 subpanel scheme.

5.5 Wake Routines

5.5.1 Initial Wake Geometry

Wakes are formed after all the surface patches have been paneled and the neighbor information stored. The user identifies strings of WAKE-SHEDDING PANELS, the side geometry of which defines the FIXED BASELINE of each wake. At the end of each string of wake-shedding panels, the user has the option of defining the initial (i.e., prior to wake relaxation) streamwise geometry of a line on the near-wake (4.2) using a set of BASIC WAKE POINTS. The function of these points is similar to that of basic points defining chordwise sections on patches (5.2.2). Node cards are used here also and allow the user to select wake panel density and form of distribution in accordance with the expected location of the relaxed wake; in this way, wake panel detail may be used efficiently in relation to the expected wake curvature and surface interference. As a minimum, one basic wake point must be provided on each streamwise line defined--this point corresponds to the downstream end of the near-wake. (The upstream end is taken automatically from the fixed base line.) Multiple basic wake points are essential only in the case of multiple high-lift devices and allow a representative initial wake geometry to be defined which should reduce the number of wake shape iterations later in the calculations. Figure 35 illustrates the case of a wing with slat and slotted

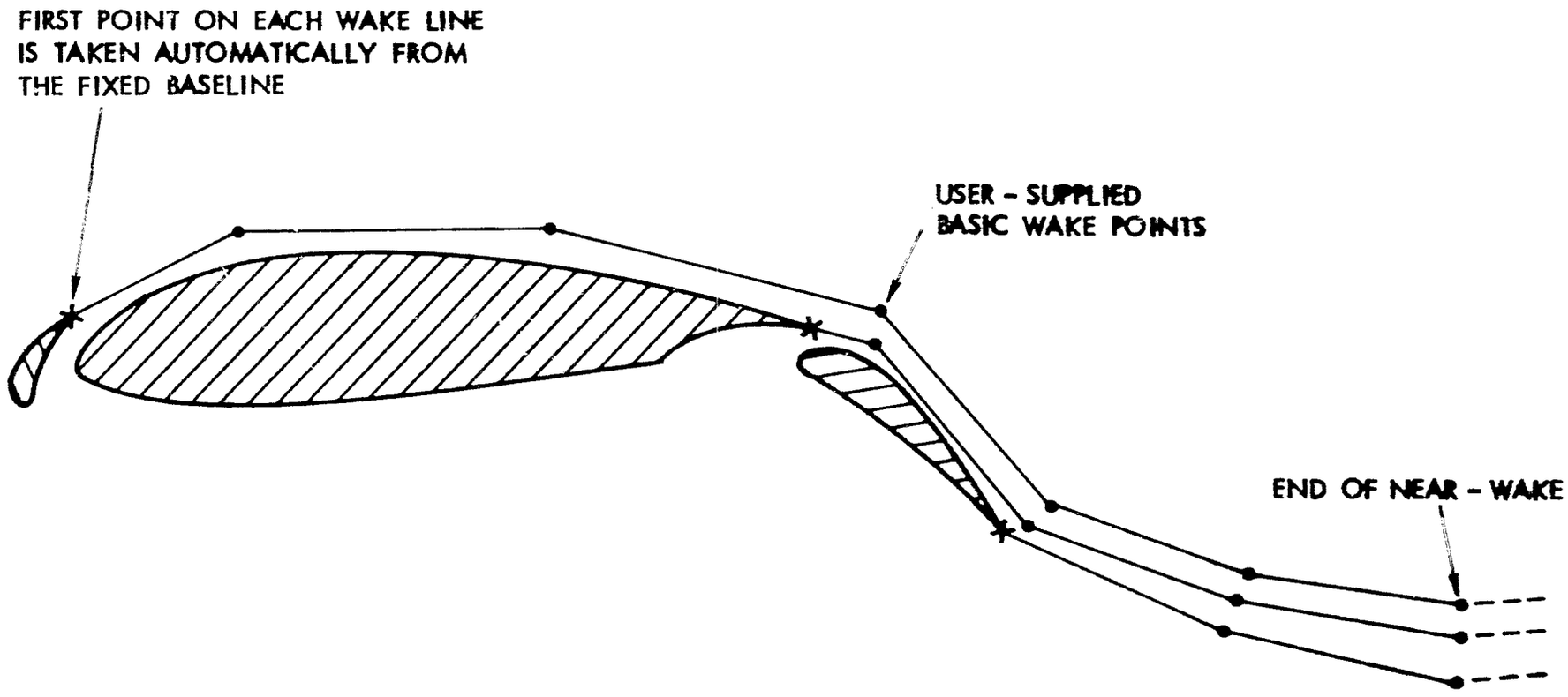

Figure 35. Basic Wake Points Define Initial Wake Streamwise Geometry.

flap and shows a typical set of basic wake points.

When the basic wake information has been supplied, the program generates streamwise sets of wake panel corner points according to the user's instructions on the node cards. A set of points is generated corresponding to each wake-shedding panel corner point on the fixed baseline and ends at the downstream edge of the near wake. Linear interpolation is used in both streamwise (between basic points) and spanwise (between streamwise lines) directions for the purpose of generating these initial sets of wake panel corner points. The user should bear this in mind when selecting the number and location of both basic points and streamwise lines. It must be emphasized, however, that this information is used only to define the preliminary wake for the purpose of the first solution--thereafter, the wake relaxation routine will redefine the wake geometry at each iteration.

5.5.2 Wake Panels and Subpanels

The program processes the streamwise sets of wake panel corner points and generates subpanel corner points using two-way biquadratic interpolation. Wake panel and subpanel parameters are then formed as in the case of surface patches (5.4.2). Although there is an obvious similarity between a patch and a wake, the doublet distribution on the latter is less complicated as it is constant along the (streamwise) columns. Doublet multipliers (see later in 6.1) associated with wake subpanels are therefore dependent only on the spanwise geometry, which changes with each wake relaxation iteration.

The doublet value on each column of wake panels is the difference between the values on the corresponding wake-shedding panel and its neighbor across the shedding line. This neighbor relationship across the shedding line is terminated once the wake has been formed, the doublet distribution then passes smoothly onto the wake from both sides of the shedding line.

5.5.3 Wake Relaxation

After the initial processing of the input, each near-wake shape is always stored in the form of the streamwise sets of wake panel corner points. After a doublet solution has been obtained, velocities are calculated at each of these points, Figure 36. Each set of points is then relaxed into the local flow direction as defined by the local velocity vectors. These calculations proceed from the (fixed) first point in each set and finish at the downstream end of the near-wake.

Based on the new sets of points, wake panels and subpanels are regenerated after each wake relaxation. The wake doublet values are assumed to move with the center subpanel in each wake panel. In this way the stretching and contraction of the wake affects the vorticity level when the spanwise gradient of the doublet distribution is evaluated.

C-2

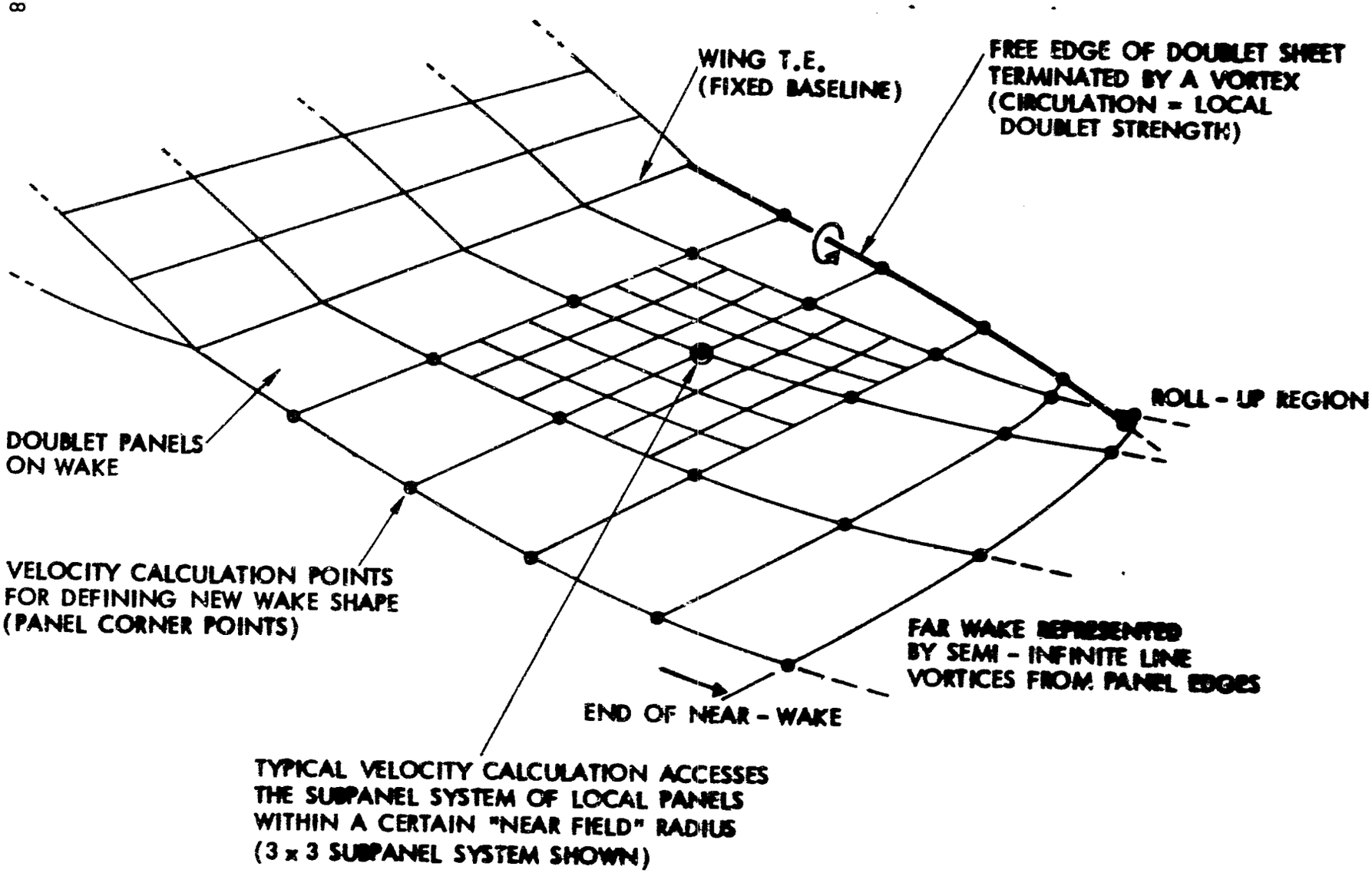

Figure 36. Wake Relaxation.

6.0 SURFACE DOUBLET DISTRIBUTION

6.1 Doublet Multipliers

In order to evaluate the doublet values at subpanel centers, we form a two-way biquadratic interpolation through neighboring panel doublet values. The interpolation is based on surface distances, p, q, respectively in the chordwise and spanwise directions over each patch. Surface distances are normalised to α, β, respectively, using local intervals between control points, Figure 37(a). Intervals in p and q are evaluated on the basis of straight-line distance across subpanels, i.e., by using the stored SM_p, SM_q information (5.4.2). The two-way biquadratic scheme requires a 4 x 4 set of panels for interpolation within the central area, Figure 37(a). One 4 x 4 set, however, only covers one quarter of the panel; four such sets are, therefore, required to cover all the subpanels on a panel. Since the four sets overlap they can be selected from a 5 x 5 panel set having the panel at the center, Figure 37(b), i.e., within this 25-panel set, the panel itself is always at location 13. with this arrangement, the selection of panel sets for subpanels within each panel follows a common rule throughout the configuration. Not all the subpanels require a 4 x 4 panel set to define their doublet value; a subpanel which lies on a grid line joining panel control points requires only 4 panels; for example, with the 3 x 3 subpanel scheme shown in Figure 37(b), subpanel number 3 is related to panels at locations 3, 8, 13, and 18. In particular, the middle subpanel takes the panel doublet value so it has just one multiplier which has unit value.

The doublet value at location α, β is given by

$$\mu(\alpha,\beta) = \sum_{\substack{i=1,4 \\ j=1,4}} \mu_{ij} D_{ij} \qquad (14)$$

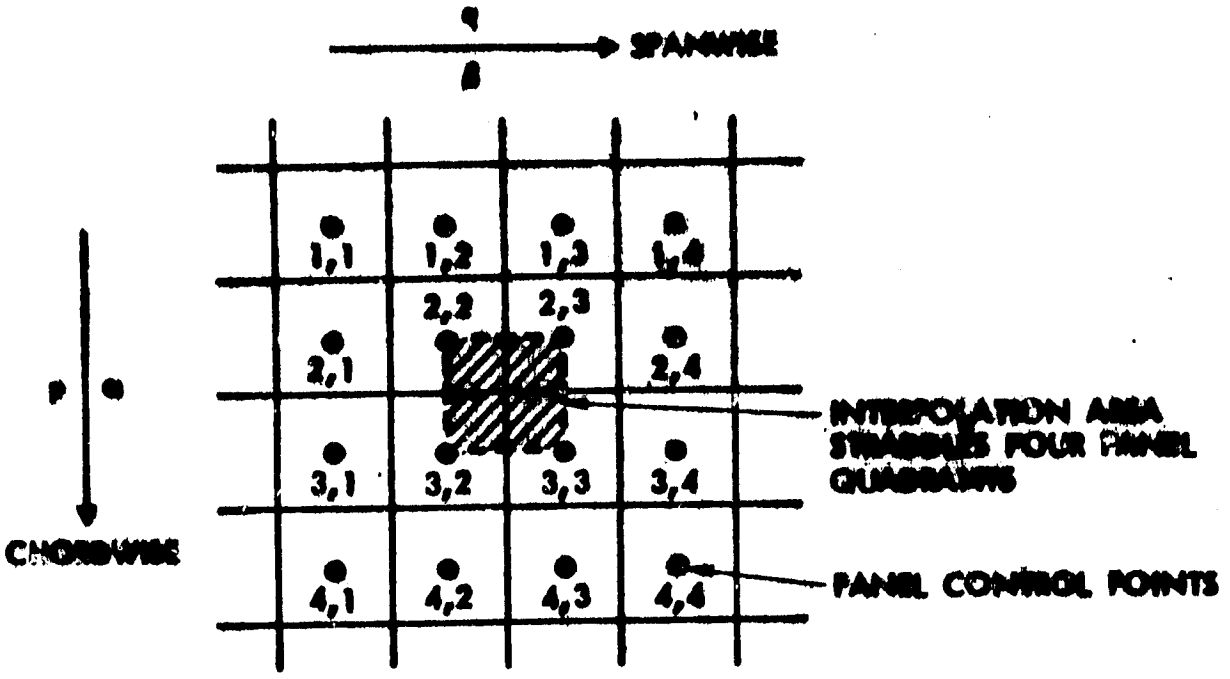

(a) LOCAL 4 x 4 PANEL SYSTEM

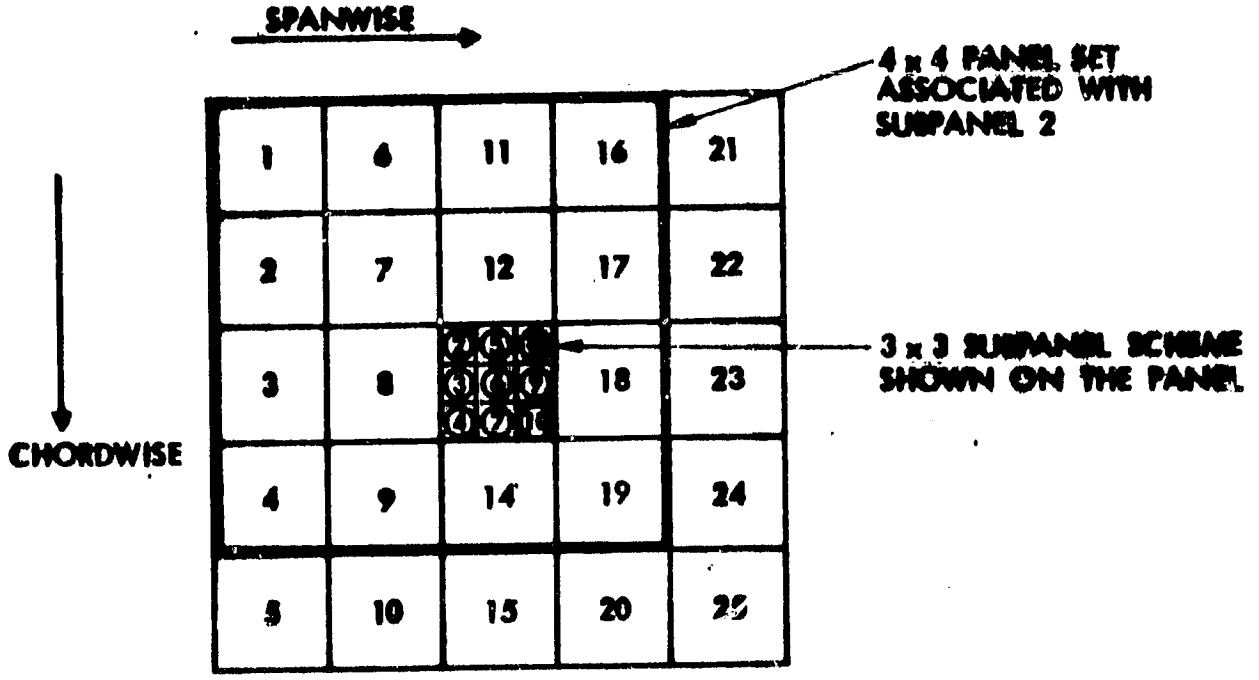

(b) THE PANEL'S 25 - PANEL SET

Figure 37. Two-Way Biquadratic Interpolation for Subpanel Doublet Values.

where i and j refer, respectively, to the row and column numbers in the 4 x 4 panel set and D_{ij} are the doublet multipliers evaluated at α, β and are given by

$$D_{ij} = d_{ij}\, e_{ij} \tag{15}$$

(This is a simplified scheme which may give distortions in extremely irregular grid patterns--an alternative, more rigorous (but also more complicated) scheme is held in reserve should the simple scheme fail.)

The d_{ij} and e_{ij} are the column-wise and row-wise biquadratic multipliers, respectively, evaluated as follows:

first define $$\alpha_{1j} = -\Delta p_{1_j} \Big/ \Delta p_{2_j} \tag{16}$$

$$\alpha_{2j} = (\Delta p_{2_j} + \Delta p_{3_j}) \Big/ \Delta p_{2_j} \tag{17}$$

where $\Delta p_{ij} = p_{i+1,j} - p_{ij}$ are the surface length increments; hence,

$$d_{1j} = G1(\alpha, \alpha_{1_j}); \quad d_{2j} = G2(\alpha, \alpha_{1_j}, \alpha_{2_j}); \tag{18}$$

$$d_{3j} = G2(1 - \alpha,\ 1 - \alpha_{2_j},\ 1 - \alpha_{1_j}); \tag{19}$$

$$d_{4j} = G1(1 - \alpha,\ 1 - \alpha_{2_j}); \tag{20}$$

with G1 and G2 being the general biquadratic multipliers (Appendix A). Similarly, in the β direction

$$\beta_{i1} = -\Delta q_{i1} \Big/ \Delta q_{i2} \tag{21}$$

$$\beta_{i2} = (\Delta q_{i2} + \Delta q_{i3}) \Big/ \Delta q_{i2} \tag{22}$$

Hence,

$$e_{i1} = G1(\beta,\beta_{i1});\ e_{i2} = G2(\beta,\beta_{i1},\beta_{i2});\tag{23}$$

$$e_{i3} = G2(1-\beta,\ 1-\beta_{i2},\ 1-\beta_{i1});\tag{24}$$

$$e_{i4} = G1(1-\beta,\ 1-\beta_{i2}).\tag{25}$$

At the beginning of the calculation, the panel doublet values, μ_{ij} (solution part) are unknown and so the subpanel doublet multipliers, D_{ij}, must be stored to be later applied to subpanel influence coefficients (6.3.3).

6.2 Augmented Patch

To facilitate the collection of the 25-panel sets in a regular manner without problems at patch edges, an AUGMENTED PATCH is temporarily formed for each patch in turn. The augmented patch has a two-panel deep fringes of panels surrounding the basic patch, Figure 38. The fringe panels are assembled from the neighboring panel information and the complete set of panels and grid distances, p, q, are formed for the entire augmented patch. Each panel in the basic patch can then quickly locate its 25-panel set together with the grid distances, even if it is a one-panel patch.

In forming grid line distances within the fringe areas, the orientation of the neighboring panels must be considered. Four panel sides and the panel polarity (4.5.3) lead to eight possible orientations of a neighboring panel across a patch side. All these possibilities are covered by the coding, but, further refinement is needed when evaluating surface distances in the fringe area in cases where there is a large mismatch in the neighboring panel alignments.

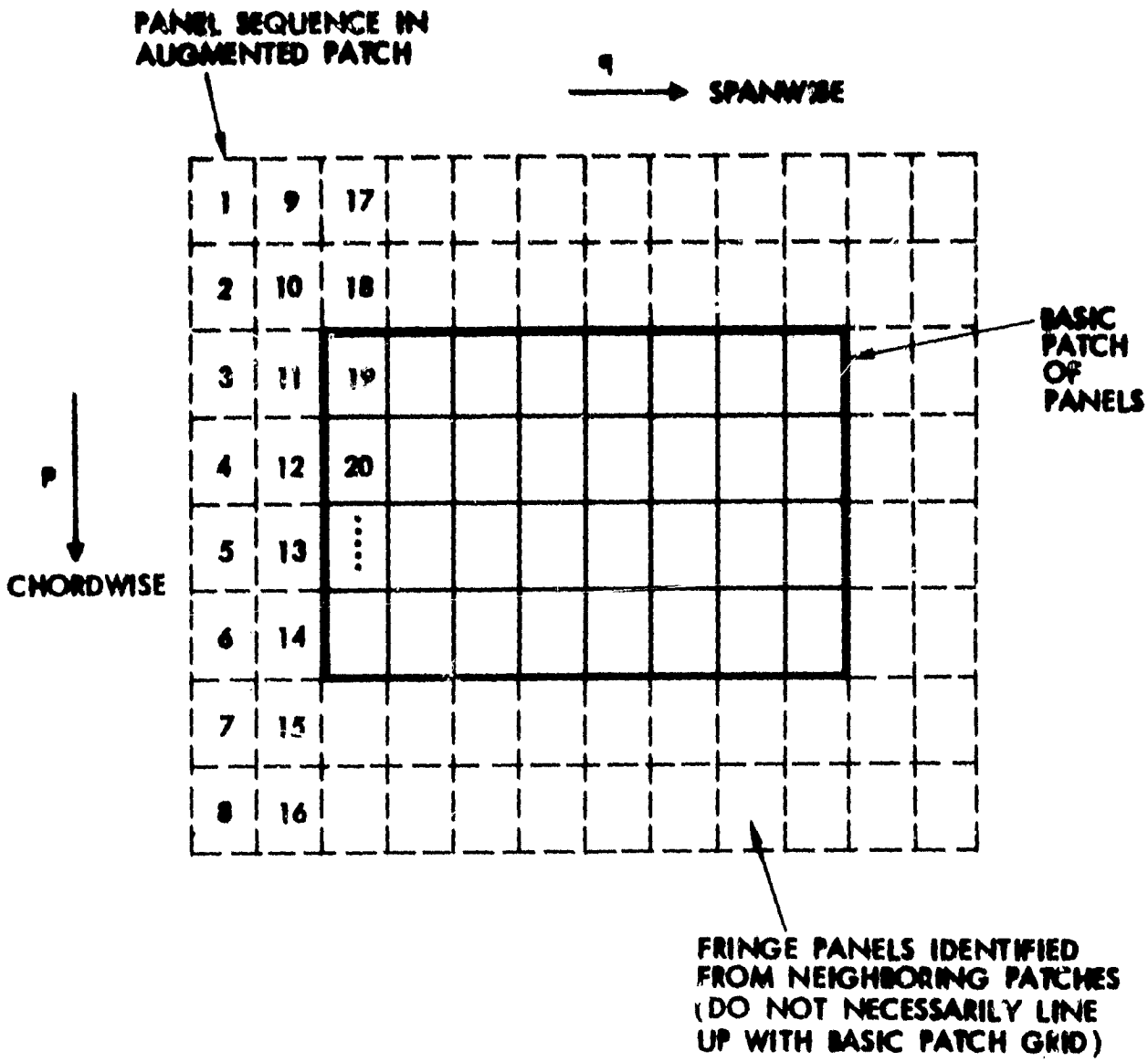

Figure 38. Augmented Patch Scheme for Doublet Interpolation.

6.3 Influence Coefficient

The influence coefficient routine for the doublet singularity model is arranged in three parts for application in far-field, middle-field or near-field velocity calculations. So far, the distances to the boundary of each of these regions has not been fully explored, but approximate guidelines are indicated below. These distances, which are measured from the panel control point, are given in terms of panel "size"; this is defined as the square root of the panel area at this time.

6.3.1 Far-Field

In the far-field, say beyond ten panel sizes away, the doublet distribution on a panel is regarded as piecewise constant. The influence coefficient is then that of a quadrilateral vortex defined by the panel's four corner points. The vortex strength, Γ, is the same as the panel doublet value. The velocity induced by each of the four sides of the quadrilateral vortex is obtained from the Biot Savart law:

$$\underline{v} = \frac{\Gamma}{4\pi} \underline{a} \wedge \underline{b}(a + b)/\{ab(ab + \underline{a} \cdot \underline{b})\} \qquad (26)$$

where $a \equiv |\underline{a}|$, etc.

where $\underline{a}$ and $\underline{b}$ are the position vectors of the velocity calculation point relative to the start, and, respectively, of the straight line segment. The lengths of these vectors are denotated by a and b, respectively.

The form of the induced velocity expression, which was developed during the course of this work (Appendix F), eliminates the numerical problem associated with earlier forms when calculating a velocity close to the extended line of the vortex. The new expression passes correctly through zero without special treatment for this condition.

6.3.2 Middle Field

Between, say, three and ten panel sizes away, a panel is regarded as having a two-way linear vorticity distribution. The vorticity value and slope are derived from the doublet distribution by passing quadratic curves in the p and q directions through the neighboring panel doublet values, Figure 39(a).

Using the nomenclature shown in Figure 39(a), the gradient and second derivative of the quadratic curves in the p and q directions are evaluated at the panel center as follows:

$$\frac{\partial \mu}{\partial p} = \left\{ \mu_B \, \Delta p_D \Big/ (\Delta p_D + \Delta p_B) - \mu_M (\Delta p_D - \Delta p_B) \Big/ \Delta p_D \right\} \Big/ \Delta p_B$$

$$- \mu_D \, \Delta p_B \Big/ \left\{ \Delta p_D (\Delta p_D + \Delta p_B) \right\} \tag{27}$$

$$\frac{\partial^2 \mu}{\partial p^2} = 2 \left\{ (\mu_D / \Delta p_D + \mu_B / \Delta p_B) \Big/ (\Delta p_D + \Delta p_B) \right.$$

$$\left. - \mu_M \Big/ (\Delta p_D \, \Delta p_B) \right\} \tag{28}$$

$$\frac{\partial \mu}{\partial q} = \left\{ \mu_C \, \Delta q_A \Big/ (\Delta q_A + \Delta q_C) - \mu_M (\Delta q_A - \Delta q_C) \Big/ \Delta q_A \right\} \Big/ \Delta q_C$$

$$- \mu_A \, \Delta q_C \Big/ \left\{ \Delta q_A (\Delta q_A + \Delta q_C) \right\} \tag{29}$$

$$\frac{\partial^2 \mu}{\partial q^2} = 2 \left\{ (\mu_A / \Delta q_A + \mu_C / \Delta q_C) \Big/ (\Delta q_A + \Delta q_C) \right.$$

$$\left. - \mu_M \Big/ (\Delta q_A \, \Delta q_C) \right\} \tag{30}$$

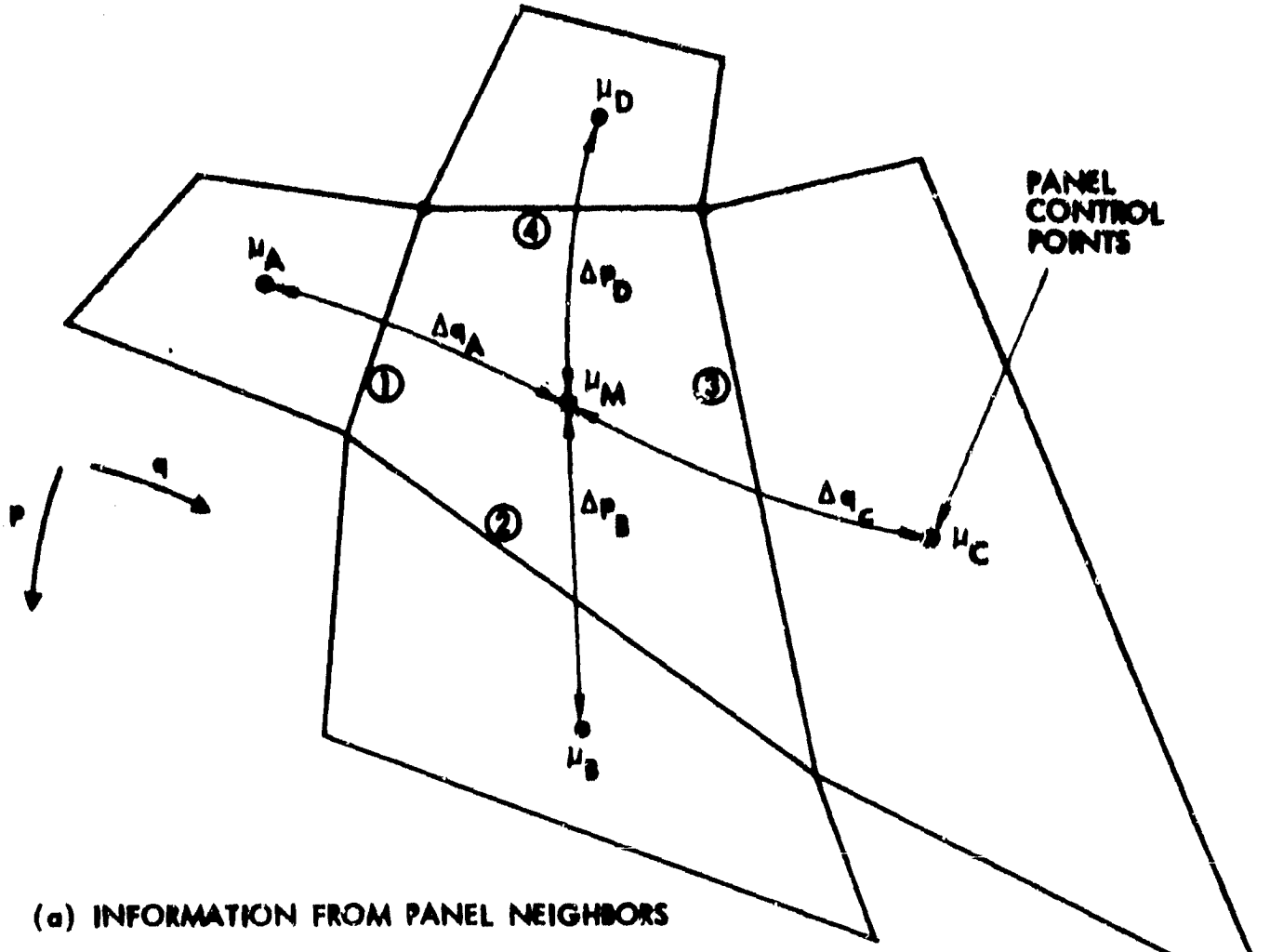

(a) INFORMATION FROM PANEL NEIGHBORS

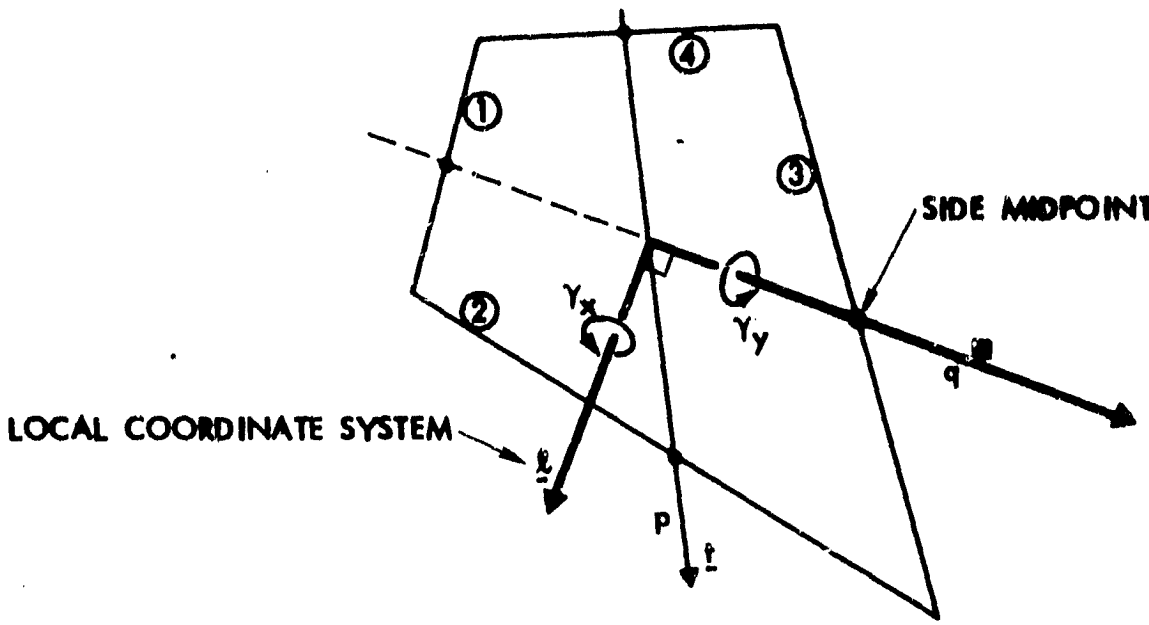

(b) PANEL VORTICITY COMPONENTS

Figure 39. Evaluation of Vorticity Value and Gradient on a Panel.

The vorticity components in the panel's local coordinate system (see Figure 39(b)) are obtained at the panel center:

$$\gamma_x = \frac{\partial \mu}{\partial q} \tag{31}$$

and

$$\gamma'_x = \frac{\partial^2 \mu}{\partial q^2} \qquad (\gamma_x \text{ gradient in the q direction}) \tag{32}$$

$$\gamma_y = \left\{ \frac{\partial \mu}{\partial q} \; \underline{m} \cdot \underline{t} - \frac{\partial \mu}{\partial p} \right\} \Big/ \underline{\ell} \cdot \underline{t} \tag{33}$$

and

$$\gamma'_y = \left\{ \frac{\partial^2 \mu}{\partial q^2} \; \underline{m} \cdot \underline{t} - \frac{\partial^2 \mu}{\partial p^2} \right\} \Big/ \underline{\ell} \cdot \underline{t} \tag{34}$$

Where $\underline{t}$ is the unit vector in the direction from the panel center to the midpoint of side 2.

The linear vorticity influence coefficient for the panel is accumulated by considering each side in turn, applying the model shown in Figure 40; for simplicity, this illustration and the following description are for the case of γ_x, but the γ_y value is treated in a similar way.

The basic linear vorticity model has two semi-infinite strips of opposing vorticity separated by a swept line (i.e., a panel side). The strips are aligned with the vorticity vector while the vorticity gradient is normal to that direction (Figure 40).

The velocity induced by the strip is

$$\underline{V} = \frac{1}{4\pi} \left\{ v\underline{m} + w\underline{n} \right\} \tag{35}$$

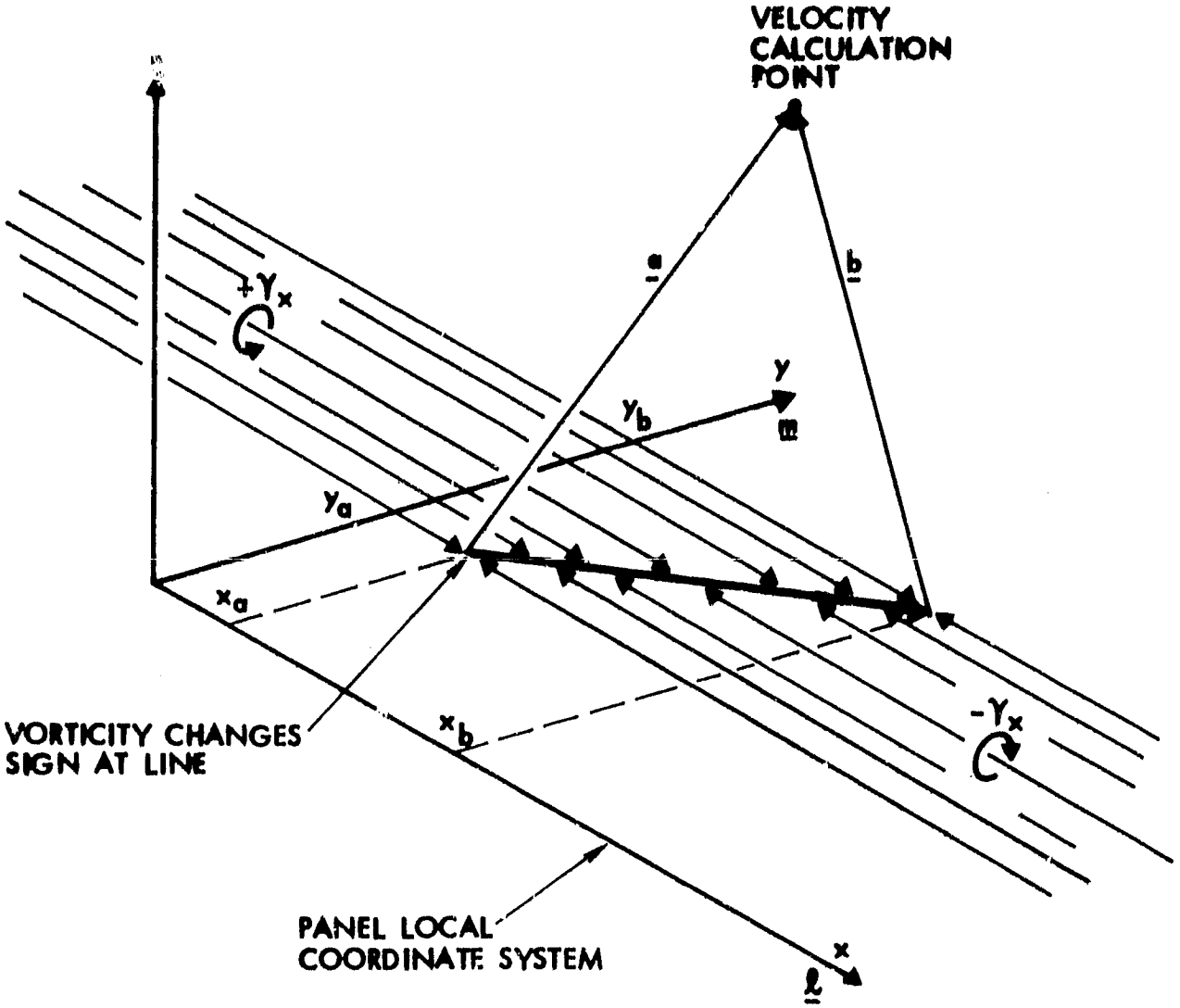

Figure 40. Basic Linear Vorticity Model (γ_x Component).

where

$$v = \gamma_{xl}\, T + \gamma'_x\, a_n (L - \lambda J)$$

and

$$w = \gamma_{xl}(L - \lambda J) - \gamma'_x \left\{ (a_1 J + \lambda (b - a)/e_3 + a_n T) \right\}$$

$$T = \tan^{-1} \left\{ a_n (a p_b - b p_a)/(p_a p_b + a_n^2\, ab) \right\}$$

$$J = \frac{1}{\sqrt{e_3}} \ell_n \left| (\sqrt{e_3}\, b - b_m - b_\ell)/(\sqrt{e_3}\, a - a_m - \lambda a_\ell) \right|$$

$$L = \tfrac{1}{2} \ell_n \left| (b - b_\ell)(a + a_\ell)/(b + b_\ell)/(a - a_\ell) \right|$$

$$p_a = \lambda (a_m^2 + a_n^2) - a_m\, a_\ell$$

$$p_b = \lambda (b_m^2 + a_n^2) - b_m\, b_\ell$$

$$\gamma_{xl} = \gamma_x + \gamma'_x (y_a + a_m)$$

$$e_3 = 1 + \lambda^2$$

$$a_1 = \lambda a_m - a_\ell$$

$$\lambda = (x_b - x_a)/y_b - y_a) \quad \text{-- slope of joint line}$$

a_ℓ, a_m, a_n, b_ℓ, b_m, b_n are the components of position vectors at a and b (Figure 40) in the panel's local coordinate system.

Applying this model to all the sides of a (closed) polygon causes the vorticity to reinforce (double) in the interior region and to cancel everywhere else. (The factor of 2 has been taken into account in the influence expression above.)

6.3.3 Near-Field

For velocity calculations within about three panel sizes from a panel's control point, the panel's subpanel set is accessed. (This includes the case for the influence of the panel on its own control point.) Each subpanel uses the linear vorticity model described in 6.3.2, except that here the vorticity value and slope are evaluated using neighboring subpanel doublet values rather than the panel values indicated in Figure 39.

As each subpanel's influence coefficient is evaluated, it is factored by its set of doublet multipliers (6.1) to get the corresponding contributions for the associated local panel set. These contributions are then accumulated in the matrix of influence coefficients.

7.0 TEST CASES

A number of preliminary tests have been carried out to check the working of the modified routines. Two of these cases are described below, but further tests need to be carried out, especially for general configurations. In particular, experimental data in part-span, high-lift devices is needed for comparison purposes to thoroughly check the code.

7.1 Geometry Code

As a preliminary check of the paneling capability, a general configuration was assembled having part-span, high-lift devices, Figure 41(a). Calculations for this case were terminated after the panels had been generated. The configuration consists of three separate COMPONENTS (limit is 10) represented by twelve PATCHES (limit is 100).

The slat is represented by three patches. Patch 1 covers the main slat surface--trailing edge through leading edge back to trailing edge, and root to tip. It is defined by two chordwise sections--one at the root, and one at the tip. The tip-edge Patches, 2 and 3, are generated automatically (5 ?.2) from the root and tip edges, respectively, of Patch 1. These two patches were specified to be flat. The option provided to generate a streamlined tip-edge patch is exercised on Patch 7--the wing tip; here, an automatic tip-edge patch was requested on the outboard edge of Panel 6, but the planform contour was described. The contour description is a set of points (any spacing and any scale) going from the trailing edge to the leading edge. The program generates tip-edge sections using semi-ellipses based on the local thickness of the basic patch edge (i.e., Patch 6), and the local offset of the tip contour planform (after internal scaling and interpolation).

Other flat-edge patch options are exercised on Patches 8, 9, 11, and 12. For patches 8 and 9, the partial section copying

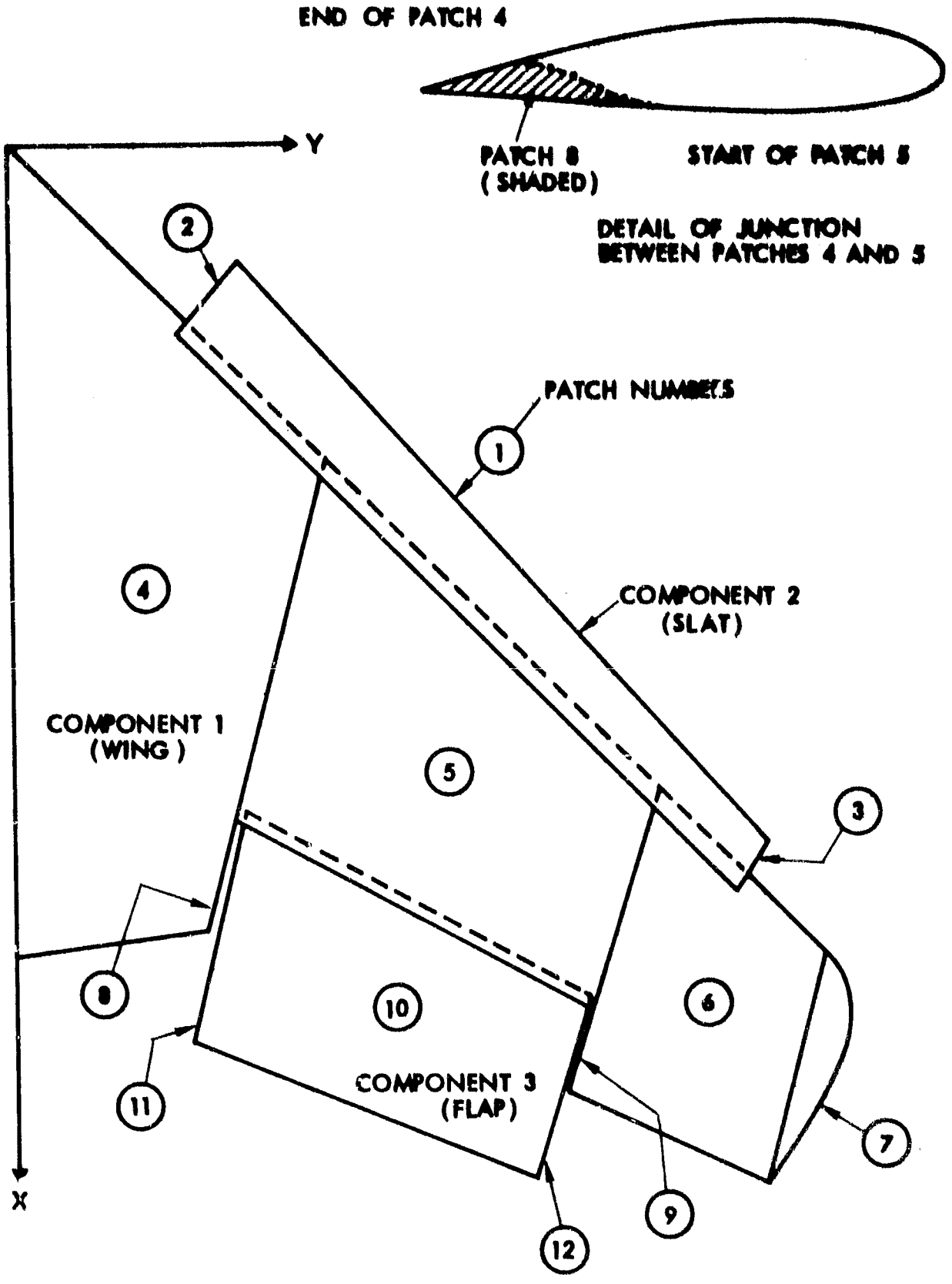

(a) WING PLANFORM INDICATING THE PATCHES OF PANELS ON THREE COMPONENTS

Figure 41. Tests for the Geometry Code.

option (5.3.2) was used; this special input requires 4 sets (one for each side of the new patch) of 4 integers. The four integers include the patch number, the section number on that patch, and the first and last point subscripts on that section which are to be copied for the new patch. A similar option is employed to define the first section of Patch 5: here, the majority of the section has already been defined on the last section of Patch 4. The first section of Patch 5 can, therefore, be defined by reading in seven new points (seven in this case) to define the cove contour (see the detail in Figure 41) followed by a copy (5.3.1) of the set of common points from Patch 4.

Figures 41(b) through 41(e) show plots of the panels and subpanels generated. Figure 41(b) shows the general view of the panels on the complete configuration and indicates the directions of detailed views shown in Figures 41(c), (d) and (e). Figure 41(c) gives the detail of panels and subpanels on the wing tip, Patch 7. The closer geometric representation offered by the subpanel scheme is obvious in this case. (Note: the control point conditions for each panel are taken from the central subpanel on that panel. Also, the panel influence on itself always uses its basic subpanel set.)

Figures 41(d) and 41(e) show similar details for Patches 10 and 11 and for Patch 8, respectively. Patch 9, at the outboard end of the flap cutout, is very similar to Patch 8.

7.2 Wing Case

The modified potential flow code was applied to a rectangular wing of aspect ratio 2 to check the routines through to the pressure calculation. The wing section was the 11.1% t/c, Boeing Section TR 17 and angle of attack 5.73^0. Figure 42(a) shows the chordwise pressure distribution at .125 semispan calculated using panels distributed in a 24 x 4 array on the main surface patch and a 2 x 12 array on a tip patch with semicircular

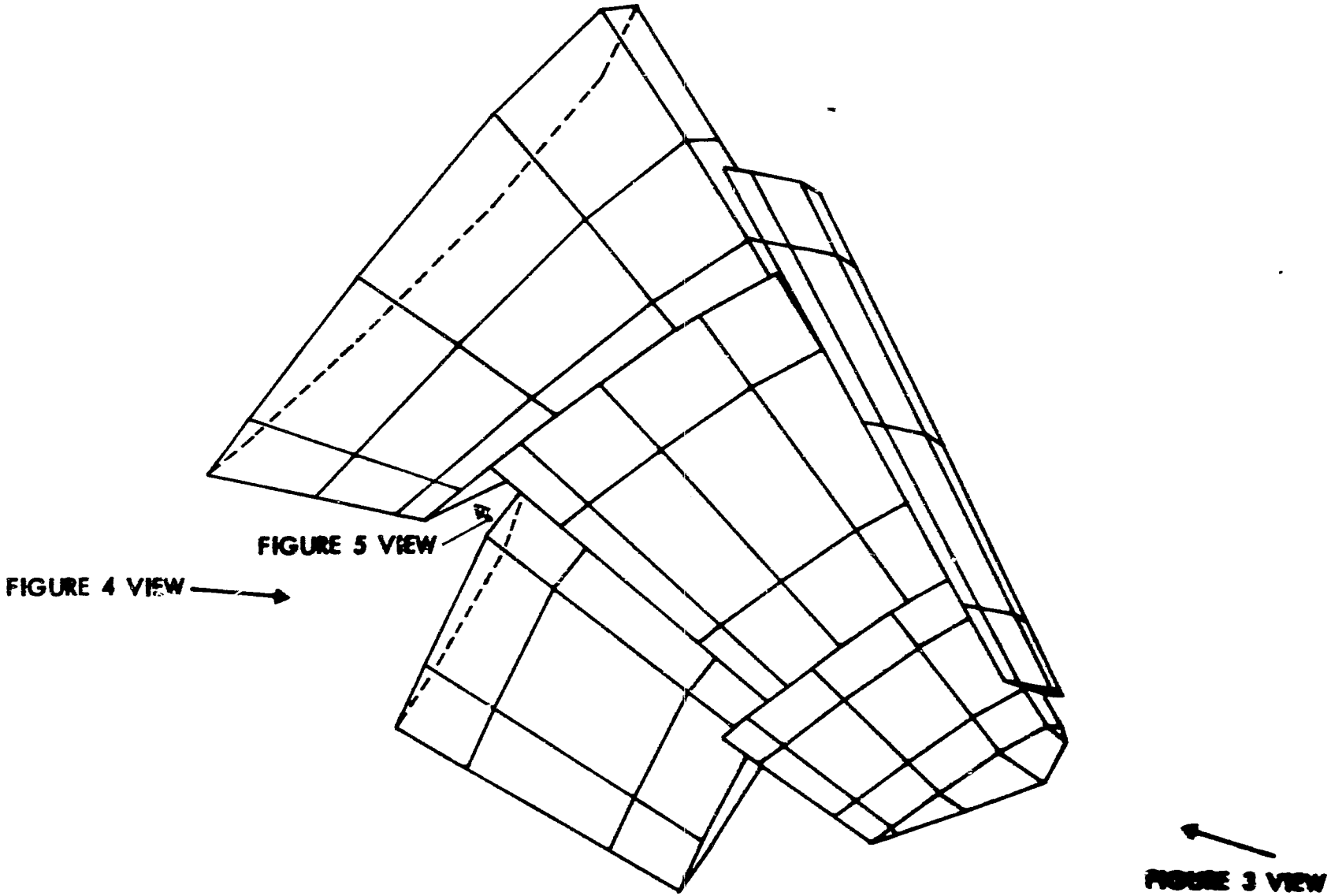

(b) GENERAL VIEWS OF PANELS

Figure 41. Continued.

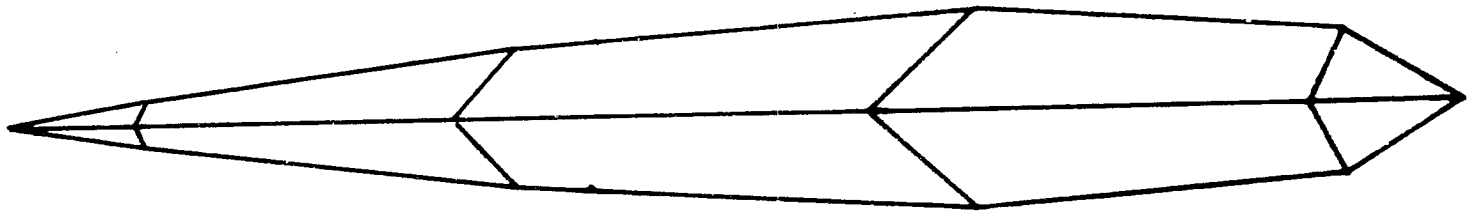

PANELS

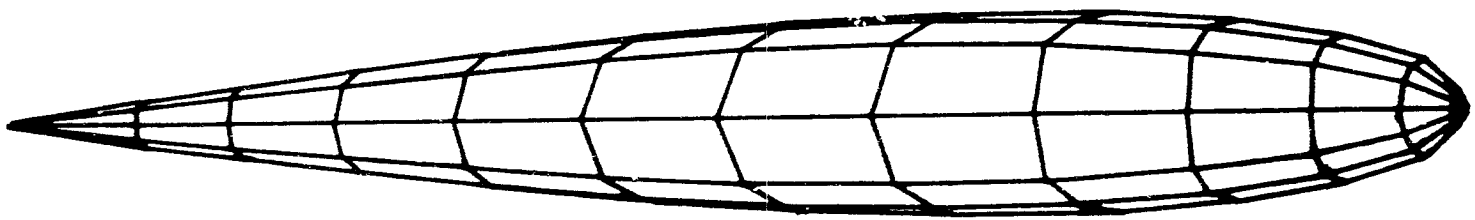

SUBPANELS (3 x 3 ON EACH PANEL)

(c) PANELS AND SUBPANELS ON THE TIP PATCH (PATCH 7)

Figure 41. Continued.

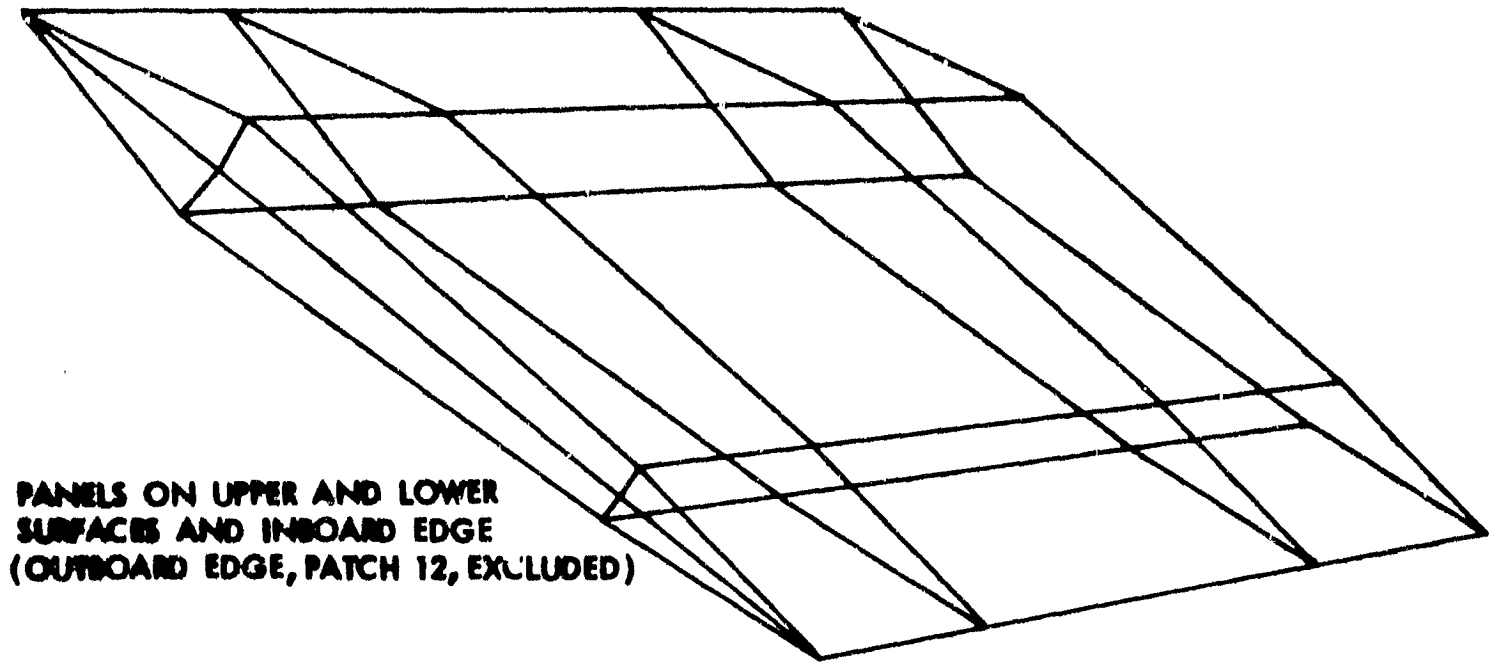

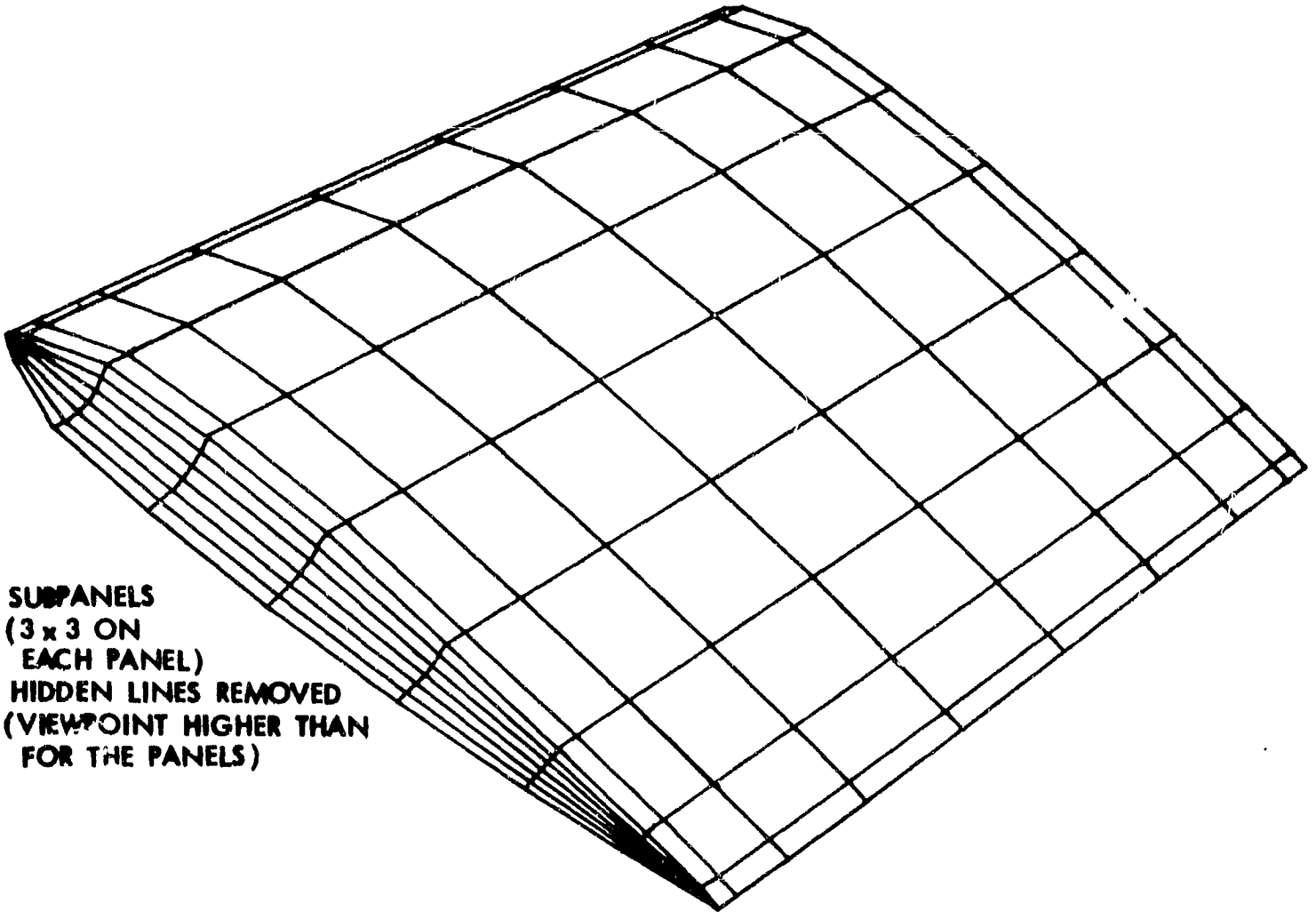

(d) PANELS AND SUBPANELS ON FLAP (PATCHES 10 AND 11 ONLY)

Figure 41. Continued.

(e) PANELS AND SUBPANELS ON EDGE OF FLAP CUTOUT ON WING MATCH 8

Figure 41. Concluded.

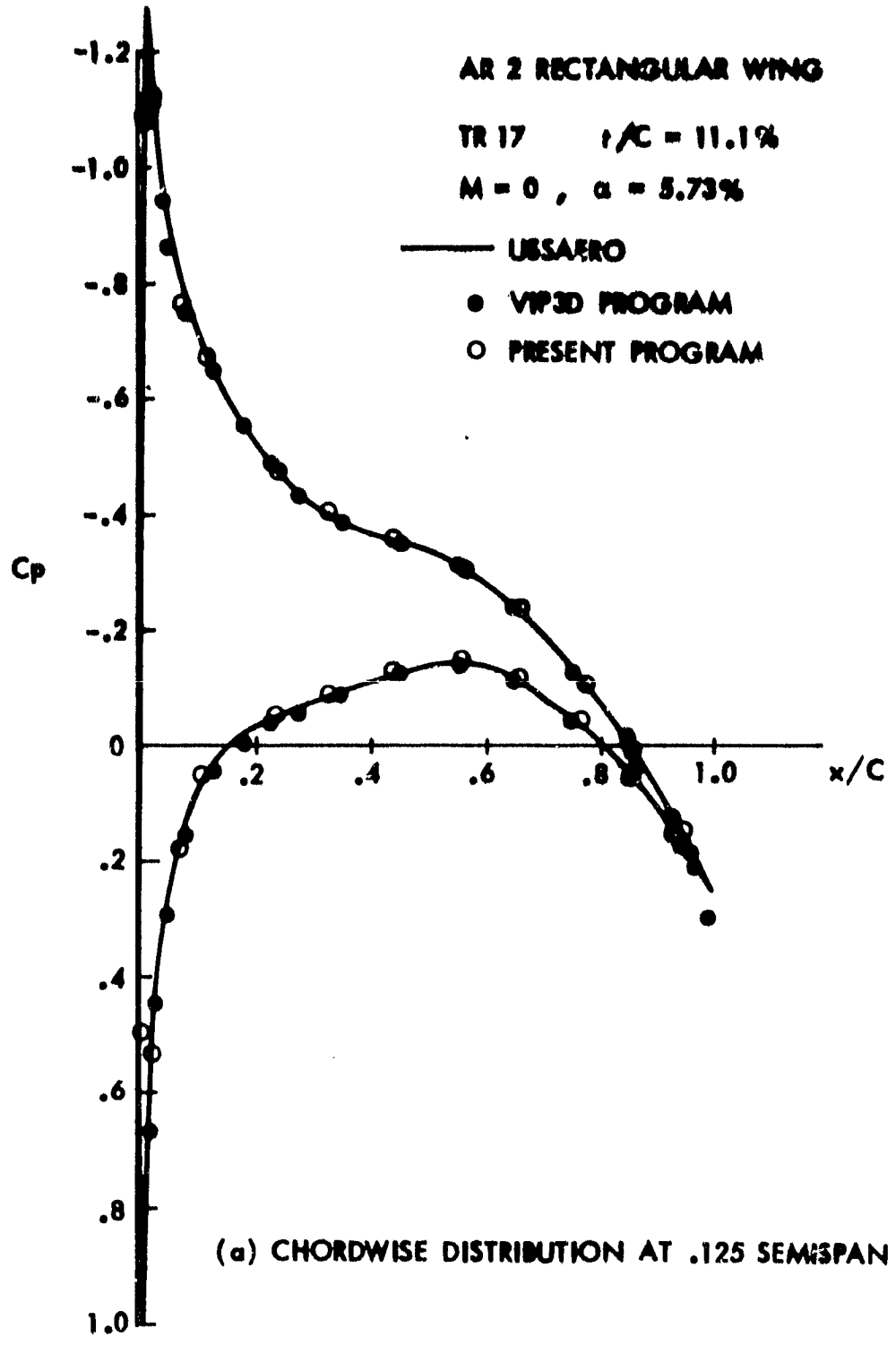

Figure 42. Rectangular Wing Pressure Distribution.

sections. For comparison, Figure 42(a) also shows solutions from the original VIP3D program (36 x 4 array) and also from the USSAERO program (Ref. 9). There is very close agreement between all three programs. This is very encouraging because the doublet solution used a less dense panel system than the others.

The tip patch paneling in the doublet model allows pressures to be calculated round the tip edge. Figure 42(b) shows pressure distributions plotted in the spanwise direction from lower surface round the tip and back along the upper surface at x-wise stations .0086 and .889. Values are plotted from two panel distributions, one with 4 equal spanwise intervals and one with 6 spanwise intervals with cosine distribution giving increased density towards the tip. The latter improves the matching in panel size between the main surface and tip patch compared with the first case which has panel size ratios of the order 50 passing onto the tip patch; this probably accounts for the discrepancies between the two solutions near the tip in Figure 42(b). Large and sudden changes in interval size can cause numerical error when interpolating or differentiating the surface doublet distribution.

At the forward station, the spanwise flow from lower surface onto upper surface clearly has a monotonically decreasing pressure. Towards the trailing edge, however, the upper surface suction level has disappeared while a peak suction has developed on the tip surface, Figure 42(b). At this station, therefore, the spanwise flow is suddenly faced with a strong adverse pressure gradient as it climbs round the tip edge and will lead to the conditions for tip edge separation.

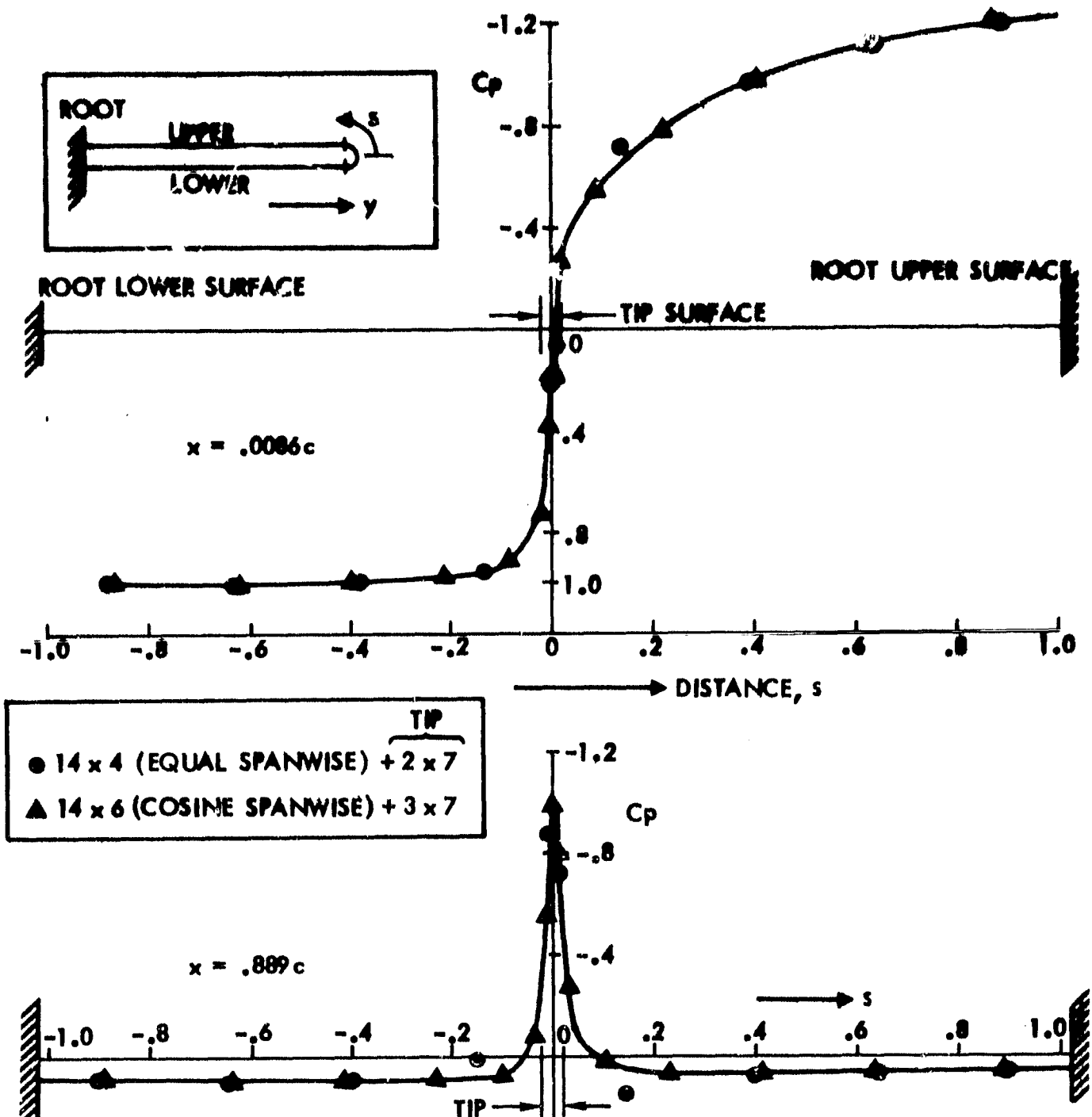

(b) SPANWISE DISTRIBUTION AT x = .0086c AND .889c

Figure 42. Concluded.

8.0 CONCLUSIONS AND RECOMMENDATIONS

An investigation in two-dimensional flow demonstrated that a doublet subpanel technique has the required behavior for calculating interference pressures in a vortex/surface interaction case: the close-approach problems associated with earlier panel methods is essentially removed without increasing the panel density. Because the subpanel model provides a better representation of curved surfaces and smooth singularity distribution, it gives the effect of increased panel density without increasing the number of unknowns. Subpanels are accessed only on panels close to the velocity calculation point.

Results from preliminary test cases of the three-dimensional form of the doublet subpanel technique have been encouraging. The VIP3D geometry routines have been extensively modified to be compatible with the technique and also to allow application to general high-lift configurations. For this purpose a versatile, user-oriented scheme has been developed based on multiple patches of panels. Preliminary test calculations have shown very close agreement with solutions from the original VIP3D singularity model.

Further test cases need to be performed, but experimental measurements on general high-lift configurations are required having detailed pressure distributions and flow visualization. In particular, cases having part-span, high-lift devices need to be examined.

9.0 REFERENCES

1. Dvorak, F.A., Woodward, F.A., and Maskew, B., "A Three-Dimensional Viscous/Potential Flow Interaction Analysis Method for Multi-Element Wings", NASA CR-152012, July 1977.

2. Maskew, B., "On the Influence of Camber and Non-Planar Wake on the Airfoil Characteristics in Ground-Effect", TT 7112, Loughborough University of Technology, England, October 1971 (See also ARC 33950, 1973, Aero. Res. Council, London).

3. Maskew, B., "A Quadrilateral Vortex Method Applied to Configurations with High Circulation", NASA SP-405, Paper No. 10, May 1976, pp. 163-186.

4. Maskew, B., "Calculation of the Three-Dimensional Potential Flow Around Lifting Non-Planar Wings and Wing-Bodies Using a Surface Distribution of Quadrilateral Vortex Rings", TT 7009, Loughborough University of Technology, England, October 1972.

5. Maskew, B., "A Subvortex Technique for the Close-Approach to a Discretized Vortex Sheet", NASA TMX 63,487, September 1975 (See also J. Aircraft, Vol. 14, No. 2, February 1977, pp. 188-193).

6. Maskew, B., and Woodward, F.A., "Symmetrical Singularity Model for Lifting Potential Flow Analysis", J. Aircraft, Vol. 13, Number 9, September 1976, pp. 733-734.

7. Maskew, B., "A Submerged Singularity Method for Calculating Potential Flow Velocities at Arbitrary Near-Field Points", NASA TMX 73,115, March 1976.

8. Rossow, V.J., "Lift Enhancement by an Externally Trapped Vortex", J. Aircraft, Vol. 15, Number 9, September 1978, pp. 618-625 (Also a private communication).

9. Woodward, F.A., "An Improved Method for the Aerodynamic Analysis of Wing-Body-Tail Configurations in Subsonic and Supersonic Flow: Part I; Theory and Application", NASA CR-2228, May 1973.

10. Hornbeck, R.W., Numerical Methods, Quantum Publishers, Inc., New York, 1975, Chapter 8.

10.0 APPENDICES

A. Biquadratic Interpolation

The biquadratic interpolation scheme described below is applied in a number of routines in the new code. Its simple multiplier form is very convenient to use and yet it is a "constrained" cubic, i.e., it cannot oscillate wildly. Experience with the routine over a number of years in the codes of References 2 through 7 have shown it to be a reliable method.

Given a set of position vectors, $\underline{P}n$, n=1,2,...,N, defining a smooth space curve, we wish to interpolate for additional values in, say, the interval between $\underline{P}_n$ and $\underline{P}_{n+1}$, Figure A1. We first generate the integrated contour length, s_n, to each point from the beginning of the curve, i.e., from $\underline{P}_1$. For convenience, the straight segment length is used across each interval, i.e., $s_n = \left| \underline{P}_{n+1} - \underline{P}_n \right|$, but arc lengths could easily be substituted--or indeed, any other parameter that varies smoothly and monotonically along the curve, i.e., without introducing multiple value problems. For example, the point subscript interval is used in some parts of the program.

Next, we generate two quadratic curves: $\underline{q}_1(\alpha,\alpha_{1_n})$ passing through points $\underline{P}_{n-1}$, $\underline{P}_n$, $\underline{P}_{n+1}$, and $\underline{q}_2(\alpha,\alpha_{2_n})$ passing through points $\underline{P}_n$, $\underline{P}_{n+1}$, and $\underline{P}_{n+2}$, Figure A1.

The normalized interpolation parameter, α, ranges from 0 to 1 in the n^{th} interval, and has value

$$\alpha_{1_n} \text{ at } \underline{P}_{n-1} \quad \text{and} \quad \alpha_{2_n} \text{ at } \underline{P}_{n+2}$$

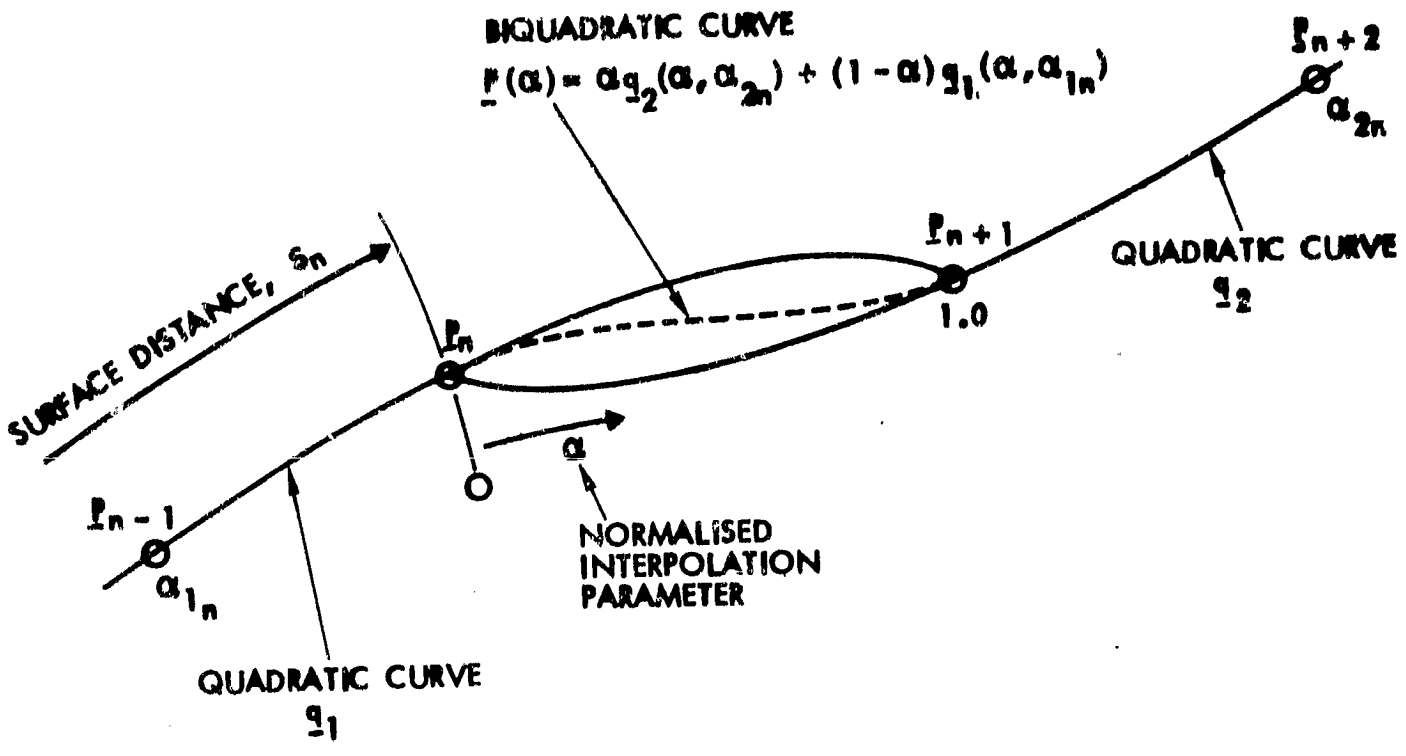

Figure A1. Biquadratic Interpolation.

where

$$\alpha_{1_n} = (s_{n-1} - s_n)/(s_{n+1} - s_n); \text{ and}$$

$$\alpha_{2_n} = (s_{n+2} - s_n)/(s_{n+1} - s_n).$$

In the n^{th} interval, we take a linear combination of $\underline{q}_1$ and $\underline{q}_2$ to define the biquadratic interpolation curve there:

$$\underline{\Gamma}(\alpha) = \alpha \underline{q}_2(\alpha,\alpha_{2_n}) + (1 - \alpha)\underline{q}_1(\alpha,\alpha_{1_n}).$$

The biquadratic is, therefore, a cubic, but it is constrained to lie between two quadratic curves. It can't therefore, behave wildly.

The value of α for a point distance, s, from the start of the curve (but located in the n^{th} interval) is

$$\alpha = s/(s_{n+1} - s_n).$$

The form of the interpolation curve can be expressed in terms of biquadratic multipliers, G1, G2, applied to the four local position vectors:

$$\underline{P}(\alpha) = \underline{P}_{n-1}\, G1(\alpha,\alpha_{1_n}) + \underline{P}_n\, G2(\alpha,\alpha_{1_n}, \alpha_{2_n})$$

$$+ \underline{P}_{n+1}\, G2(1 - \alpha, 1 - \alpha_{2_n}, 1 - \alpha_{1_n})$$

$$+ \underline{P}_{n+2}\, G1(1 - \alpha, 1 - \alpha_{2_n}).$$

The forms of G1, G2 are:

$$G1(a,b) = a(1 - a)^2/\{b(1 - b)\}$$

$$G2(a,b,c) = (1 - a)\{1 - a(1 - a)/b - a^2/c\} .$$

These multipliers, based on the linear combination of two quadratics, give continuous slope and a piecewise linear--but not necessarily continuous--variation of second derivative across each interval. A similar set of multipliers has been formed which gives continuous second derivatives, but it has not been thoroughly checked out at this time.

The G multipliers can be differentiated to give the tangent vector:

$$\underline{t}(\alpha) = \underline{P}_{n-1}\, H1(\alpha,\alpha_{1_n}) + \underline{P}_n\, H2(\alpha, \alpha_{1_n}, \alpha_{2_n})$$

$$- \underline{P}_{n+1}\, H2(1 - \alpha, 1 - \alpha_{2_n}, 1 - \alpha_{1_n})$$

$$- \underline{P}_{n+2}\, H1(1 - \alpha, 1 - \alpha_{2_n})$$

Where the tangent multipliers are:

$$H1(a,b) = (1 - 4a + 3a^2)/\{b(1 - b)\}$$

$$H2(a,b,c) = (4a - 3a^2 - 1)/b + (3a^2 - 2a)/c - 1$$

Note: this is not a unit vector; $\left|\underline{t}(\alpha)\right| = \frac{ds}{d\alpha}$.

The G multipliers can also be integrated to give the area under the curve between the n^{th} and $(n + 1)^{th}$ points:

$$\underline{A}_n = \left[\underline{P}_{n-1} \, F1(\alpha_{1_n}) + \underline{P}_n \, F2(\alpha_{1_n}, \alpha_{2_n}) \right.$$

$$\left. + \underline{P}_{n+1} \, F2(1 - \alpha_{2_n}, 1 - \alpha_{1_n}) + \underline{P}_{n+2} \, F1(1 - \alpha_{2_n}) \right] \frac{ds}{d\alpha}$$

where the integral multipliers are:

$$F1(b) = 1/\{12b(1 - b)\}$$

$$F2(b,c) = \{1 - (1/b + 1/c)/6\}/2$$

This assumes that the value of $\frac{ds}{d\alpha}$ is constant over the interval. In this case, therefore, it would be an advantage to use the arc length intervals rather than straight line intervals when calculating surface distances.

The F multipliers are used in the integration of surface pressures to obtain forces and moments.

B. Numerical Integration for Doublet Influence Coefficient

A doublet singularity can be regarded as the limiting condition when a source and sink of equal strength became coincident in such a way that the product of their strength and distance apart remains constant. This constant is the doublet strength, μ, and the unit vector, n, in the direction source-to-sink defines the axis of the doublet. The velocity induced by the point doublet is then

$$\underline{V} = \frac{\mu}{4\pi a^3} \left\{ \underline{n} - \frac{3\underline{a} \cdot \underline{n}\, \underline{a}}{a^2} \right\}$$

Where $\underline{a}$ is the position vector of the velocity calculation point relative to the doublet.

The velocity induced by a doublet distribution on a flat surface, Figure B1, has the form

$$\underline{V} = \frac{1}{4\pi} \iint \left\{ \underline{k} - \frac{3\underline{a}(\alpha,\beta) \cdot \underline{k}\ \ \underline{a}(\alpha,\beta)}{a^2(\alpha,\beta)} \right\} \frac{\mu(\alpha,\beta)\ d\beta d\alpha}{a^3(\alpha,\beta)}$$

where

$$a^2(\alpha,\beta) = r^2(\alpha,\beta) + z^2$$

and

$$r^2(\alpha,\beta) = (x - \alpha)^2 + (y - \beta)^2$$

The component of velocity normal to the surface has polar symmetry about the doublet axis, $\underline{k}$, and the integrand is

$$Iw(r) = \frac{r^2 - 2z^2}{\{r^2 + z^2\}^{5/2}}$$

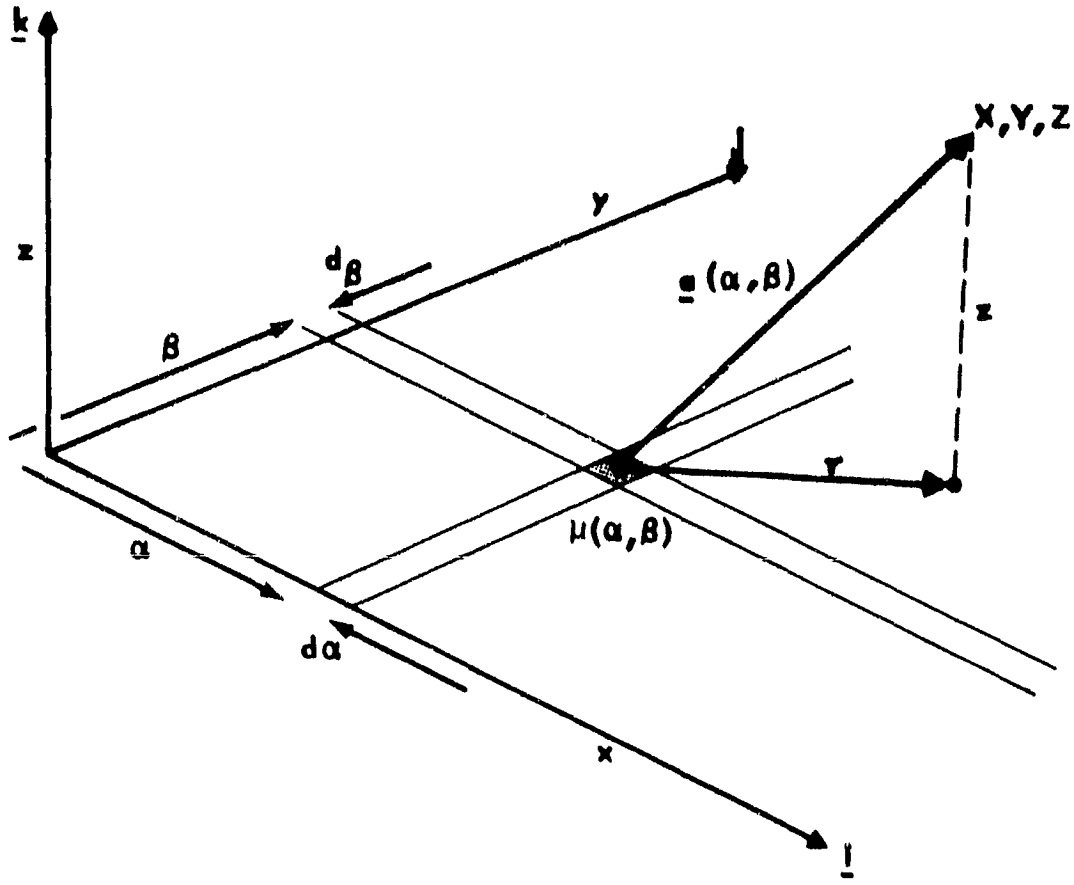

Figure B1. Nomenclature for the Doublet Integration.

This has the form illustrated in Figure B2(a). A number of interesting features can be evaluated.

The negative peak value occurring at r = 0 depends on the height, z, of the point above the sheet.

$$Iw(o) = \frac{-2}{z^3}$$

The radius at which Iw passes through zero is

$$r_1 = \sqrt{2}|z|$$

The secondary (positive) peak value is

$$Iw(r_2) = \frac{2}{5^{5/2} z^3}$$

and is located at

$$r_2 = 2|z|$$

It is important to note that both Iw(o) and $IW(r_2)$ go singular (in opposite directions) as z tends to zero.

The velocity component tangential to the sheet also has polar symmetry and is radial. The integrand for this has the form

$$Iv(r) = \frac{3zr}{(r^2 + z^2)^{5/2}}$$

which is illustrated in Figure B2(b).

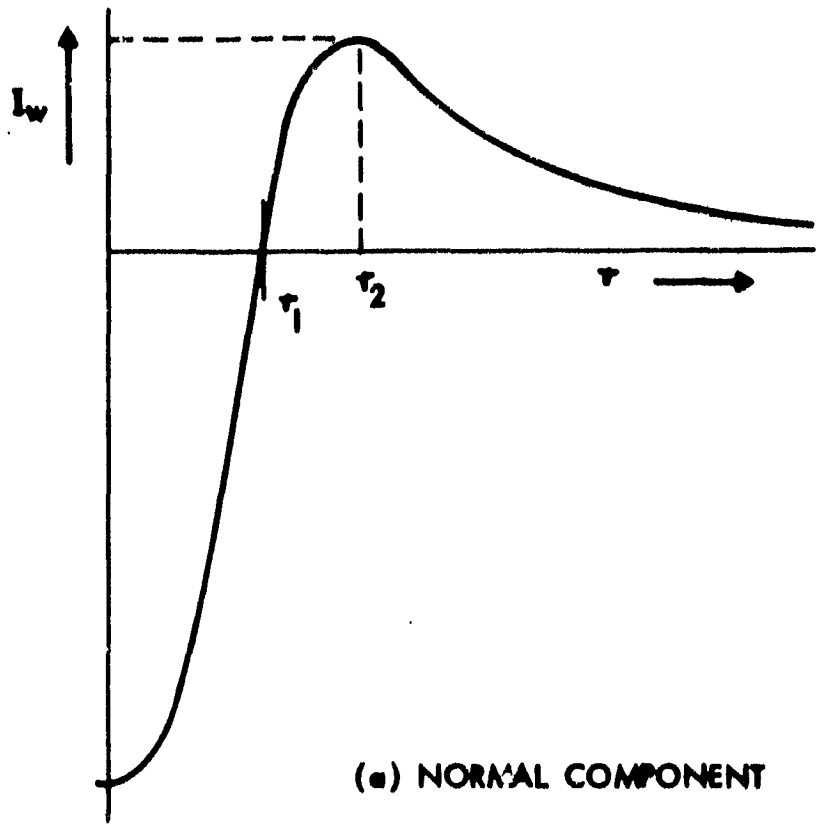

(a) NORMAL COMPONENT

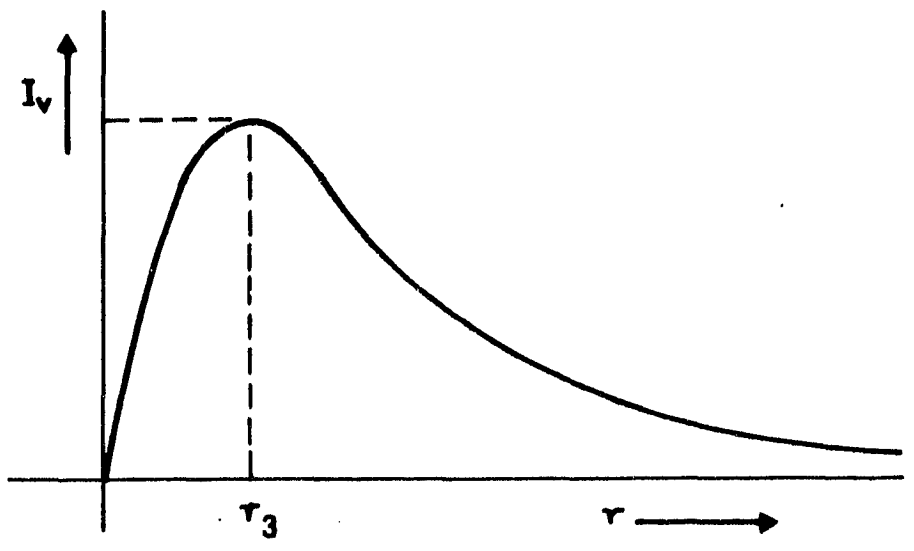

(b) TANGENTIAL COMPONENT

Figure B2. Behavior of the Doublet Integrand.

The peak value is

$$Iv(r_3) = \frac{48}{5^{5/2} z^3}$$

and occurs at

$$r_3 = |z|/2.$$

The locations of the peaks in both velocity components were used to define separate regions in which the Romberg integration technique, Reference 10, was applied. Transformations were applied in each region according to the local behavior of each integrand. The aim was to obtain a more linear variation across each region. This would allow the Romberg Integration technique to converge more rapidly since it is based on the trapezoidal rule.

C. Linear Vorticity Influence Coefficient in Two Dimensions

There are a number of two-dimensional potential flow codes based on linear vorticity panels; however, the influence coefficient used in the present work was formulated differently from earlier forms and is based on the panel center rather than the panel ends, Figure C1. This is more convenient when working with the surface doublet model.

The induced velocity is

$$\underline{V} = V_T \underline{t} + V_N \underline{n}$$

Where the velocity components tangential and normal to the panel are, respectively:

$$V_T = \frac{1}{2\pi} \gamma_o T + \gamma'(T a_t + L a_n)$$

$$V_N = \frac{1}{2\pi} \gamma_o L + \gamma'(s - T a_n + L a_t)$$

where γ_o and γ' are, respectively, the vorticity value and gradient at the panel center, and

$$T = \mathrm{Tan}^{-1} \; a_n s/(a^2 - .25s^2)$$

$$L = \tfrac{1}{2} L_n \left\{ (a^2 - a_t s + .25s^2)/(a^2 + a_t s + .25s^2) \right\}$$

$$a_t = \underline{a} \cdot \underline{t}$$

$$a_n = \underline{a} \cdot \underline{n}$$

and s is the panel length.

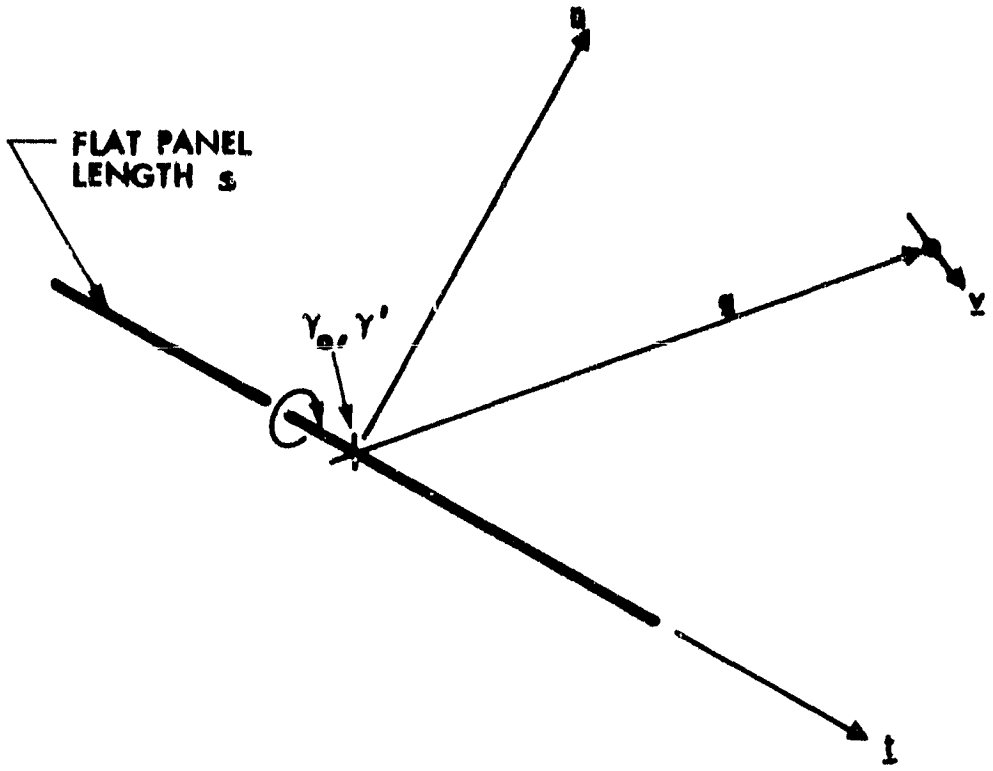

Figure C1. Linear Vorticity on a Flat Panel.

D. Neumann Boundary Condition Applied to a Surface Doublet Model

When the Neumann boundary condition is applied to a surface doublet distribution, the solution can diverge near the airfoil trailing edge. To find the source of the problem, we examine the simplified situation where the doublet sheets on the upper and lower surfaces are close to each other and are parallel, Figure D1. Consider the Neumann boundary condition applied to a control point on the upper surface. The major terms are

$$\tfrac{1}{2}(\mu_u - \mu_L) = V_N$$

Where μ_u, μ_L are the local upper and lower doublet values, respectively, and V_N is the local normal component of the onset flow.

Next, divide the doublet values into symmetrical and anti-symmetrical parts:

$$\mu_u = \mu_s + \mu_A$$

and

$$\mu_L = \mu_s - \mu_A$$

The equation above then becomes

$$\tfrac{1}{2}\left\{\mu_s + \mu_A - (\mu_s - \mu_A)\right\} = V_N$$

or

$$\mu_A = V_N$$

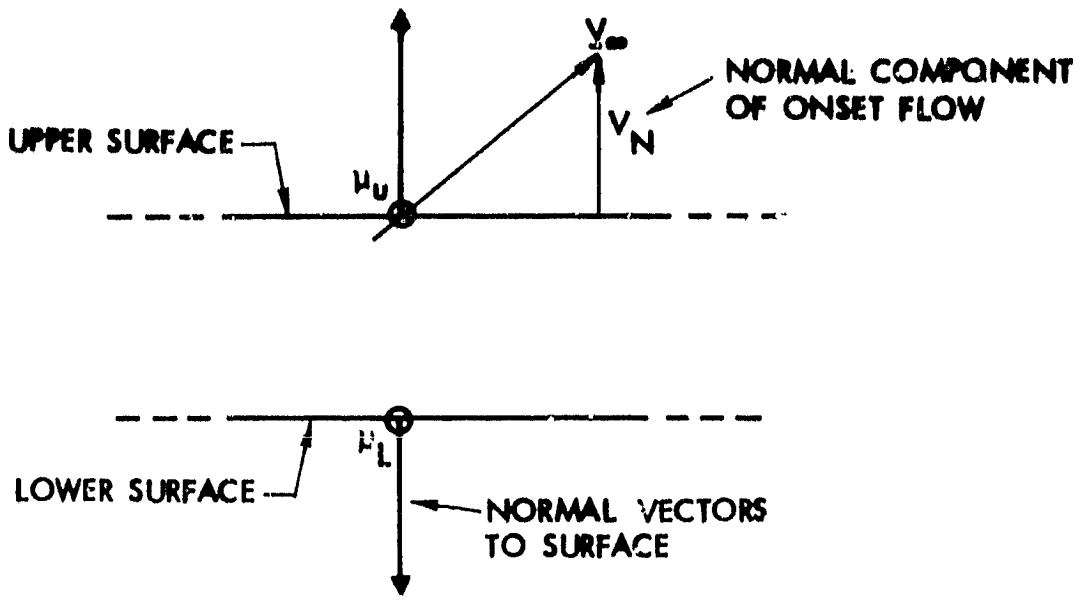

Figure D1. Parallel Doublet Sheets in Close Proximity.

That is, the symmetrical part, μ_s, has disappeared. In this simplified situation, therefore, the symmetrical part could take any value and yet the Neumann boundary condition would still be satisfied. Thus μ_s is indeterminate.

In practical cases, this condition is rarely met with exactly; however, it is approached in the neighborhood of sharp, trailing edges. In these circumstances the Neumann boundary condition is weak, and we sometimes observe that the upper and lower doublet values deviate from the exact solution, but they move together. The difference between them, i.e., the antisymmetrical part, is generally close to the exact value. This numerical ill-conditioning is especially serious when using iterative solution techniques.

E. Streamline Calculation Routine

A numerical procedure was developed for calculating streamline paths. The procedure is based on finite intervals, a mean velocity vector being calculated in the middle of each interval as we proceed along the path, Figure E1. The velocity calculation point, RP, is obtained by extrapolation from the two previous intervals on the basis of constant rate of change in the velocity vector direction; i.e.,

$$\underline{RP} = \underline{R}_n + .5\, S_n\, \underline{t}$$

where $\underline{R}_n$ is the previous point calculated on the streamline, S_n is the present interval length, and $\underline{t}$ is a projected tangent vector.

$$\underline{t} = \left(\frac{S_n + S_{n-1}}{S_{n-2} + S_{n-1}} \right) \left(\underline{t}_{n-1} - \underline{t}_{n-2} \right) + \underline{t}_{n-1}$$

where $\underline{t}_{n-1} = \dfrac{\underline{V}_{n-1}}{|\underline{V}_{n-1}|}$, etc. $\underline{V}_{n-1}$ is the velocity calculated in the middle of the previous interval.

RP does not necessarily lie on the streamline path. When we have calculated the velocity, $\underline{V}_n$, at RP we use this to evaluate the next point on the streamline, i.e.,

$$\underline{R}_{n+1} = \underline{R}_n + \frac{S_n\, \underline{V}_n}{|\underline{V}_n|}$$

An automatic procedure is included in the routine which changes the interval length, S_n, in accordance with the change in tangent direction. If a large change in direction is calculated, the value of S_n is decreased and the calculation is repeated

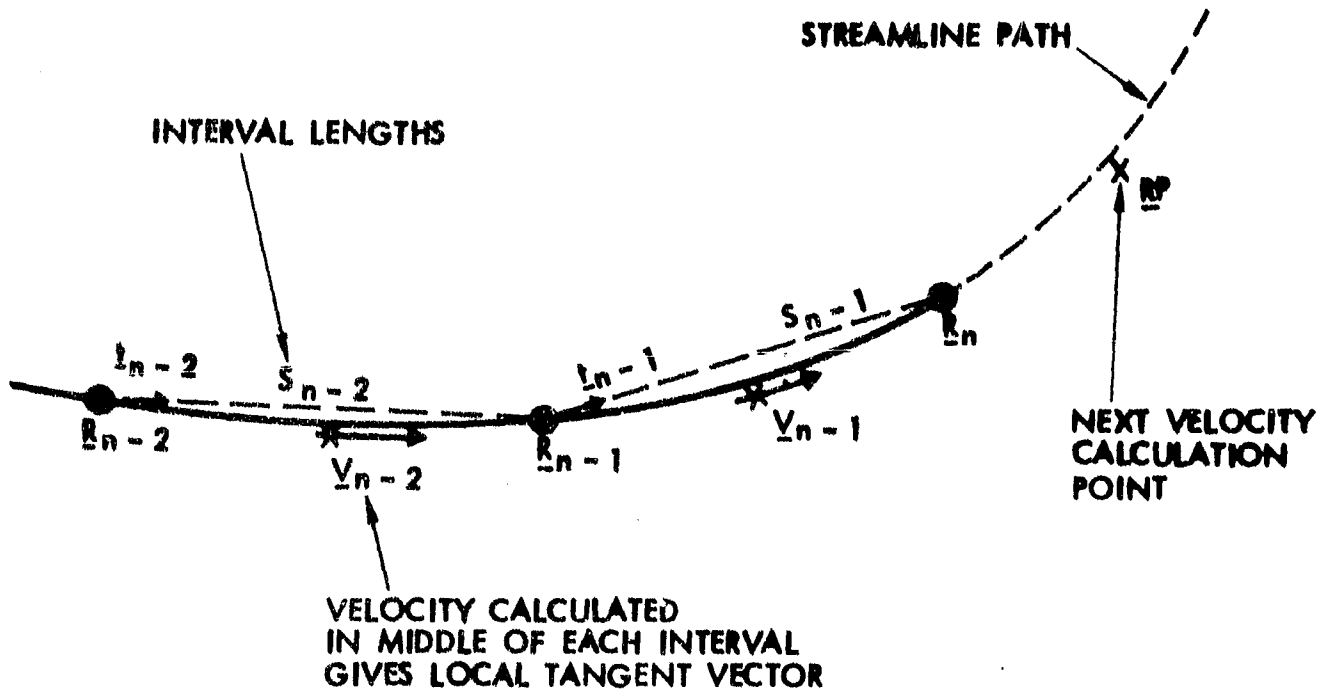

Figure E1. Streamline Calculation.

until the change in direction is within a specified amount. If the change in direction is smaller than a certain amount, then the interval length for the next step is increased.

F. Vortex Segment Influence Coefficient

The familiar expression for the velocity induced at a point, P, by a straight vortex segment is, referring to Figure F1:

$$\underline{V} = \frac{\Gamma}{4\pi h}\left(\cos\theta_1 + \cos\theta_2\right)\underline{n}$$

$\underline{n}$ is the unit vector normal to the plane containing the segment and the point, P.

A more convenient form for three-dimensional analyses (Ref. 4) is

$$\underline{V} = \frac{\Gamma}{4\pi}\,\frac{\underline{a}\wedge\underline{b}}{(\underline{a}\wedge\underline{b}\cdot\underline{a}\wedge\underline{b})}\,(a+b)\left(1-\frac{\underline{a}\cdot\underline{b}}{ab}\right)$$

which avoids the evaluation of trigonometric quantities.

Both expressions have a numerical problem when P approaches the extension of the segment. (The case where P approaches the segment is a separate problem requiring special treatment, such as a core model.)

The computer is then faced with dividing one small number by another small number. The result should pass smoothly through zero as P passes through the in-line condition. In practice, round-off in the computer creates spurious results which necessitate a special local treatment.

A solution to this problem has been found in the present work by rearrangement of the second expression. This can be written

$$\underline{V} = \frac{\Gamma}{4\pi}\,\frac{\underline{a}\wedge\underline{b}(a+b)(1-\cos\theta)}{a^2b^2\sin^2\theta}$$

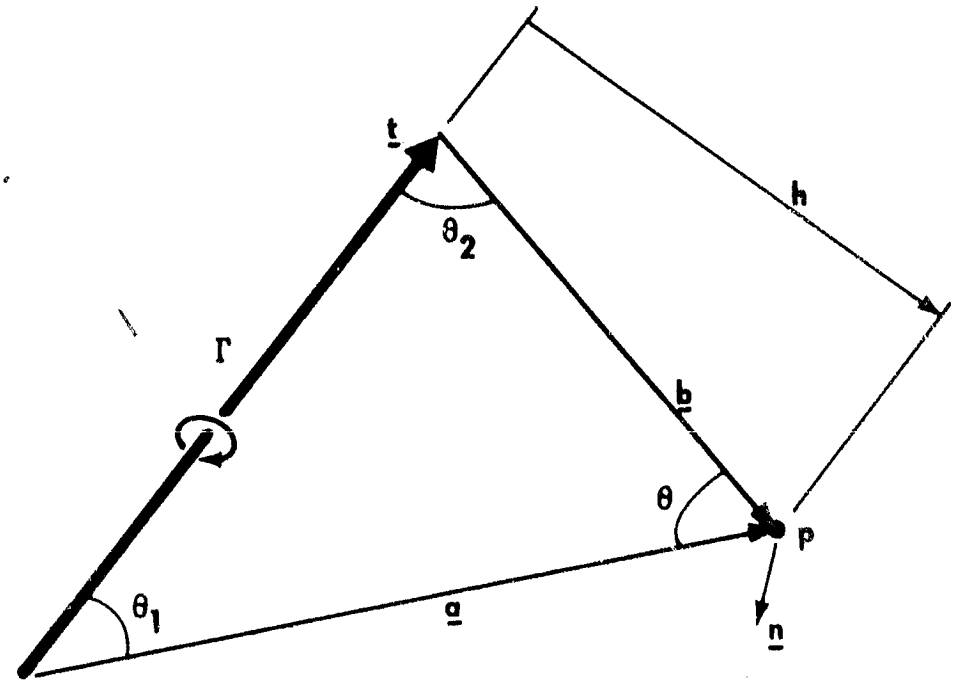

Figure F1. Vortex Segment Nomenclature.

The cause of the numerical problem is clearly the $\sin^2\theta$ term in the denominator--θ being 0 when P is in line with the segment. This term can be cancelled after multiplying numerator and denominator by $(1 + \cos\theta)$, leaving:

$$\underline{V} = \frac{\Gamma}{4\pi} \frac{\underline{a} \wedge \underline{b}(a + b)}{a^2b^2(1 + \cos\theta)}$$

or

$$\underline{V} = \frac{\Gamma}{4\pi} \frac{\underline{a} \wedge \underline{b}(a + b)}{ab(ab + \underline{a} \cdot \underline{b})}$$

This expression passes through zero correctly without special treatment as P passes through the in-line condition.

The corresponding form for the semi-infinite vortex is

$$\underline{V} = \frac{\Gamma}{4\pi} \frac{\underline{a} \wedge \underline{t}}{a(a + \underline{a} \cdot \underline{t})}$$

where $\underline{t}$ is the unit vector along the vortex.